J-Proteins in Plant Development and Stress Response

Dissertation der Fakultät für Biologie

der Ludwig-Maximilians-Universität

München

vorgelegt von

Sophie Isabell Dittmer

aus München

München, Oktober 2020

Diese Dissertation wurde angefertigt unter der Leitung von PD Dr. Serena Schwenkert an der Fakultät für Biologie der Ludwig-Maximilians-Universität München.

Erstgutachterin: PD Dr. Serena Schwenkert

Zweitgutachter: Prof. Dr. Thomas Nägele

Tag der Abgabe: 27.10.2020

Tag der mündlichen Prüfung: 17.12.2020

Summary

Molecular chaperones are involved in a broad range of different processes, like protein folding, trafficking or degradation. Furthermore, many chaperones also play an important role during the response to different stresses. Since plants are sessile organisms, they need to be able to quickly adapt to different conditions. To do so, plants possess a complex chaperone machinery, composed of HSP70, HSP90, J-proteins and other factors. How the different chaperones cooperate, and in which processes they are involved in is so far not well understood. DJC31 and DJC62 are two J-proteins in *Arabidopsis thaliana* and have previously been described to be located inside the chloroplast. Using GFP localization studies and splitGFP, the actual localization could be determined to be the cytosolic side of the endoplasmic reticulum membrane, which could be confirmed by sucrose density centrifugation using isolated microsomes. Moreover, they were found to be attached to the membrane, which is presumably mediated by the N-terminal halves. Both proteins are composed of a long, disordered N-terminal part followed by several TPR repeats, forming two TPR domains, and a J-domain at the C-terminus. This domain composition hints towards a function as co-chaperones of both HSP70 and HSP90. An interaction with cytosolic HSP70 and HSP90 could be shown by bimolecular fluorescence complementation. Additionally, performing a yeast two-hybrid library screening, potential client proteins of DJC31 could be identified. Knockout of either *DJC31* or *DJC62* caused only a mild phenotype, which was overall comparable to wild type. However, the double mutant exhibited severe defects in growth and development, which affected almost all organs. Furthermore, it could be shown that the double mutant is more sensitive to osmotic stress and treatment with abscisic acid, but surprisingly exhibited enhanced tolerance to drought. On the molecular level, up- or downregulation of *DJC31* or *DJC62* could not be observed under different stress conditions by qPCR. However, salt treatment of protoplasts, expressing the respective N-terminus of DJC31 or DJC62 fused to GFP, revealed that both proteins are released from the ER membrane into the cytosol under salt stress conditions, which indicates a regulation of DJC31 and DJC62 on the protein level. Transcriptome analysis could show, that under non-stress conditions expression levels of factors involved in biotic or abiotic stress response, as well as hormonal signaling are altered in the mutants. Taken together, these findings indicate that DJC31 and DJC62 might be regulators of different signaling pathways involved in development and stress response.

Zusammenfassung

Molekulare Chaperone sind an einer Vielzahl unterschiedlicher Prozesse beteiligt, wie z.B. der Proteinfaltung, dem Proteintransport in Organellen oder dem Abbau von Proteinen. Darüber hinaus spielen viele Chaperone auch eine wichtige Rolle bei der Reaktion auf unterschiedliche Stressbedingungen. Da Pflanzen sessile Organismen sind, sind sie darauf angewiesen sich schnell an unterschiedliche Bedingungen anpassen zu können. Zu diesem Zweck besitzen Pflanzen ein komplexes Chaperon-System, welches aus HSP70, HSP90, J-Proteinen und anderen Faktoren besteht. Wie die verschiedenen Chaperone zusammenarbeiten und an welchen Prozessen sie beteiligt sind, ist bisher nicht genau bekannt. DJC31 und DJC62 sind zwei J-Proteine in *Arabidopsis thaliana* und wurden zuvor als Chloroplastenproteine beschrieben. Durch GFP-Lokalisierungsstudien und splitGFP konnte jedoch gezeigt werden, dass DJC31 und DJC62 an der cytosolischen Seite des endoplasmatischen Retikulums lokalisiert sind, was biochemisch nochmals bestätigt werden konnte. Darüber hinaus wurde festgestellt, dass sie an die Membran angeheftet sind, was vermutlich durch die N-terminalen Hälften der Proteine vermittelt wird. Beide Proteine bestehen aus einem langen, ungeordneten N-terminalen Teil, gefolgt von mehreren *TPR-Repeats*, die jeweils zwei TPR-Domänen bilden, und einer *J-Domain* am C-Terminus. Diese Domänenzusammensetzung deutet auf eine Funktion als Co-Chaperone von HSP70 und HSP90 hin. Eine Interaktion mit cytosolischem HSP70 und HSP90 konnte durch bimolekulare Fluoreszenzkomplementation gezeigt werden. Zusätzlich konnten durch die Durchführung eines *Yeast Two-Hybrid library screenings* potentielle Klientproteine von DJC31 identifiziert werden. Die *DJC31* und *DJC62* Einzelmutanten wiesen nur einen milden Phänotyp auf, der insgesamt mit dem Wildtyp vergleichbar ist. Die Doppelmutante zeigte jedoch schwere Wachstums- und Entwicklungsstörungen, wobei fast alle Organe betroffen waren. Darüber hinaus konnte gezeigt werden, dass die Doppelmutante sensitiver gegenüber osmotischem Stress und der Behandlung mit Abscisinsäure reagiert, jedoch wies sie überraschenderweise eine erhöhte Trockenheitstoleranz auf. Auf molekularer Ebene konnte mittels qPCR unter verschiedenen Stressbedingungen keine vermehrte oder reduzierte Expression von *DJC31* oder *DJC62* beobachtet werden. Die Salz-Behandlung von Protoplasten, die ein Fusionskonstrukt bestehend aus dem N-terminus von DJC31 bzw. DJC62 und GFP exprimierten, zeigte, dass beide Proteine unter Salzstress von der ER-Membran ins Cytosol entlassen werden, was auf eine Regulierung von DJC31 und DJC62 auf Proteinebene hinweist. Eine Transkriptomanalyse konnte zeigen, dass die Expression von Faktoren der biotischen oder abiotischen Stressantwort, sowie der hormonellen Signalübertragung, unter normalen Bedingungen in den Mutanten verändert ist. Zusammenfassend deuten diese Ergebnisse darauf hin, dass DJC31 und DJC62 an der Regulierung verschiedener Entwicklungs- und Stress-Signalwege beteiligt sind.

Abbreviations

ABA	abscisic acid
Ade	adenine
ADP	adenosine diphosphate
Asp	aspartic acid
ATP	adenosine triphosphate
BASTA	ammonium glufosinate
BiFC	bimolecular fluorescence complementation
BiP	binding-immunoglobulin protein
bp	base pair
cDNA	complementary DNA
Col-0	ecotype Columbia, wild type
C-terminus	carboxy-terminus
CTD	carboxy-terminal domain
DNA	deoxyribonucleic acid
DMSO	dimethyl sulfoxide
EDTA	ethylenediaminetetraacetic acid
ER	endoplasmic reticulum
EtOH	ethanol
GA	gibberellin
GAL4-AD	GAL4 activation domain
GAL4-BD	GAL4 DNA binding domain
gDNA	genomic DNA
GFP	green fluorescent protein
Glu	glutamic acid
HOP	HSP70-HSP90 organizing protein
HSF	heat shock factor
HSP	heat shock protein
His	histidine
Ile	isoleucine
kDa	kilodalton
KEGG	Kyoto encyclopedia of genes and genome
Leu	leucine
MD	middle domain
MES	2-(N-morpholino) ethanesulfonic acid
Met	methionine
NaCl	sodium chloride
NBD	nucleotide binding domain
NEF	nucleotide exchange factor
NTD	amino-terminal domain
N-terminus	amino-terminus
PAGE	polyacrylamide gel electrophoresis
PCR	polymerase chain reaction

Phe	phenylalanine
Pro	proline
PVP	polyvinylpyrrolidone
qPCR	quantitative polymerase chain reaction
RNA	ribonucleic acid
RNAi	RNA interference
RNAseq	RNA sequencing
RT-PCR	reverse transcription polymerase chain reaction
SBD	substrate binding domain
SCFP	cyan fluorescent protein
SD	standard deviation
SDS	sodium dodecyl sulfate
TP	transit peptide
TPR	tetratricopeptide repeat
Trp	tryptophan
Tyr	tyrosine
Val	valine
VYNE	venus, yellow fluorescent protein
X-α-Gal	5-Bromo-4-chloro-3-indolyl-α-D-galactopyranoside
Y2H	yeast two-hybrid
ZFLR	zinc finger like region

Table of Contents

1. Introduction

1.1. Protein folding and proteostasis

In order to function, proteins must fold into their native three-dimensional structure. With approximately 27416 protein coding genes, *Arabidopsis thaliana* is challenged with the production and regulation of several thousand proteins, different in size, structure and stability[2] . Since a polypeptide chain can adopt a multitude of different conformations, protein folding is an error prone process and relies on cooperation of many weak, non-covalent interactions (Hartl et al., 2011). First insights into how proteins attain their functional structure, were gained in the 1950s. *In vitro* experiments on chemically denatured proteins could show, that upon removal of the denaturant, some proteins were able to refold without the help of additional factors. This demonstrated that the amino acid sequence itself contains all information necessary for correct folding (Anfinsen, 1973). Decades of research later, it became evident, that some proteins, especially large proteins, require help of molecular chaperones in order to fold correctly and efficiently (Balchin et al., 2016).

In contrast to *in vitro* conditions, complete polypeptide chains *in vivo* barely move freely inside the cytosol. Synthesis of new proteins occurs at ribosomes and resembles a rather slow process with a speed of ~4 amino acids per second. As a consequence, the polypeptide leaves the ribosome step by step, which restricts productive folding, especially in formation of long-range interactions and assembly of larger multidomain proteins. Compared to the speed of translation, protein folding is a rather fast process. After emerging from the ribosomal exit tunnel, the nascent chain is exposed in an unfolded, aggregation prone state for several seconds, in which it might form non-native intra- or intermolecular interactions (Kim et al., 2013). To prevent misfolding, molecular chaperones interact with nascent chains, but also the ribosome is suggested to prevent aberrant interactions and might contribute to proper folding (Kaiser et al., 2011).

Another difference to *in vitro* conditions is that the cellular environment contains a large number of different macromolecules, which constitute 20-30% of the total volume. This macromolecular crowding makes proper protein folding even more challenging and increases the risk of accumulation of partially folded intermediates or misfolded proteins (Balchin et al., 2016; Ellis & Minton, 2006). These intermediates or misfolded states often expose features, like hydrophobic residues, which are usually buried within the protein because they might promote aggregation in a concentration-dependent manner. Since presence of aggregates can be toxic, maintenance of proteome homeostasis (also termed proteostasis) is of special importance for an organism's viability. Therefore, a complex network, consisting of molecular chaperones, regulatory proteins, the ubiquitin-proteasome system and the autophagy system, guides the proteome throughout a protein's life cycle (Hartl et al., 2011).

1.2. Chaperones and their co-chaperones

Molecular chaperones are defined as proteins which interact with, stabilize or help other proteins to attain their functional structure, without being part of the final structure. They act in many different cellular processes, like *de novo* folding and refolding, assembly of oligomers, protein trafficking and protein degradation. Since some of these proteins were observed to be upregulated during stress, they are also called heat shock proteins. These proteins can be grouped into several structurally unrelated classes, which were named after the molecular weight of their typical members (Balchin et al., 2016; Hartl et al., 2011). Among them HSP70, HSP90 and HSP40, which are described in more detail in the following.

1.2.1. The HSP70 chaperone family

Chaperones of the HSP70 protein family are central players in protein folding and protein homeostasis and are therefore involved in a wide range of different cellular processes (Hartl et al., 2011). Members of this protein family can be found in different organisms, from eubacteria to eukaryotes and also in some archaea and share at least two of the four structural features of the bacterial HSP70, DnaK (Lin et al., 2001; Young, 2010). DnaK is composed of an N-terminal nucleotide binding domain (NBD) of 45 kDa in size, a 15 kDa substrate binding domain (SBDβ), containing a hydrophobic groove for polypeptide binding, with a 10 kDa helical lid domain (SBDα) and a disordered C-terminal region, which contains, at least in the cytosolic and nuclear HSP70 family members, the conserved charged Glu-Glu-Val-Asp (EEVD) motif (Balchin et al., 2016; Rosenzweig et al., 2019; Young, 2010). The NBD consists of two lobes, which can be subdivided into the subdomains 1a and 1b on one side, 2a and 2b on the other side. Subdomains 1a and 2a form the bottom of the nucleotide pocket, to which the nucleotides bind (Young, 2010). NBD and SBD are connected by a hydrophobic linker, which is essential for coupling ATP binding and hydrolysis at the NBD to substrate binding to the SBD (Balchin et al., 2016; Rosenzweig et al., 2019). This interplay between nucleotide binding and client binding or release must be tightly regulated to ensure rapid association and timely release to prevent client protein aggregation, but also to ensure proper folding. In the ADP-bound state, the SBD tightly binds a five amino acid long hydrophobic segment of the client protein with high affinity but very low association and dissociation rates. Binding of ATP weakens the interaction between client protein and SBD, by increasing the association rate 100-fold and the dissociation rate 1000-fold (Kampinga & Craig, 2010; Rosenzweig et al., 2019). HSP70 cycles between these two states through ATP hydrolysis and a nucleotide exchange reaction. However, the basal HSP70 ATPase activity is rather low and nucleotides stably bind to the NBD. Therefore, additional factors are needed. J-proteins stimulate the HSP70 ATPase activity, which leads to hydrolysis from ATP to ADP thus inducing client binding. Subsequent dissociation of ADP,

stimulated by a nucleotide exchange factor (NEF), induces client release and recycling of HSP70 for another cycle of client binding and release (Kampinga & Craig, 2010) (Figure 1).

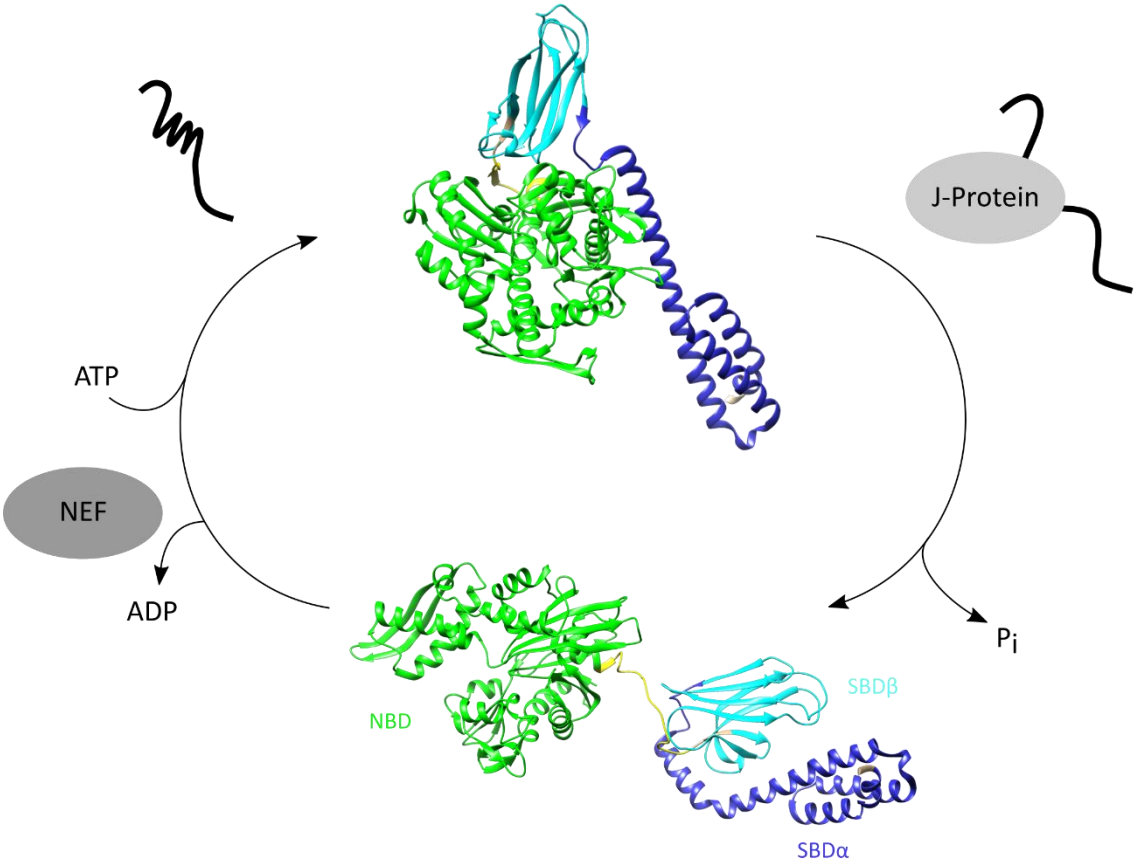

Figure 1: The HSP70 cycle of the *E.coli* HSP70 homolog DnaK. HSP70/DnaK consists of a nucleotide binding domain (NBD, green), which is connected via a flexible linker (yellow) with the substrate binding domain (SBDβ, cyan) and the lid domain (SBDα, blue). A J-protein delivers the client to HSP70 in the ATP-bound open conformation (PDB: 4B9Q, (Kityk et al., 2012)). The J-domain activates the ATPase activity of HSP70, which leads to client binding and transition to the ADP bound closed conformation (PDB: 2KHO, (Bertelsen et al., 2009)). A nucleotide exchange factor (NEF) induces release of ADP. After binding of ATP, the client protein is released.

HSP70 is known to bind a broad range of different client proteins, including newly synthesized proteins at the ribosome, folding intermediates and misfolded proteins as well as aggregates and complexes that need to be correctly assembled. This multitude of different clients and conformations raises the question of how HSP70 chooses its clients. Studies on the *E.coli* HSP70, DnaK, using cellulose-bound peptide libraries revealed, that DnaK prefers peptides composed of a hydrophobic core, especially enriched in Leu, Ile, Val, Phe, and Tyr, flanked by regions with predominantly basic residues. These motifs are abundant in different protein sequences, but mostly not accessible in correctly folded proteins (Rüdiger et al., 1997). Although the structure of the SBD is conserved, HSP70 proteins from different organisms and cellular compartments show preferences for different peptide compositions.

Whereas the cytosolic HSP70 prefers peptides enriched in leucine, the ER resident HSP70 family protein, BiP, rather binds to peptides with aromatic residues (Rosenzweig et al., 2019).

Besides proteins of the HSP70/DnaK type, orthologs of the cytosolic mammalian HSP110, the yeast SSE proteins and the ER localized orthologs of the mammalian GRP170 proteins are part of the HSP70 superfamily because of structural and functional similarities. The *Arabidopsis* genome contains 18 members of the HSP70 superfamily, whereas 14 of them belong to the HSP70/DnaK type and four to the HSP110/SSE subfamily. From the HSP70/DnaK subfamily proteins, AtHSP70-1, AtHSP70-2, AtHSP70-3, AtHSP70-4 and AtHSP70-5 contain the C-terminal EEVD motif and were predicted to be located in the cytosol. Additionally, AtHSP70-1 and AtHSP70-5 carry consensus nuclear localization signals. AtHSP70-6, AtHSP70-7 and AtHSP70-8 contain predicted chloroplast transit peptides. Mitochondrial transit peptides could be found in AtHSP70-9 and AtHSP70-10. In the endoplasmic reticulum, three HSP70 family proteins can be found. AtHSP-18 shows highest similarity to the cytosolic members of the HSP70/DnaK subfamily but lacks the EEVD motif at the C-terminus. Since it could not be detected so far, it might be a pseudogene. For the HSP110/SSE subfamily, three proteins (AtHSP70-14, AtHSP70-15, AtHSP70-16) could be identified in the *Arabidopsis* genome and were predicted to be located in the cytosol, whereas AtHSP70-14 and -15 additionally possess a nuclear localization signal. As a representative of the GRP170 subfamily, AtHSP70-17 could be identified (Lin et al., 2001).

The ER resident HSP70 proteins BiP1, 2 and 3 play an important role in the unfolded protein response and gametogenesis. The chloroplast located HSP70 members maintain the chloroplast structure and are important for plant development. Furthermore, plastidal and mitochondrial HSP70 are involved in translocation of proteins into the organelle (Leng et al., 2017). Because of the high sequence identity of over 80%, knowledge about precise roles of the cytosolic HSP70s is limited and indicates high functional redundancy (Leng et al., 2017; Lin et al., 2001). Two studies have examined the expression pattern of the individual HSP70 proteins but came to different results. Lin et al. detected all cytosolic HSP70s to be widely expressed in 9-day-old seedlings and 4-6-week old plants, whereas Sung et al found HSP70-1, -2, -3 to be expressed in roots, leaves, stems, flowers and siliques, HSP70-4 predominantly expressed in roots and leaves and HSP70-5 could not be detected at all. Both reported that the different HSP70s are expressed differentially in response to environmental stimuli (Lin et al., 2001; Sung et al., 2001). Knockout of only one HSP70 gene does not exhibit a mutant phenotype, supporting the idea of overlapping functions and functional redundancy between the different HSP70s. However, the double and triple knockouts *hsp70-1/4* and *hsp70-2/4/5* exhibit a pleiotropic phenotype, demonstrating the importance of HSP70 in growth and development and furthermore, that the individual HSP70 proteins must have specialized functions. Another argument for specialized functions,

comes from qPCR experiments under stress conditions. Treatment of plants with different stress agents or hormones leads to up and downregulation of different HSP70 genes, indicating a specific role in stress response (Leng et al., 2017).

1.2.2. The HSP40 chaperone family

Proteins of the HSP40 chaperone family, also known as J-proteins, are a large group of multidomain proteins, which contain the highly conserved J-domain. The J-domain is approximately 70 amino acids in length and consists of four α-helices, with the functionally important His, Pro, Asp (HPD) motif between helix II and III, which stimulates the ATPase domain of HSP70 (Kampinga & Craig, 2010). J-proteins can be divided according to their domain composition into three groups. Class A contains J-proteins harboring domains and motifs, which are most similar to the *E.coli* DnaJ, the founding member of this protein family. These proteins carry the J-domain at the N-terminus, followed by a glycine/phenylalanine (G/F) rich region and two C-terminal domains (CTD), of which CTD-I contains a zinc finger like region (ZFLR). Additionally, they contain a dimerization domain at the very C-terminal end. Class B J-proteins are similar in structure and domain composition to class A J-proteins. They also contain the J-domain at the N-terminus with the adjacent glycine/phenylalanine rich region, the CTD and a C-terminal dimerization domain, but they lack the zinc finger like domain. Class C is the most diverse group. Members of this group only have the J-domain in common, which can be located N- as well as C-terminally. Besides the J-domain, class C J-proteins can contain additional domains, like tetratricopeptide repeat (TPR) domains, thioredoxin domains or kinase domains (Kampinga & Craig, 2010; Rosenzweig et al., 2019) (Figure 2).

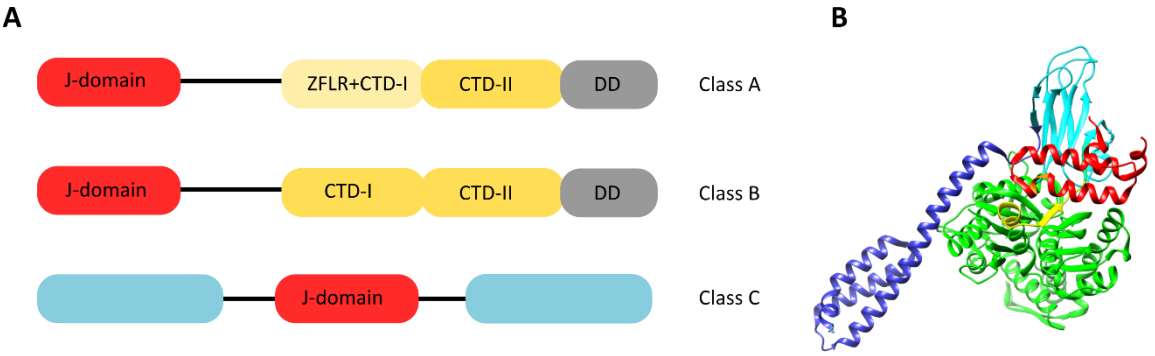

Figure 2: Domain composition of J-proteins.

A.) J-proteins can be divided into three groups according to their domain composition. Class A J-proteins are composed of an N-terminal J-domain, a G/F rich linker, a Zinc finger like region (ZFLR) within the C-terminal domain I (CTD-I), followed by CTD-II and a dimerization domain (DD). Class B J-proteins exhibit an N-terminal J-domain with an adjacent G/F rich linker, two C-terminal domains and a C-terminal dimerization domain. Class C J-proteins only have the J-domain in common, which can be located either N- or C-terminally. Additionally, class C J-proteins can contain various other domains.

B.) Structural Model of the E.coli HSP70 homolog DnaK (NBD green, SBDβ cyan, SBDα blue) with a bound J-domain (red) (PDB:5NRO,(Kityk et al., 2018)).

So far, 118 J-proteins could be identified in *Arabidopsis*. Some of them exhibit a broad or unspecific client range, like atDjA1, which is required for correct folding of a vast number of proteins synthesized in the cytosol. Others have a more specialized function and bind only a few clients, like atDjC3, an auxilin-like J-protein, which catalyzes the coat disassembly of clathrin coated vesicles. Most of the HSP70 proteins interact with multiple different J-proteins, which enable HSP70 to function in a multitude of cellular processes, like protein folding, regulation of multimeric protein complexes or translocation of proteins across membranes (Craig & Marszalek, 2017; Rajan & D'Silva, 2009). Binding of clients by J-proteins was observed to increase the number of HSP70 binding sites, e.g. by inducing conformational changes or preselecting proteins in a conformation, which is best accessible for HSP70, but how J-proteins choose their clients is not fully understood yet. Screening experiments using a peptide library with the *E.coli* DnaJ showed, that class A J-proteins prefer binding of linear sequence motifs of eight amino acids in length, enriched in predominantly hydrophobic, aromatic residues (Rüdiger et al., 2001). A similar finding was obtained for class B J-proteins. Yeast Sis1 was also observed to bind peptides composed of predominantly hydrophobic and aromatic residues, but in a different composition (Fan et al., 2004). Besides the CTD, also the G/F rich region could contribute to client binding. Whereas binding of unfolded client proteins appeared to be unaffected, deletion of the G/F rich region in the class A J-protein DnaJ from *E.coli* reduced affinity to folded or partially unfolded client proteins (Perales-Calvo et al., 2010). Since members of the J-protein class C are very diverse in structure and function, no general pattern for client recognition could be determined so far. Additionally, they are often specialized on a certain subset of client proteins and might have special client binding domains. Once a client is bound, it is transferred to HSP70, which binds the client upon activation of the ATPase by the J-domain (Kampinga & Craig, 2010; Rosenzweig et al., 2019).

1.2.3. The HSP90 chaperone family

HSP90 is a highly conserved member of the gyrase, HSP90, His kinase and MutL (GHKL) superfamily of split ATPases. As many chaperones, HSP90 was discovered as a specific and upregulated factor during the heat shock response. Besides a role in response to heat, HSP90 was also observed to be involved in numerous cellular processes, like protein maturation, stability, activity and degradation, under stressed and non-stressed conditions (di Donato & Geisler, 2019; Schopf et al., 2017). Whereas in bacteria only one HSP90 can be found, yeast and higher eukaryotes possess more than one HSP90 homolog but only in higher eukaryotes, HSP90 can also be found in organelles like mitochondria, chloroplasts and the endoplasmic reticulum. HSP90 is composed of an amino-terminal domain (NTD), which mediates ATP binding, the middle domain (MD), important for ATP hydrolysis and client binding, and the carboxy-terminal domain (CTD), mediating homodimerization, which is essential for HSP90 function (Schopf et al., 2017). In cytosolic HSP90 proteins, the CTD also contains the Met-Glu-Glu-Val-Asp (MEEVD) motif, which allows binding to TPR domain containing co-chaperones. NTD and MD are

connected by a long, flexible and charged linker that modulates HSP90 function and co-chaperone binding. This linker can be found in cytosolic and ER resident HSP90 proteins of eukaryotes but is lacking in bacteria and the mitochondrial HSP90 (Genest et al., 2019). In an ATP-free state, the HSP90 homodimer has an open, V-shaped conformation. Binding of ATP leads to structural rearrangements. The NTDs rotate and dimerize, leading to an N-terminally closed state (Figure 3). HSP90 has low enzymatic activity and low affinity to ATP. For ATP hydrolysis the NTD must interact with the MD. To do so, large conformational changes are required, which involve all three domains and interaction between the two NTDs. When ATP binds, rearrangements take place in the NTD and the lid, which is composed of a loop containing several conserved amino acids, closes over the ATP bound NTD. This represents the intermediate state. Dimerization of the NTD and association to the MDs induce the closed state, which is crucial for ATP hydrolysis. After ATP hydrolysis, the NTDs dissociate, ADP is released and HSP90 changes back into the open conformation (Genest et al., 2019; Schopf et al., 2017).

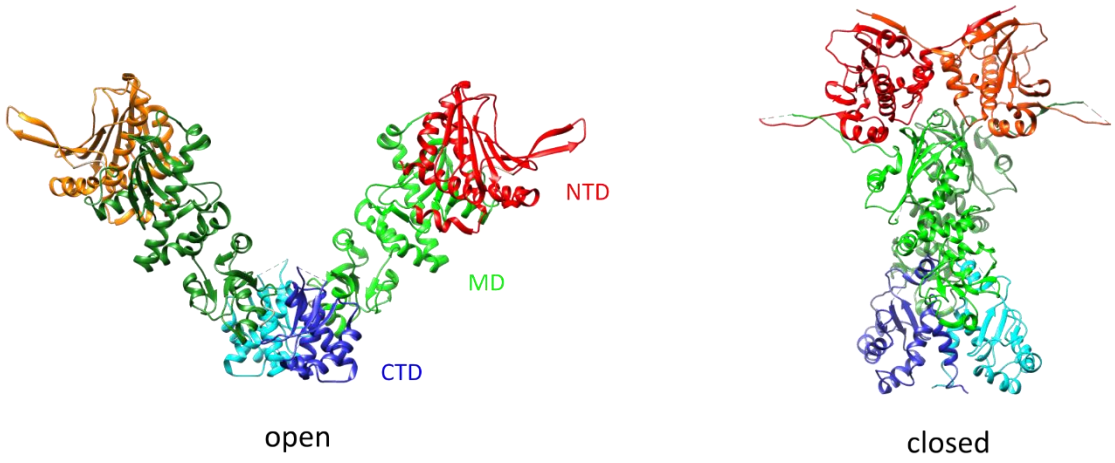

Figure 3:Structure and domain composition of HSP90. HSP90 forms a dimer, with each monomer consisting of a C-terminal domain (CTD, blue/cyan), a middle domain (MD, green/dark green) and a N-terminal domain (NTD, red/orange). In the ATP-free state, the HSP90 dimer exhibits a V-shaped conformation (PDB: 2IOQ, HSP90/HtpG from *E.coli*, (Shiau et al., 2006). Binding of ATP leads to a closed conformation by dimerization and rotation of the NTD (PDB: 2CG9, HSP90 from *S.cerevisiae*, (Ali et al., 2006)).

Whereas HSP70 appears to interact with all unfolded proteins, the number of HSP90 clients seems to be limited to several hundred proteins involved in e.g. stress regulation, protein folding, DNA repair and development. The interaction with clients occurs in three different ways: facilitating the formation of a specific active conformation, supporting assembly of multiprotein complexes and promoting binding of ligands to proteins by stabilizing a binding competent conformation. Therefore, HSP90 acts as a central conformational regulator, which impacts a multitude of different signaling processes (Schopf et al., 2017). In contrast to HSP70, it is so far not understood how HSP90 identifies its clients, especially because client-HSP90 complexes are rather dynamic and transient. Consistent with the fact,

that HSP90 acts downstream of HSP70, the hydrophobicity of the client interaction site is less hydrophobic compared to HSP70 clients and contains a higher fraction of positively charged residues. However, for some clients an overall negatively charged binding region was determined (Radli & Rüdiger, 2018). Since HSP90 clients are structurally and sequentially unrelated, different studies suggest that the overall structural stability determines the dependency to HSP90 rather than distinct structural motifs (Genest et al., 2019; Schopf et al., 2017). Additionally , different clients seem to bind to different regions and at different nucleotide states of HSP90 (Genest et al., 2019).

HSP90 can be regulated in many ways, including transcriptional regulation, post-translational modifications, co-chaperones and regulation by its clients. On the transcriptional level, HSP90 is regulated by heat shock factor 1 (HSF1), which is at the same time a HSP90 client. Under non-stressed conditions, HSP90 and HSP70 bind to HSF1 to keep it in an inactive state. Under stress conditions, HSP70 and HSP90 are no longer available for keeping HSF1 inactive. Therefore, HSF1 is released and increases the expression of stress related genes, like genes for HSP90 and other chaperones (Schopf et al., 2017). Besides regulation on the transcriptional level, post-translational modifications play a role in the modification of HSP90 activity. HSP90 is phosphorylated predominantly at different serine residues, but it also occurs at threonine and tyrosine residues. Many of these residues are conserved between the different HSP90 proteins, but some are also isoform specific (Sima & Richter, 2018). Phosphorylation slows down the conformational HSP90 cycle and was observed to affect the interaction with co-chaperones, as well as client maturation. Also acetylation is an important regulator of the HSP90-co-chaperone interaction. Whereas acetylation was described to promote complex formation between HSP90 and its co-chaperones, hyperacetylation was found to interfere with co-chaperone interaction and consequently leads to a loss of chaperone activity and disturbed client activation (Schopf et al., 2017; Sima & Richter, 2018). Furthermore, HSP90 can be S-nitrosylated at its C-terminal domain, which affects the ATPase activity, as well as its chaperone activity (Retzlaff et al., 2009). Further modifications that adapt and regulate the HSP90 activity include SUMOylation and methylation (Sima & Richter, 2018). Another mode of regulation can be mediated by co-chaperones, which either bind to the MEEVD motif in the CTD via their tetratricopeptide repeat (TPR) domain or, if lacking a TPR domain, to different regions on HSP90 (Schopf et al., 2017).

The *Arabidopsis thaliana* genome harbors seven HSP90 isoforms, of which HSP90.1, Hsp90.2, HSP90.3 and HSP90.4 are located in the cytosol, HSP90.5 in the chloroplast, HSP90.6 in mitochondria and HSP90.7 in the endoplasmic reticulum. The cytosolic HSP90 proteins share a very high amino acid sequence identity and single knockout mutants exhibit only mild phenotypes, which hints to a high degree of functional redundancy. RNAi mediated silencing of all four isoforms is lethal, underlining the importance of HSP90 for plant viability. HSP90.1 is thought to be heat shock induced, whereas the

other three isoforms are constitutively expressed in high amounts (di Donato & Geisler, 2019). However, expression of HSP90.1 and HSP90.3 was found to be elevated in embryo development (Prasinos et al., 2005).

1.2.4. Co-chaperones of HSP90

Many of the HSP90 co-chaperones are tetratricopeptide repeat (TPR) containing proteins. These proteins are involved in many different processes and act as interaction modules or mediators for multiprotein complexes. A TPR domain consists of several TPR repeats, which consist of 34 amino acids, sharing a degenerate consensus sequence (Zeytuni & Zarivach, 2012). Although different TPR domains do not share a high degree of similarity, they exhibit some residues which are highly conserved, among them A/G_8, A_{20} and A_{27}. The consensus residues 4, 7, 11 and 24 predominantly exhibit hydrophobic residues. Furthermore, position 32 contains a helix-breaking amino acid like proline (D'Andrea & Regan, 2003). The TPR motif adopts a basic helix-turn-helix fold. Due to their antiparallel packing, adjacent TPR repeats form repeating antiparallel α-helices, which creates an overall super-helix structure. This super-helix fold forms concave and convex surfaces, which provide a binding groove for different peptides. The ligands usually do not exhibit similarity in structure or sequence. However, binding of ligands to TPR containing proteins is usually highly specific (Schopf et al., 2017; Zeytuni & Zarivach, 2012).

Among the proteins, which carry TPR domains, several co-chaperones can be found, which may influence the HSP90 ATPase activity, select client proteins and recruit additional factors. One of them is HOP, a TPR containing protein, composed of two TPR domains, which mediate interaction with HSP70 and HSP90 (di Donato & Geisler, 2019; Genest et al., 2019). The first TPR domain, TPR1, specifically recognizes the C-terminal heptapeptide of HSP70, whereas the TPR2A domain binds the pentapeptide of the HSP90 C-terminus (Figure 4). Both HSP70 and HSP90 possess the conserved EEVD motif at their C-terminus, which mediates binding to the TPR domains. Therefore, it was thought that HOP has the role as an adaptor for the two chaperones. Studies on the yeast HOP homolog Sti1 revealed, that it stabilizes the weak interactions between HSP70 and HSP90 and facilitates functional collaboration between the two chaperones by keeping HSP90 in an open conformation (Genest et al., 2019; Schopf et al., 2017). In *Arabidopsis*, three HOP homologs could be identified, which play a role in heat stress and acclimation to high temperatures (Fernández-Bautista et al., 2018). Another group of co-chaperones are the TPR domain containing immunophilins. Besides the TPR domain, they possess peptidylprolyl-isomerase activity and were described to be involved in regulation of steroid receptor action, transcriptional activity, protein conformation and many more processes (Zgajnar et al., 2019). In plants, immunophilins are represented by five genes. Four of them belong to the FKBP family and are involved in stress response and hormone related processes. The fifth gene is the cyclophilin 40

(CYP40) homolog Squint (SQN), important for shoot development and Clavata signaling. A co-chaperone involved in degradation of proteins is the Carboxyl terminus of Hsc70-interacting protein (CHIP). CHIP is a TPR containing U-box ubiquitin ligase, which acts in the quality control of protein folding in the HSP70/HSP90 pathway and targets client proteins to proteasomal degradation (di Donato & Geisler, 2019).

Not all HSP90 co-chaperones contain TPR domains, e.g. p23 and Activator of HSP90 ATPase (Aha1). The co-chaperone p23 is known for stabilizing the progesteronreceptor-HSP90 complex in animals (Figure 4). In *Arabidopsis* two homologs could be identified, which play a role in root development and auxin signaling (D'Alessandro et al., 2015). Activator of HSP90 ATPase (Aha1), which binds to the HSP90 N-terminus and regulates ATPase activity, might be represented in *Arabidopsis* by the so far uncharacterized protein AT3G12050 (di Donato & Geisler, 2019).

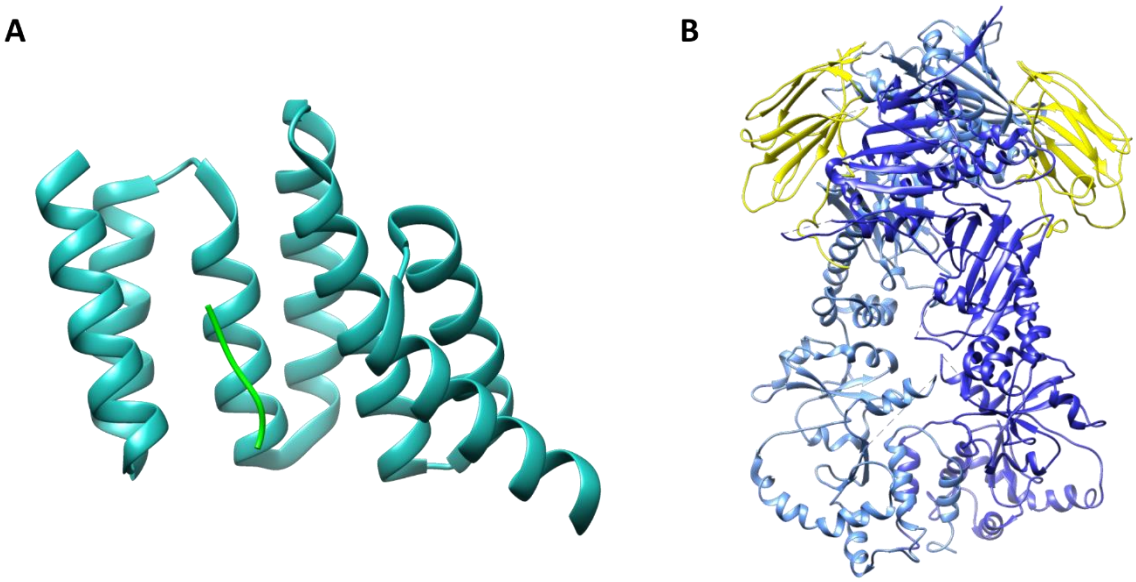

Figure 4: Interaction of co-chaperones with HSP90.

A.) The TPR domain of the human HOP (TPR2A, cyan) binds to the HSP90 C-terminal MEEVD peptide (green) (PDB: 1ELR, (Scheufler et al., 2000)).

B.) The co-chaperone p23 (yellow) binds to the NBD of yeast HSP90 (blue/light blue) in a closed conformation (PDB: 2CG9, (Ali et al., 2006)).

Many more co-chaperones, already known from the yeast and mammalian system, were predicted in *Arabidopsis*, which play important roles in different developmental and stress related processes. However, for some already described co-chaperones, no orthologues could be identified so far in *Arabidopsis*, indicating that plants have evolved different functionally analogous mechanisms (di Donato & Geisler, 2019).

1.3. Aim of the study

As sessile organisms, plants need to cope with a fast-changing environment and different conditions. Therefore, a versatile chaperone machinery is essential for the response and adaptation to various stresses, like heat, drought and soil salinity. J-proteins, as determinators of HSP70 function, play an important role during this process. Additional to their J-domain, DJC31 and DJC62 carry several TPR repeats, which form two TPR domains and might mediate binding to HSP90 (Prasad et al., 2010). A previous study has determined the two proteins to be located in the chloroplast by chloroplast import experiments (Chiu et al., 2013). However, since the import efficiency was very low and more than one mature form was observed after the import, doubts remained regarding a plastidal localization. Therefore, the subcellular localization should be confirmed in this study by a different method. Furthermore, single and double knockout mutants should be analyzed to find out more about the function of DJC31 and DJC62. In general, co-chaperones were reported to be involved in the response to different stresses. Therefore, a potential role of DJC31 and DJC62 in stress response should be analyzed on the phenotypic and molecular level under different conditions. According to their domain composition, DJC31 and DJC62 might act as co-chaperones of HSP70 and HSP90. This interaction should be confirmed and a screening for potential client proteins and additional factors should be performed.

2. Material

2.1. Chemicals

Chemicals were purchased from Sigma-Aldrich (Taufkirchen, Germany), Roth (Karlsruhe, Germany), Merck (Darmstadt, Germany), New England BioLabs (NEB, Frankfurt am Main, Germany), ThermoFisher Scientific (Braunschweig, Germany) and Serva (Heidelberg, Germany) in high quality. Exceptions are stated in the respective sections.

2.2. Molecular weight markers and DNA standards

For agarose-gel electrophoresis, HindIII/EcoRI digested λ-Phage DNA (NEB, Frankfurt am Main, Germany) was used as DNA marker for molecular size estimation. For SDS-PAGE, the PageRuler^{TM} Plus Prestained Protein Ladder (ThermoFisher Scientific, Braunschweig, Germany) was used as a molecular size marker.

2.3. Plant and bacterial strains

2.3.1. Plant material

Arabidopsis thaliana ecotype Columbia (Col-0) was used as wild type strain. The *djc31 djc62 Arabidopsis* double mutant was generated by crossing of *djc31* (SALK_034886) and *djc62* (SALK_050913). For transient gene expression *Nicotiana benthamiana* was used.

2.3.2 Plant lines generated in this study

The following plant lines were either generated by crossing or by stable agrobacteria mediated transformation.

Table 1: Plant lines generated in this study

Name	**Genotype**	**Description**
djc31 djc62	*djc31* x *djc62*	Double mutant
35S::*DJC31*	*djc31 djc62* 35S::*DJC31*	Complementation line
35S::*DJC62*	*djc31 djc62* 35S::*DJC62*	Complementation line
DJC31 H1052Q	*djc31 djc62* 35S::*DJC31 H1052Q*	DJC31 with mutated HPD motif
DJC62 H1006Q	*djc31 djc62* 35S::*DJC62 H1006Q*	DJC62 with mutated HPD motif
GFP-DJC31+S	*djc31 djc62* 35S::*GFP-DJC31*	DJC31 with N-terminal GFP
GFP-DJC62+S	*djc31 djc62* 35S::*GFP-DJC62*	DJC62 with N-terminal GFP

2.3.2. Bacterial strains

For molecular cloning and plasmid propagation *E.coli* Top10 and *E.coli* NEB stable cells were used. Protein overexpression was performed using *E.coli* BL21-CodonPlus(DE3)-RIPL. For transient gene expression in tobacco, *Agrobacterium tumefaciens* strains AGL1 or GV3101 were used. GV3101 was also used for stable transformation of *Arabidopsis thaliana* by floral dipping.

2.4. Accession numbers

Sequences and information for the genes and proteins used in this study can be found under the accession numbers given in Table 2.

Table 2: Accession numbers of genes and proteins used in this study

Name	**Organism**	**Identifier**
DJC31	*Arabidopsis thaliana*	AT5G12430
DJC62	*Arabidopsis thaliana*	AT2G41520
TPR2	*Homo sapiens*	NP_003306
DnaJ	*Escherichia coli*	NP_414556
BiP2	*Arabidopsis thaliana*	AT5G42020
HSP70.1	*Arabidopsis thaliana*	AT5G02500
HSP90.2	*Arabidopsis thaliana*	AT5G56030
HOP3	*Arabidopsis thaliana*	AT4G12400
ABI5	*Arabidopsis thaliana*	AT2G36270
RD29a	*Arabidopsis thaliana*	AT5G52310
CaM4	*Arabidopsis thaliana*	AT1G66410
IQD11	*Arabidopsis thaliana*	AT5G13460
ENO2	*Arabidopsis thaliana*	AT2G36530

2.5. Oligonucleotides

Oligonucleotides were purchased from Metabion (Martinsried, Germany), desalted and in standard quality. Sequences and applications can be found in Table 3.

Table 3: Primer sequences used in this study

Name	**Sequence (5'-3')**	**Application**
LBb1.3	ATT TTG CCG ATT TCG GAA C	Genotyping
DJC31Intron_rev	ATT TAA ATG CAT AGA AAT AGC AGA C	Genotyping
DJC31-2-for	GCA GAA TTT GAA TTC TAG CT	Genotyping
DJC31-XhoI-for	ACG TCT CGA GAT GAG CAA GTT CGG CGA ATT G	Genotyping
DJC31Int-BlpI-rev	AGC TGC TCA GCC TAT GCT TCT TGC GCT GCA TTA	Genotyping
DJC62-1-for	CTA ACG GTA CTG TGT AGA AG	Genotyping
DJC62-2-rev	CCA GCT TCC GTT AAC AAC AC	Genotyping
DJC62-XhoI-for	ACG TCT CGA GAT GTC TCC TGC GGC GGT GGA G	Genotyping
DJC62Int-BlpI-rev	GCT GCT CAG CCT AGA CAT CAG GCA TCA TCG AT	Genotyping
35S-Prom-for	CAA TTT ACT ATT CTA GTC g	Sequencing
35S-Term-rev	TGC GGA CTC TAG CAT GGC CG	Sequencing
M13_for	GTA AAA CGA CGG CCA GT	Sequencing
M13_rev	GGA AAC AGC TAT GAC CAT G	Sequencing
T7_Prom	TAA TAC GAC TCA CTA TAG G	Sequencing
T7_Term	GCT AGT TAT TGC TCA GCG G	Sequencing
pDONR207_for	TCG CGT TAA CGC TAG CAT GGA TCT	Sequencing
pDONR207_rev	GTA ACA TCA GAG ATT TTG AGA CAC	Sequencing
GFP_rev	CTC GCC GGA CAC GCT GAA CTT G	Sequencing
GFP_for_pB7WGF2	TGA ACT TCA AGA TCC GCC ACA ACA	Sequencing
pAUL2_for	GAG AGG GGC GCG CCA AGC TA	Sequencing
35S_for_BiFC	GAC GCA CAA TCC CAC TAT CC	Sequencing
NosT_BiFC	CAT CTC ATA AAT AAC GTC ATG CAT TAC	Sequencing
3'DNA-BD_Seq_rev	TTT TCG TTT TAA AAC CTA AGA GTC	Sequencing
Djc31seq_for	TTA ACT GGT GTG CAG TCA CA	Sequencing
Djc31seq_rev	TGT GTA GAC GAG TAA GCG	Sequencing
Djc62seq_for	GAT GTC TGT GAG GTT TGG	Sequencing
Djc62seq_rev	GTG TGT AAC ATT CCT CAG CT	Sequencing

DJC31pDONR207_for	GGG GAC AAG TTT GTA CAA AAA AGC AGG CTT CAT GAG CAA	Gateway Cloning
DJC31pDONR207_rev	GGG GAC CAC TTT GTA CAA GAA AGC TGG GTC CGG GTA TCT	Gateway Cloning
DJC62pONR207_for	GGG GAC AAG TTT GTA CAA AAA AGC AGG CTT CAT GTC TCC	Gateway Cloning
DJC62pDONR207_rev	GGG GAC CAC TTT GTA CAA GAA AGC TGG GTC CCA CCA AGA	Gateway Cloning
DJC31_mut_for	CAA ACA GAT ACC CGT AAG ACC CAG CTT TC	Site directed mutagenesis
DJC31_mut_rev	CGG GTA TCT GTT TGA TCG GTT TGG A	Site directed mutagenesis
62neb_for	TAG GAC CCA GCT TTC TTG TAC AAA G	Site directed mutagenesis
62neb_rev	CCA CCA AGA AGG CGT GTT	Site directed mutagenesis
DJC31-80AA-rev	GGA AAA AGA TCC ACG GAA GTG	TOPO Cloning
DJC31-TOPO-for	CAC CAT GAG GTT CGG CGA ATT G	TOPO Cloning
DJC62-80AA-rev	AAA AGA AGG TTT TTT CAC CTC	TOPO Cloning
DJC62-TOPO-for	CAC CAT GTC TCC TGC GGC GGT GGA G	TOPO Cloning
DJC31Int_rev	GGG GAC CAC TTT GTA CAA GAA AGC TGG GTC TGC TTC TTG CGC TGC ATT AG	Gateway Cloning
DJC62Int_rev	GGG GAC CAC TTT GTA CAA GAA AGC TGG GTC GAC ATC AGG CAT CAT CGA TG	Gateway Cloning
31TPR+J GWfor	GGG GAC AAG TTT GTA CAA AAA AGC AGG CTT CTC TCC GTT AAC TGG TGT GCA G	Gateway Cloning
31TPR+J GWrev	GGG GAC CAC TTT GTA CAA GAA AGC TGG GTC TTA CGG GTA TCT GTT TGA TCG GTT	Gateway Cloning
62TPR+J GWfor	GGG GAC AAG TTT GTA CAA AAA AGC AGG CTT CCA AGC TGT AAA GAA ATA TAG GAG	Gateway Cloning
62TPR+J GWrev	GGG GAC CAC TTT GTA CAA GAA AGC TGG GTC CTA CCA CCA AGA AGG CGT GT	Gateway Cloning
DJC31 AK NheI for	CGA TGC TAG CAT GTC ATC TCA TGT TGA TAA ATT GC	Cloning into pET21a
DJC31 AK XhoI rev	CGA TCT CGA GAG CAT CTG TATA TAG AAA GGG	Cloning into pET21a
DJC62 AK NheI for	CGA TGC TAG CAT GGC TAG TGG GAA CAG TTC TGG	Cloning into pET21a
DJC62 AK XhoI rev	CGA TCT CGA GGA CAT CAG GCA TCA TCG ATG	Cloning into pET21a
GFP-GW_for	GGG GAC AAG TTT GTA CAA AAA AGC AGG CTT CAT GGT GAG CAA GGG CGA GGA	Gateway Cloning
GFP-GW_rev	GGG GAC CAC TTT GTA CAA GAA AGC TGG GTC TTA CTT GTA CAG CTC GTC CAT GCC G	Gateway Cloning
DJC31-HPD-f	TCA AAC ATC AAC CCG ACA AGG	Site directed mutagenesis

DJC31-HPD-r	GTG CGG CCT TCC TAT ATG	Site directed mutagenesis
62HPDlong_f	TTA GAC ATC AAC CAG ACA AAG CTG CAC A	Site directed mutagenesis
62HPDlong_r	GAG CTG CTT TGC GGT ATG CCT TTT TG	Site directed mutagenesis
Y2H_DJC31_for	GGC CGA ATT CCC GGG GAT GAG CAA GTT CGG CGA ATT GAA T	Cloning into pGBKT7
Y2H_DJC31_rev	GCC GCT GCA GGT CGA CTT ACG GGT ATC TGT TTG ATC GGT T	Cloning into pGBKT7
Y2H_DJC62_for	GGC CGA ATT CCC GGG GAT GTC TCC TGC GGC GGT GGA GAT T	Cloning into pGBKT7
Y2H_DJC62_rev	GCC GCT GCA GGT CGA CCT ACC ACC AAG AAG GCG TGT TTT G	Cloning into pGBKT7
5’ AD Screening	CTA TTC GAT GAT GAA GAT ACC CCA CCA AAC CC	Y2H Library Screening
3’ AD Screening	GTG AAC TTG CGG GGT TTT TCA GTA TCT ACG ATT	Y2H Library Screening
CaM4_for	GGG GAC AAG TTT GTA CAA AAA AGC AGG CTT CAT GGC GGA TCA GCT AAC TGA TG	Gateway Cloning
CaM4_rev	GGG GAC CAC TTT GTA CAA GAA AGC TGG GTC TCA CTT AGC CAT CAT AAT CTT GAC A	Gateway Cloning
IQD11_for	GGG GAC AAG TTT GTA CAA AAA AGC AGG CTT CAT GGC TAA GAA GAA GGG CTT G	Gateway Cloning
IQD11_rev	GGG GAC CAC TTT GTA CAA GAA AGC TGG GTC TCA TCT CAA GCT GCT CTG CTT G	Gateway Cloning
ENO2_for	GGG GAC AAG TTT GTA CAA AAA AGC AGG CTT CAT GGC TAC TAT CAC CGT TGT TAA G	Gateway Cloning
ENO2_rev	GGG GAC CAC TTT GTA CAA GAA AGC TGG GTC TTA GTA GGG TTC CAC AGG TTT GC	Gateway Cloning
qDJC31_for	GCA TAT AGG AAG GCC GCA CT	qPCR
qDJC31_rev	GAG AAC GCT TTG CAG GGT CT	qPCR
qDJC62_for	AAC TAA AGC AGG CCC GTC AA	qPCR
qDJC62_rev	GTG CAG CTT TGT CTG GGT GA	qPCR
qBiP1/2_for	GGT GAC ACT CAC TTG GGA GGT GA	qPCR (Schott et al., 2010)
qBiP1/2_rev	CTC ACA TTC CCT TCG GAG CTT A	qPCR (Schott et al., 2010)
HOP3 qPCR for	TGA GGG CAT ATA GCA ACA GAG	qPCR (Fernández-Bautista et al., 2018)
HOP3 qPCR rev	CAC GGC TCG CTT TGT TTA TCT	qPCR (Fernández-Bautista et al., 2018)
qOEP24_for	CTT TTA CTA CTA ATT GGA CTC ACT AAT A	qPCR
qOEP24_rev	GGG ACT TTG CGA TTT CT	qPCR

qABI5-for	GAC AGA GGA GGA TGA TCA AGA AC	qPCR (Park & Kim, 2014)
qABI5-rev	CAT CTT CCT ATT GTT TGT TTA GAG TG	qPCR (Park & Kim, 2014)
qRD29a-for	CTT GGC TCC ACT GTT GTT CC	qPCR (Clément et al., 2011)
qRD29a-rev	CAT CAA AGA CGT CAA ACA AAA CA	qPCR (Clément et al., 2011)

2.6. Vectors and DNA-constructs

Vectors and DNA-constructs used in this work are given in Table 4.

Table 4: Constructs used in this study

Name	**Application**	**Source**
DJC31 pDONR207	Entry vector for Gateway cloning	This work
DJC62 pDONR207	Entry vector for Gateway cloning	This work
DJC31+S pDONR207	Entry vector for Gateway cloning	This work
DJC62+S pDONR207	Entry vector for Gateway cloning	This work
DJC62TP pENTR/dTOPO	First 80 amino acids of DJC62, Entry vector for Gateway cloning	This work
DJC31TP pENTR/dTOPO	First 80 amino acids of DJC31, Entry vector for Gateway cloning	This work
DJC31Int pDONR207	DJC31 N-terminus, Entry vector for Gateway cloning	This work
DJC62Int pDONR207	DJC62 N-terminus; Entry vector for Gateway cloning	This work
31TPR+J+S pDONR207	TPR domains and J-domain of DJC31 with stop codon; Entry vector for Gateway cloning	This work
62TPR+J+S pDONR207	TPR domains and J-domain of DJC62 with stop codon; Entry vector for Gateway cloning	This work
DJC31AK pET21a	Antigen for antibody production	This work
DJC62AK pET21a	Antigen for antibody production	This work
DJC31TP pK7FWG2	First 80 amino acids of DJC31 fused to GFP (C-term)	This work
DJC62TP pK7FWG2	First 80 amino acids of DJC62 fused to GFP (C-term)	This work
DJC31+S pK7WGF2	DJC31 with N-terminal GFP	This work
DJC62+S pK7WGF2	DJC62 with N-terminal GFP	This work
DJC31+S pB7WGF2	DJC31 with N-terminal GFP; BASTA	This work
DJC62+S pB7WGF2	DJC62 with N-terminal GFP; BASTA	This work
DJC31Int pK7FWG2	DJC31 N-terminus fused to GFP	This work
DJC62Int pK7FWG2	DJC62 N-terminus fused to GFP	This work
31TPR+J+S pB7WGF2	TPR domains and J-domain of DJC31 with N-terminal GFP	This work

62TPR+J+S pB7WGF2	TPR domains and J-domain of DJC362 with N-terminal GFP	This work
ER marker		(Nelson et al., 2007)
Golgi marker		(Nelson et al., 2007)
DJC31+S pB7FWG2	Complementation construct	This work
DJC62+S pB7FWG2	Complementation construct	This work
DJC31Int pGW-GFP11	DJC31 split GFP construct	This work
DJC62Int pGW-GFP11	DJC62 split GFP construct	This work
HSP70.1 pDONR207	HSP70.1 without ATG; Entry vector for Gateway cloning	Regina Schweiger
HSP90.2 oATG pDONR207	HSP90.2 without ATG; Entry vector for Gateway cloning	Regina Schweiger
BiP2 pDONR207	Entry vector for Gateway cloning	Regina Schweiger
BiP2 pGW-GFP11	BiP2 split GFP construct	This work
HSP70.1 pGFP11-GW	HSP70.1 split GFP construct	This work
GFP1-10	Split GFP, cytosolic	(Xie et al., 2017)
SP-GFP1-10-HDEL	Split GFP, ER luminal	(Xie et al., 2017)
GFP pDONR207	Entry vector for Gateway cloning	This work
GFP pAUL2	GFP only; Localization control	This work
DJC31+S pDest-SCYCE(R) GW	The C-terminal part of sCFP N-terminally fused to DJC31; BiFC	This work
DJC62+S pDest-SCYCE(R) GW	The C-terminal part of sCFP N-terminally fused to DJC62; BiFC	This work
HSP70.1 pDest-VYNE(R) GW	The N-terminal part of Venus N-terminally fused to HSP70.1; BiFC	This work
HSP90.2 pDest-VYNE(R) GW	The N-terminal part of Venus N-terminally fused to HSP90.2; BiFC	This work
BiP2 pDest-VYNE(R) GW	The N-terminal part of Venus N-terminally fused to BiP2; BiFC	This work
DJC31+S H/Q pDONR207	DJC31 H1052Q; Entry vector for Gateway cloning	This work
DJC62+S H/Q pDONR207	DJC62 H1006Q; Entry vector for Gateway cloning	This work
DJC31+S H/Q pB7FWG2	DJC31 H1052Q complementation construct	This work
DJC62+S H/Q pB7FWG2	DJC62 H1006Q complementation construct	This work
DJC31 pCR-Blunt	DJC31 for restriction/ligation-based cloning	This work
DJC62 pCR-Blunt	DJC62 for restriction/ligation-based cloning	This work
DJC31 pGBKT7	DJC31 Y2H bait construct	This work
DJC62 pGBKT7	DJC62 Y2H bait construct	This work
ENO2 pDONR207	Entry vector for Gateway cloning	This work

CAM4 pDONR207	Entry vector for Gateway cloning	This work
IQD11 pDONR207	Entry vector for Gateway cloning	This work
ENO2 pDest-VYNE(R) GW	The N-terminal part of Venus was N-terminally fused to ENO2; BiFC	This work
CAM4 pDest-VYNE(R) GW	The N-terminal part of Venus was N-terminally fused to CAM4; BiFC	This work
IQD11 pDest-VYNE(R) GW	The N-terminal part of Venus was N-terminally fused to IQD11; BiFC	This work

2.7. Antibodies

Primary antisera against DJC31 and DJC62 were generated for this study by Eurogentec (Seraing, Belgium). Fragments of the DJC31 and DJC62 N-terminus were used as antigens. Antigen expression and purification conditions can be found in sections 3.4.1 and 3.4.2. The DJC31 antiserum was used in a 1:500 dilution, the DJC62 antiserum was purified, as described in 3.4.3 and the purified antibody was used in a 1:500 dilution. Other antibodies used in this study can be found in Table 5.

Table 5: Antibodies used in this study

Name	**Dilution**	**Source**
Anti-DJC31	1:500	AG Soll, LMU
Anti-DJC62	1:500	AG Soll, LMU
Anti-BiP	1:2000	Agrisera (Vännäs, Schweden)
Anti-FNR	1:1000	AG Soll, LMU
Anti-c-myc	1:1000	Santa Cruz Biotechnology (Dallas, USA)

2.8. Media

The following media were used after autoclaving for cultivation of bacteria, yeast and plants

Table 6: Composition of media used for cultivation of bacteria, yeast and plants.

YPDA (without Adenine sulfate = YPD)	10 g/L Bacto yeast extract 20 g/L Bacto peptone 20 g/L Glucose Monohydrate 40 mg/L Adenine sulfate (20 g/L Bacto agar for plates)
10x Dropout Mix	20 g L-Alanine 20 g L-Arginine 20 g L-Asparagine 20 g L-Aspartic Acid 20 g L-Cysteine 20 g L-Glutamine 20 g L-Glutamic acid 20 g Glycine 20 g Myo-inositol 20 g L-Isoleucine 20 g L-Lysine 20 g L-Methionine 2 g Para-Aminobenzoic acid 20 g L-Phenylalanine 20 g L-Proline 20 g L-Serine 20 g L-Threonine 20 g L-Tyrosine 20 g L-Valine 36,2 g of the basic mix are supplemented with the following amino acids, depending on the resistance gene used: 0.5 g Alanine 2 g L-Histidine 4 g L-Leucine 2 g Uracil 2 g L-Tryptophan
SD medium	6.7 g/L Yeats nitrogen base w/o amino acids 2 g/L Dropout Mix 20 g/L Glucose monohydrate (20 g/L Bacto agar for plates)
½ MS medium	0.05% MES 0.237% MS salts adjusted to pH 5.8 with KOH For plates the medium was supplemented with either 0.6% Gelrite or 0.8% agar
LB medium	10 g/L Tryptone 5 g/L Yeast extract 10 g/L NaCl (15 g/L Agar for plates)

2.9. Bioinformatic tools and software

2.9.1. Online tools

DNA and protein sequences were obtained from "The Arabidopsis Information Ressource" (TAIR, www.arabidopsis.org, (Lamesch et al., 2012)) or aramemnon ((Schwacke et al., 2003), http://aramemnon.uni-koeln.de). Primers for qPCR were generated using NCBI Primer BLAST (https://www.ncbi.nlm.nih.gov/tools/primer-blast). Primers for site-directed mutagenesis were designed using NEBaseChanger (http://nebasechanger.neb.com). Annealing temperatures for PCR were calculated with the NEB Tm Calculator (http://tmcalculator.neb.com). Identification of genes found in the yeast two-hybrid screening was performed using NCBI BLAST ((Altschul et al., 1997), https://blast.ncbi.nlm.nih.gov). Prediction of potential signal peptides was performed using TargetP1.1 and 2.0 (Almagro Armenteros et al., 2019; Emanuelsson et al., 2000). The domain composition was determined by using the NCBI Conserved Domain search tool (Lu et al., 2020). The PHYRE2 web portal was used for structure prediction (Kelley et al., 2015). Prediction of disorder was performed using IUPred2A (Mészáros et al., 2018). For visualization of publicly available gene expression data, the AtGenExpress eFP viewer was used (Waese et al., 2017). Functional annotation was performed using the Database for Annotation, Visualization an Integrated Discovery Version 6.8 (DAVID 6.8, (Huang da et al., 2009)). For KEGG pathway analysis g:Profiler was used (Raudvere et al., 2019).

2.9.2. Software

For generation of sequence alignments, the sequence alignment editor BioEdit (Hall, 1999) was used. Multiple sequence alignments, using default settings, and analysis of protein hydrophobicity using the Kyte-Doolitle scale with a window size of 21, were performed using CLC Main Workbench Version 7.7 (Qiagen Digital Insights). Structural models were generated with UCSF Chimera (Pettersen et al., 2004). Image analysis of western blots and root length measurements were performed using ImageJ (National Institutes of Health, Bethesda, USA).

3. Methods

3.1. Plant physiological methods

3.1.1. Growth conditions

Arabidopsis seeds were either put out on soil (Stender substrate A210, Stender AG, Schermbeck, Germany) or on sterile solid ½ MS medium. For selection of transformed plants, 0.8% agar containing ½ MS medium was supplemented with either 25 µg/ml hygromycin or 50 µg/ml glufosinate-ammonium (BASTA). For chemical stress treatment, ½ MS medium with 0.8% agar was supplemented with the respective stress inducing agent. To the non-stressed control plates, the respective solvent was added.

Before sowing on sterile media, seeds were surface sterilized with 0.05% Triton X-100 in 70% ethanol for 10 min on a rotor, followed by several washing steps with ethanol. Seeds on either soil or sterile plates were kept in the dark at 4°C for one to three days, to synchronize germination. All *Arabidopsis* plants were grown under long day conditions (Day: 16 h 100 µmol photons m^{-2} s^{-1}, 21°C; Night: 8 h dark, 16°C) in climate chambers or the greenhouse.

Nicotiana benthamiana was grown under long day conditions (Day: 16 h 100 µmol photons m^{-2} s^{-1}, 21°C; Night: 8 h dark, 16°C) in the greenhouse.

3.1.2. Stable transformation of *Arabidopsis thaliana* by floral dipping

Stably transformed *Arabidopsis* plants were generated using the floral dip method. *Agrobacterium tumefaciens* strain GV3101, carrying the desired vector construct, was cultivated under the conditions described in 3.3.1. Cells were harvested by centrifugation at 3500 g, 4°C, 20 min. The pellet was resuspended in Silwet medium (5% sucrose, 0.05% Silwet L-77) and adjusted to a final OD_{600} of 0.8. Flowering plants were dipped into the agrobacteria suspension for several seconds. After seven days, the dipping was repeated. After seed harvesting, seeds were either grown on soil for selection by ammonium glufosinate (BASTA) spraying or grown on sterile ½ MS plates supplemented with the respective selection antibiotic, as described in 3.1.1. After selection on plates, seedlings were transferred to soil.

3.1.3. Transient gene expression in *Nicotiana benthamiana*

For transient transformation of *Nicotiana benthamiana*, *Agrobacterium* strain AGL1 or GV3101, carrying the respective construct of interest, were cultivated under the conditions described in 3.3.1. The cells were harvested by centrifugation at 3225 g, 4°C, 15 min. The pellet was resuspended in infiltration medium (10 mM MES pH 5.7, 1 mM $MgCl_2$, 150 µM acetosyringone) and adjusted to a final OD_{600} of 1. The agrobacteria suspension was incubated at room temperature, covered, on a tube roller

for two hours. The tobacco leaves were infiltrated with the bacterial suspension at the abaxial side, using a 1 ml syringe. Subsequently, the infiltrated tobacco plants were covered and used for the respective experiment after two to three days. In case of co-infiltration of different constructs, the respective agrobacteria suspensions were mixed 1:1 prior to infiltration.

3.1.4. *In vitro* pollen germination assay

Pollen germination was examined according to a modified method from Boavida and McCormick and Johnson-Brousseau and McCormack (Boavida & McCormick, 2007; Johnson-Brousseau & McCormick, 2004). Open flowers from Col-0 and *djc31 djc62* were dipped onto solid germination medium (0.01% boric acid, 5 mM $CaCl_2$, 5 mM KCl, 1 mM $MgSO_4$, 10% sucrose pH 7.5, 1% agarose) on a microscope slide. The slides were placed in a germination box, made of an empty tip box, filled with water and a moistened tissue placed on the grid. The prepared glass slides were placed on the moistened tissue, the box was closed and incubated for 6 hours at room temperature.

3.1.5. Phenotypic analysis regarding growth and development

To compare growth and development between wild type, single and double mutants, the approach suggested by Boyes et al. was used with modifications (Boyes et al., 2001). Plate based phenotyping was performed on horizontal ½ MS plates under standard climate chamber conditions, considering the following developmental stages: Seed Imbibition, radicle emergence, hypocotyl and cotyledon emergence, cotyledons fully opened, two rosette leaves >1 mm, four rosette leaves >1 mm.

For phenotyping on soil, single seeds were placed in individual pots and grown under standard climate chamber conditions. When first flowers appeared, the experiment was continued in the greenhouse. The following growth stages were used for observation: Four rosette leaves >1 mm, six rosette leaves, ten rosette leaves >1 mm, first flower buds visible, first flower open, flowering complete.

3.2. Molecular biological methods

3.2.1. Isolation of DNA and RNA

3.2.1.1. Isolation of plasmid DNA

For small scale isolation of plasmid DNA (Mini-Prep) from *E.coli,* the NucleoSpin Plasmid EasyPure Kit (Macherey and Nagel, Düren, Germany) was used. Larger scale plasmid isolation (Midi-Prep) was performed using the NucleoBond PC 100 Kit (Macherey and Nagel, Düren, Germany). Both kits were used according to the instructions of the manufacturer.

3.2.1.2. Isolation of RNA

For isolation of RNA, plant material was either ground in liquid nitrogen or homogenized using an electronic pestle. Isolation of RNA was performed with the RNeasy Plant Mini Kit according to the manufacturer's instructions, including the recommended DNA digestion step using DNAseI (Roche, Mannheim, Germany)

3.2.1.3. cDNA Synthesis

For synthesis of cDNA for RT-PCR, 1 µg RNA was reverse transcribed using the M-MLV reverse transcriptase (Promega, Mannheim, Germany). For qPCR, cDNA was synthesized by reverse transcription of 1 µg RNA, using the iScript™ cDNA Synthesis Kit (Bio-Rad, Feldkirchen, Germany). For both enzymes, the recommendations of the manufacturer were followed.

3.2.1.4. Isolation of gDNA from Arabidopsis

Leaf material was homogenized in 500 µl High Purity Extraction Buffer (0.1 M Tris-HCl pH 7.5, 0.05 M NaCl, 0.05 M EDTA pH 8, 1% (w/v) PVP 40) using either an electronic pestle or a TissueLyser (Retsch/Qiagen) at maximum speed for 3 min. After homogenization, 66 µl 10% (w/v) SDS and 166 µl Potassium Acetate Buffer (5 M potassium acetate, 11.5% (v/v) acetic acid, pH 5.8) were added. After centrifugation at 16000 g for 15 min, the supernatant was transferred into new tubes and mixed with 500 µl isopropanol. After incubation at -20°C for at least 15 min, the samples were centrifuged at 16000 g for 15 min. The supernatant was discarded and the pellet washed with 500 µl 70% (v/v) ethanol by centrifugation at 16000 g for 5 min. The supernatant was discarded and the pellet dried at 50°C. The gDNA was reconstituted in 50 µl ddH_2O.

3.2.2. Polymerase chain reaction (PCR)

For cloning, site-directed mutagenesis and RT-PCR, the respective fragment was amplified using the Phusion polymerase with HF-Buffer (NEB, Frankfurt am Main, Germany). Genotyping and colony PCR were performed using the Taq polymerase (Bioron, Ludwigshafen, Germany). Annealing temperatures were adapted for each primer pair and the elongation time was chosen according to the length of the desired PCR product. Subsequently, PCR products were mixed with DNA loading dye (33% glycerol, 2.5 mg/ml bromphenol blue) and loaded onto an 1% agarose gel in TAE Buffer (40 mM Tris, 2.5 mM EDTA, 1% acetic acid) containing ethidium bromide.

3.2.3. Quantitative polymerase chain reaction (qPCR)

For qPCR, seven days old seedlings, grown on vertical ½ MS plates with 6% Gelrite, were transferred into liquid ½ MS medium and cultivated under standard growth chamber conditions for 24 hours. On the next day, the medium was removed and replaced by fresh ½ MS medium with or without a stress agent. After incubation under standard growth chamber conditions for an appropriate time period, RNA was extracted and cDNA was synthesized as given in 3.2.1.

For qPCR, the cDNA was diluted 1:10 and 2 µl were added to a master mix as described in the manual of the FastStart Essential DNA Green Master kit (Roche Diagnostics GmbH, Mannheim, Germany). The following Lightcycler program was used:

- Pre-incubation 1x 95°C, 600 s
- 3-Step Amplification 45x 95°C, 10 s; 60°C, 10 s; 72°C, 10 s
- Melting 1x 95°C, 10 s; 65°C, 60 s; 97°C, 1 s
- Cooling Hold

As reaction control, the qPCR product was loaded onto a 2% agarose gel containing ethidium bromide. For qPCR three biological replicates with each three technical replicates were used. The resulting data were analyzed using the ΔΔCt method.

3.2.4. Cloning

Different cloning strategies were performed, depending on the experiment and design of the respective vectors. All cloning products were transformed in *E.coli* as described in 3.3.3, screened by colony PCR and sequenced prior to use.

3.2.4.1. Restriction digestion and ligation

For cloning via restriction digest and ligation, the gene of interest was amplified via PCR, with primers harboring the desired restriction sites, using the Phusion polymerase. The PCR product was loaded onto an agarose gel with ethidium bromide. Subsequently, the bands were excised and extracted from the gel using the NucleoSpin Gel and PCR Clean-up Kit (Macherey-Nagel, Düren, Deutschland). 1 µg of plasmid DNA or purified PCR product was digested with the respective restriction enzymes, according to the manufacturer's recommendations. The restriction digest product was separated by agarose gel electrophoresis and the respective DNA bands were excised and extracted. For ligation with the T4 ligase, insert and vector were mixed in a molar ratio of 3:1 (insert : vector) and the reaction was set up according to the manufacturer's instructions. The ligation product was transformed into *E.coli.*

Some PCR products were ligated into the pCR®-Blunt Vector prior to restriction digest, using the Zero Blunt® PCR Cloning Kit, following the instructions of the manual (Invitrogen, Darmstadt, Germany).

3.2.4.2. Gateway cloning

For cloning with the GATEWAY system (Invitrogen, Darmstadt, Germany), PCR products carrying attB sites were generated using the Phusion polymerase (NEB, Frankfurt am Main, Germany). The PCR product was loaded onto an agarose gel. Afterwards, the bands were excised and purified using the NucleoSpin Gel and PCR Clean-up kit (Macherey-Nagel, Düren, Deutschland). The following BP reaction and subcloning into GATEWAY destination vectors by LR reaction were performed according to the manufacturer's instructions. The reaction product was transformed in *E.coli*.

3.2.4.3. TOPO cloning

As an alternative to generation of GATEWAY entry vectors by BP reaction, TOPO® cloning was used with the pENTR/D-TOPO Cloning kit (Invitrogen, Darmstadt, Germany). PCR products, with a 5' CACC overhang, were generated using the Phusion polymerase (NEB, Frankfurt am Main, Germany) and were excised and extracted after agarose gel electrophoresis. The TOPO® reaction was set up as described by the manufacturer. The resulting product was transformed in *E.coli*.

3.2.5. Site-directed mutagenesis

For exchange of amino acids, the Q5 Site-Directed Mutagenesis Kit (NEB, Frankfurt am Main, Germany) was used. For amplification of the respective construct, either the Q5 Master Mix provided by the kit, or the Phusion polymerase (NEB, Frankfurt am Main, Germany) was used. The following steps were performed as recommended by the manufacturer and the mutagenesis product was transformed into *E.coli* as described in 3.3.3.

3.2.6. Sequencing

Sequencing of plasmids and DNA fragments was performed by the Sequencing Service of the Genomics Service Unit (Ludwig-Maximilians University, Munich, Germany). For plasmids, 200-300 ng DNA was used. For sequencing of DNA fragments of 200-1000 bp in length, 50 ng DNA was used. The DNA was mixed with appropriate primers in a total volume of 7 µl in 10 mM Tris-HCl pH 8.5.

3.2.7. RNA sequencing (RNAseq) and data analysis

RNAseq was performed in cooperation with PD Dr. Tatjana Kleine (Ludwig-Maximilians University Munich).

Plants grown on soil at the four-leaves stage were ground in liquid nitrogen. Total RNA from plants was isolated using Trizol (Invitrogen, Carlsbad, USA) and purified using Direct-zol™ RNA MiniPrep Plus columns (Zymo Research, Irvine, USA) according to the manufacturer's instructions. RNA integrity and quality were assessed with an Agilent 2100 Bioanalyzer (Agilent, Santa Clara, USA). Messenger RNA enrichment, generation of mRNA-Seq libraries and 150-bp paired-end sequencing on an Illumina HiSeq 2500 system (Illumina, San Diego, USA) were conducted at Novogene Biotech (Beijing, China) with standard Illumina protocols. Three independent biological replicates were used per genotype.

RNA-Seq reads were analyzed on the Galaxy platform (Afgan et al., 2016) essentially as described (Xu et al., 2019) with one exception: reads were mapped to the Arabidopsis TAIR10 genome with the gapped-read mapper RNA STAR (Dobin et al., 2013) using standard settings.

3.3. Microbiological methods

3.3.1. Growth conditions

E.coli and *A.tumefaciens* were cultivated in LB medium on a shaker or on LB-agar plates, supplemented with antibiotics, as required. *E.coli* was cultivated at 37°C, *A.tumefaciens* at 28°C.

S.cerevisiae was grown in YPDA or on YPDA plates at 30°C. For plasmid selection, SD-medium without the respective amino acids, used as selection markers, was used in liquid culture or SD-agar plates at 30°C.

3.3.2. Generation of competent cells

3.3.2.1. Generation of competent E.coli

E.coli was grown in 5 ml LB medium (with antibiotics, if required) at 37°C over night on a shaker. The pre-culture was transferred into fresh 100 ml LB medium (with antibiotics, if required) and incubated at 37°C on a shaker until an OD_{600} of 0.4-0.6 was reached. Bacteria were harvested by centrifugation at 3000 g, 5 min, 4°C. Subsequently, the pellet was resuspended in Buffer 1 (30 mM KAc., 50 mM, $MnCl_2$*2 H_20, 100 mM KCl, 10 mM $CaCl_2$*2 H_20, 15% glycerol; sterile). After 5 min incubation on ice, the cells were again centrifuged at 3000 g, 5min, 4°C. The pellet was resuspended in 4 ml Buffer 2 (10 mM MOPS, 10 mM KCl, 73 mM $CaCl_2$*2 H_2O, 15% glycerol; sterile). Cells were aliquoted, frozen in liquid nitrogen and stored at -80°C.

3.3.2.2. Generation of competent Agrobacteria

Agrobacteria were grown in 20 ml LB medium with the respective antibiotics at 28°C for two days. 10 ml of the pre-culture were transferred into 500 ml LB medium with appropriate antibiotics and grown at 28°C for four hours. Cells were pelleted at 3000 g for 15 min. The pellet was resuspended in 10 ml sterile 10 mM $CaCl_2$. Cells were aliquoted, frozen in liquid nitrogen and stored at -80°C.

3.3.2.3. Generation of competent yeast cells

Cells were grown in 50 ml YPD at 30°C until an OD_{600} of 0.5-0.6 was reached. After centrifugation at 700 g, 5min, 4°C, the pellet was resuspended in 50 ml sterile ddH_2O and again centrifuged at 700 g, 5min, 4°C. The cells were resuspended in 12.5 ml LiSorb (100 mM lithium acetate, 10 mM Tris pH 8, 1 mM EDTA pH 8, 1 M sorbitol; sterile). After centrifugation at 700 g, 5 min, 4°C, the supernatant was discarded and the pellet resuspended in 300 µl LiSorb. Carrier-DNA (2 mg/ml) was denatured by heat treatment and syringe shearing. 42 µl denatured carrier-DNA were added to the yeast suspension. Cells were aliquoted, frozen in liquid nitrogen and stored at -80°C.

3.3.3. Transformation of competent cells

3.3.3.1. Transformation of E.coli

1 µl plasmid DNA was added to 50 µl competent *E.coli* and mixed by tapping. After 30 min incubation on ice, the cells were heat shocked at 42°C for 90 s. After addition of 450 µl LB medium, the cells were incubated at 37°C for one hour in a thermomixer. Cells were plated on LB-agar plates, containing appropriate antibiotics for selection.

In case of transformation after cloning, the whole cloning product was added to competent *E.coli* and prior to plating, the cells were centrifuged for 2 min at 1500 g and resuspended in 200 µl LB medium.

The plates were incubated at 37°C over night.

3.3.3.2. Transformation of Agrobacteria

5 µl plasmid DNA were added to 100 µl competent *A.tumefaciens*. After 5 min incubation on ice, the cells were frozen in liquid nitrogen for 5min. Subsequently, heat shock was performed at 37°C for 5 min. After addition of 800 µl LB medium, the bacteria were incubated at 28°C for 2-4 hours. Cells were harvested by centrifugation for 2 min at 1500 g, resuspended in 200 µl LB medium and spread on LB-agar plates containing appropriate antibiotics. The plates were incubated at 28°C for 2-3 days.

3.3.3.3. Transformation of yeast

5 µl plasmid DNA were added to 50 µl competent yeast cells and mixed by tapping. 300 µl LiPEG (100 mM lithium acetate, 10 mM Tris pH 8, 1 mM EDTA pH 8, 40% PEG3500; sterile) was added and mixed by vortexing. The cells were incubated for 20 min at room temperature. After addition of 35 µl DMSO, heat shock was performed at 42°C for 15 min. Cells were centrifuged at 700 g for 1.5 min. The supernatant was discarded and the pellet resuspended in 150 µl sterile 0.9% NaCl. Cells were spread on SD medium plates without the amino acid used for selection. The plates were incubated at 30°C.

3.3.4. Long term storage

E.coli and *A.tumefaciens* were grown over night in 5 ml LB medium with appropriate antibiotics under standard conditions described above. 300 µl sterile glycerol were added to 700 µl of the over night culture and mixed by vortexing. The cells were frozen in liquid nitrogen and stored at -80°C.

3.3.5. Yeast Two-Hybrid library screening

3.3.5.1. Test experiments for bait expression, autoactivation and toxicity

For testing toxicity of the bait construct, 100 ng DJC31+S pGBKT7, DJC62+S pGBKT7 or empty pGBKT7 were transformed into competent Y2HGold cells. The cells were plated in a 1:10 and 1:100 dilution on SD-Trp plates and incubated at 30°C for three days.

For testing autoactivation of the reporter genes by the bait construct, 100 ng DJC31+S pGBKT7 and DJC62+S pGBKT7 were transformed into competent Y2HGold cells and plated in a 1:10 and 1:100 dilution on SD-Trp plates containing 40 µg/ml X-α-Gal (Clontech, Mountain View, USA) and SD-Trp plates with 40 µg/ml X-α-Gal and 200 ng/ml Aureobasidin A (Clontech, Mountain View, USA). The plates were incubated at 30°C and evaluated after three days.

For testing expression of the bait proteins, DJC31+S pGBKT7, DJC62+S pGBKT7 and empty pGBKT7 were inoculated in 5 ml SD-Trp medium and incubated over night at 30°C on a shaker. On the next day, the over night culture was used to inoculate 50 ml SD-Trp medium with an OD_{600} of 0.150. The cultures were incubated at 30°C until they reached an OD_{600} of 0.4 – 0.6. The cells were harvested by centrifugation at 1000 g for 5 min at 4°C. The pellets were resuspended in cold ddH_2O and centrifuged again at 1000 g, 5 min, 4°C. 1 ml cracking buffer (8 M Urea, 5% SDS, 40 mM Tris/HCl pH 6.8, 0.1 mM EDTA, 0.4 mg/ml bromphenol blue) was mixed with 10 µl β-mercaptoethanol, 70 µl 10x protease inhibitor (cOmplete EDTA-free Protease Inhibitor; Roche, Mannheim, Germany) and 50 µl 100 mM PMSF and heated to 60°C. 100 µl warm cracking buffer with supplements was added per 7.5 OD_{600} units. Additionally, 3 µl 100 mM PMSF were added from time to time during protein extraction. The cracking buffer – cell suspension was transferred into a 1.5 ml reaction tube with glass beads and heated to 70°C for 10 min. Cells were vortexed for 1 min and subsequently centrifuged at 18400 g for 5 min at 4°C. The supernatants were transferred into new tubes and placed on ice. The pellets were heated to 95°C for 5 min and vortexed for 1 min. After centrifugation at 18400 g for 5 min at 4°C, the supernatants were combined with the supernatants from the previous step. The samples were mixed with 5x SDS loading buffer and loaded onto a 10% SDS gel. After gelelectrophoresis, the proteins were transferred onto a PVDF membrane via a wet blot system and probed with an anti-c-myc antibody.

3.3.5.2. Library mating

DJC31+S pGBKT7 or DJC62+S pGBKT7 was transformed into competent Y2HGold cells, as described above, and plated onto SD-Trp plates (=bait strain). 50 ml SD-Trp were inoculated with a colony of the bait strain and incubated at 30°C until an OD_{600} of 0.8 was reached. The cells were centrifuged at 1000 g for 5 min, resuspended in SD-Trp medium and adjusted to a cell density of $>1x10^8$ cells/ml. 5 ml of the bait strain were combined with 1 ml library strain (Mate & Plate library – Universal Arabidopsis, normalized; Takara Bio USA) in 45 ml 2x YPDA medium with 50 µg/ml kanamycin in a 2 L flask. The cells were incubated at 30°C under slow shaking. After 20-24 hours, the culture was checked for the presence of zygotes under the microscope. The cells were centrifuged at 1000 g for 10 min. The 2 L flask was rinsed with 50 ml 0.5x YPDA with 50 µg/ml kanamycin and the rinsing fluid was used to resuspend the pellet. The cells were centrifuged again at 1000 g for 10 min and the pellet resuspended in 10 ml 0.5x YPDA with 50 µg/ml kanamycin. The mating culture was plated on SD-Leu-Trp plates containing 200 ng/ml Aureobasidin A and 40 µg/ml X-α-Gal. As a control, 100 µl of 1:10, 1:100, 1:1000

and 1:10000 dilutions were spread on SD-Trp, SD-Leu and SD-Trp-Leu plates, to check viability of the bait strain, the library strain and the diploids. All plates were incubated at 30°C for 3-5 days.

All blue colonies from the mating plates were streaked out on SD-Leu-Trp-Ade-His plates containing 200 ng/ml Aureobasidin A and 40 µg/ml X-α-Gal. The plates were incubated at 30°C for three days.

3.3.5.2. Screening

After the library mating, blue colonies from the SD-Leu-Trp-Ade-His plates with Aureobasidin A and X-α-Gal were tested via colony PCR to identify the prey peptide. For this, single colonies were transferred into 15 µl ddH_2O and 15 µl PCR master mix were added. The fragment was amplified using the Taq polymerase with the respective screening primers. 3 µl of the PCR product were mixed with 2.5 µl loading dye and loaded onto an 1% agarose gel with ethidium bromide. The residual PCR product was purified using the NucleoSpin Gel and PCR Clean-up kit (Macherey-Nagel, Düren, Germany) with the following modifications: 100 µl NTI were mixed with the PCR product and loaded onto the column. After centrifugation at 11000 g for 30 s, 680 µl NT3 were added and the columns centrifuged at 11000 g for 2:30 min. The columns were transferred to 1.5 ml reaction tubes and 20 µl NE was pipetted onto the membrane. After 5 min incubation at room temperature the PCR product was eluted via centrifugation at 11000 g for 1.5 min. 50 ng purified PCR product were used for sequencing and the sequences were identified using NCBI BLAST.

3.4. Biochemical methods

3.4.1. Protein expression in *E.coli*

A pre-culture of 10 ml LB, containing appropriate antibiotics, was set up with *E.coli* harboring the plasmid encoding the gene of interest and was incubated at 37°C over night on a shaker. This pre-culture was used on the following day to inoculate 1 L LB, containing antibiotics, with an OD_{600} of 0.0125. The cells were grown at 37°C until an OD_{600} of 0.6 – 0.8 was reached. Protein expression was induced by addition of 1 mM IPTG and carried out at 18°C over night. On the next day, cells were harvested by centrifugation at 3500 g, 20 min, 4°C. The pellets were either frozen in liquid nitrogen and stored at -80°C or used immediately for protein purification.

3.4.2. Protein purification

For purification of His-tagged protein, the pellet was resuspended in 30 ml lysis buffer (20 mM Tris/HCl pH 7.5, 200 mM NaCl, 20 mM imidazole) and the cells were disrupted by passing the suspension two times through a microfluidizer (Microfluidics, Westwood, USA). After centrifugation at 20000 g for 30 min at 4°C, the supernatant was transferred into a 50 ml reaction tube and mixed with 300 µl Ni-NTA agarose beads (Macherey-Nagel, Düren, Germany). After incubation at 4°C on a roller over night, the

suspension was transferred onto a gravity flow column (Econo-Pac; Bio-Rad, Munich, Germany). The beads were washed three times with 5 ml wash buffer (20 mM Tris/HCL pH 7.5, 200 mM NaCl, 40 mM Imidazole). For elution 300 µl elution buffer (20 mM Tris/HCl pH 7.5, 200 mM NaCl, 200 mM imidazole) were added onto the beads and incubated for 5 min. This step was repeated three times. Purity of the isolated protein was checked via SDS-PAGE. The proteins were frozen in liquid nitrogen and stored at -80°C.

3.4.3. Antibody purification

For purification of antibodies from serum, the respective purified antigen was loaded onto a 12% SDS gel and subsequently blotted onto a PVDF membrane using a semi-dry blot system at 100 mA for one hour. The membrane was stained with ponceau staining solution and the antigen region was cut out. The membrane strip was transferred into a 15 ml reaction tube and blocked with 5% milk powder in PBS (0.14 M NaCl, 2.7 mM KCl, 10 mM $Na_2HPO_4*2H_2O$, 1.8 mM KH_2PO_4) for 30 min at room temperature. The strip was washed three times with 10 ml PBS. Afterwards, 10 ml serum were added and incubated at 4°C on a roller over night. On the next day, the serum was removed, and the strip washed with PBS-T (PBS + 0.05% Tween20). The antibody was eluted from the membrane by addition of 800 µl 100 mM glycine pH 2.8 – 2.5 for 30 min at room temperature. The eluate was neutralized by addition of 50 µl 100 mM Tris/HCl pH 8. The antibody was aliquoted, frozen in liquid nitrogen and stored at -80°C

3.4.4. Small scale chloroplast isolation

For small scale isolation of chloroplasts from *Arabidopsis*, leaves were transferred into a petri dish with 1 ml isolation buffer (50 mM Tris/HCl pH 8, 330 mM sorbitol, 0.1 mM EDTA, 0.1% BSA, 1 mM PMSF) on ice. Using a razor blade, the leaves were cut in small pieces. The suspension was filtered through one layer of gauze, rinsed with 1 ml isolation medium and centrifuged at 1000 g for 5 min at 4°C. The supernatant was removed, and the pellet resuspended in an appropriate volume of isolation buffer.

3.4.5. Isolation of microsomes

Leaves were homogenized with approximately 20 ml MF buffer (0.05 M Tris/HCl pH 7.5, 0.5 M sucrose, 0.001 M EDTA) using a polytron homogenizer. After filtration through one layer of gauze, the suspension was centrifuged at 4200 g for 10 min at 4°C. The supernatant was transferred into new centrifuge tubes and centrifuged at 10000 g for 10 min at 4°C. The supernatant was again transferred into new centrifuge tubes and microsomal membranes were pelleted via ultracentrifugation at 100000 g for one hour at 4°C. The pellet was resuspended either in MF buffer or other buffers suitable for the subsequent experiment. The sample was frozen in liquid nitrogen and stored at -80°C.

3.4.6. Sucrose density centrifugation

Microsomal membranes were isolated in either Mg-MF buffer (0.05 M Tris/HCl pH 7.5, 0.5 M sucrose, 5 mM $MgCl_2$) or EDTA-MF buffer (0.05 M Tris/HCl pH 7.5, 0.5 M sucrose, 5 mM EDTA) as described in 3.4.5. After ultracentrifugation, the pellets were resuspended in 1 ml Mg-MF2 (0.01 MTris/HCl pH 7.5, 0.25 M sucrose, 0.5 mM $MgCl_2$) or EDTA-MF2 (0.01 M Tris/HCl pH 7.5, 0.25 M sucrose, 0.5 mM EDTA), respectively. Isolated microsomes were loaded onto linear gradients ranging from 15% to 50% sucrose in Mg-MF2 or EDTA-MF2 buffer. The samples were separated on the gradient by ultracentrifugation at 166900 g in a swing out rotor for two hours at 4°C. After ultracentrifugation, the gradient was divided into fractions from top to bottom. 35 µl of each fraction were loaded onto an 8% SDS-Gel. After wet-blotting, the membranes were probed with antibodies against DJC31, DJC62 and BiP as ER control.

3.4.7. Membrane attachment

80 µg microsomal membranes were pelleted at 100000 g for one hour at 4°C. The pellets were resuspended in different buffers and incubated on ice for 30 min.

1) 50 mM Tris/HCl pH 7.5 (Control)
2) 0.1 M Na_2CO_3 (~ pH 11)
3) 1 M NaCl in 50 mM Tris/HCl pH 7.5
4) 6 M Urea in 50 mM Tris/HCl pH 7.5
5) 1% SDS in 50 mM Tris/HCl pH 7.5

The samples were centrifuged at 100000 g, 4°C for one hour. Pellet and soluble fractions were loaded onto a 10% SDS Gel. After wet-blotting, the membranes were probed with antibodies against DJC31 and DJC62.

3.4.8. Bradford protein assay

For determination of the protein concentration according to Bradford (Bradford, 1976), 200 µl 5x Bradford reagent (0.01% Brilliant Blue G250, 5% ethanol p.a., 8.5% phosphoric acid) were added to 799 µl ddH_2O and 1 µl sample. After vortexing, the mixture was incubated at room temperature for 10 min and photometrically measured at 595 nm. 1 µl sample buffer instead of sample was used as control. For generation of a calibration curve BSA was used in a concentration range of 0-5 mg/ml.

3.4.9. SDS-Polyacryladmide gelelectrophoresis

SDS-polyacrylamide gelelectrophoresis was performed as described by Laemmli (Laemmli, 1970). Depending on the size of the protein of interest, 8%, 10% or 12% acrylamide were used. The stacking gel contained 5% acrylamide. Samples were mixed with SDS loading buffer (62.5 mM Tris/HCl pH 6.8, 2.25% SDS, 10% glycerin, 5% β-mercaptoethanol, 0.004% bromphenol blue) and separated on the gel in SDS running buffer (25 mM Tris, 192 mM glycine, 0.1% SDS) at 30 mA/gel.

3.4.10. Western blot

Proteins, separated via SDS-PAGE, were transferred onto PVDF membranes via either semi-dry blotting (small proteins) or wet-blotting (proteins >100 kDa). For both methods the blot was assembled as follows (from anode to cathode): Three filter papers (Blotting-Paper, Macherey-Nagel, Düren, Germany) were soaked in Towbin buffer (25 mM Tris, 192 mM glycine, 0.001% SDS, 10-20% methanol). A PVDF membrane (Immobilon-P, Millipore, Darmstadt, Germany) was activated in methanol and placed on the filter papers. The SDS-gel was placed onto the PVDF membrane and covered by three filter papers soaked in Towbin buffer.

For semi-dry blotting, the transfer was performed at 0.8 mA/cm^2 for one hour at room temperature. Wet blotting was performed at 400 mA, for two hours at 4°C or at 50 mA, over night at 4°C.

For immunodetection, the membranes were blocked with 5% milk powder in TBS-T (20 mM Tris, 135 mM NaCl, pH 7.5, 0.05% Tween20) for 30 min at room temperature. Incubation with the primary antibody was either carried out at room temperature for two hours or at 4°C over night. The antibodies were diluted in 1% milk powder in TBS-T as given in Table 5. After washing in TBS-T for 3 x 10 min, the membrane was treated with an appropriate secondary antibody, coupled to a horseradish peroxidase, for two hours at room temperature. After washing in TBS-T for 3 x 10 min, the membrane was covered with a 1:1 mixture of ECL1 solution (100 mM Tris/HCl pH 8.5, 1% luminol, 0.44% coumaric acid) and ECL2 solution (100 mM Tris pH 8.5, 0.018% H_2O_2). The luminescence signal was recorded using an ImageQuant LAS 4000 (GE Healthcare).

3.4.11. Protein staining

To visualize proteins in SDS-gels or on a membrane, gels or membranes were incubated in Coomassie solution (45% (v/v) methanol, 9% (v/v) acetic acid, 0.2% (w/v) Brilliant Blue R-250) for 20 min at room temperature. To destain the background, gels or membranes were incubated in Coomassie destain solution (45% (v/v) methanol, 9% (v/v) acetic acid, 0.2% (w/v)) until the band pattern was clearly visible.

For reversible staining of western blot membranes, Ponceau staining solution (5% (v/v) acetic acid, 0.3% (w/v) Ponceau S) was used. The membranes were incubated in staining solution and destained in ddH_2O until the band pattern was clearly visible.

3.5. Cellbiological methods

3.5.1. Protoplast isolation from *Arabidopsis thaliana*

Leaves were placed in a petri dish with 10 ml enzyme solution (1% (w/v) cellulase R10, 0.3% (w/v) macerozyme R10, 400 mM mannitol, 20 mM KCl, 20 mM MES pH 5.7, 10 mM $CaCl_2$, 0.1% (w/v) BSA), cut in small pieces and incubated in the dark at room temperature for 90 min. Protoplasts were released by gently swirling the petri dish. The protoplasts were filtered through a nylon mesh and pelleted at 100 g for 4 min (low brake). The pellet was resuspended in MMg buffer (0.4 M mannitol, 15 mM $MgCl_2$, 4 mM MES pH 5.7). Subsequently, the protoplasts were layered onto a step gradient consisting of 9 ml MSC buffer (10 mM MES, 20 mM $MgCl_2$, 120 g/L sucrose, adjusted to 550 mOsm) and 2 ml MMg. After centrifugation at 70 g for 10 min, intact protoplasts were transferred into a new tube and diluted with 5 ml W5 buffer (2 mM MES pH 5.7, 154 mM NaCl, 125 mM $CaCl_2$, 5 mM KCl). After centrifugation at 100 g for 4 min, the pellet was resuspended in 500 µl MMg.

3.5.2. Transfection of *Arabidopsis* protoplast

Transfection of *Arabidopsis* protoplasts was performed as described in Yoo et al. 2007 with modifications (Yoo et al., 2007). 10 µg plasmid DNA were transferred into a 2 ml reaction tube. 100 µl protoplasts in MMg buffer were added and mixed by tapping. 110 µl PEG solution (40% PEG4000, 0.2 M mannitol, 100 mM $CaCl_2$) were added and mixed by tapping. The protoplasts were incubated at room temperature for 15 min. The transfection was stopped by addition of 440 µl W5 buffer followed by gentle inversion of the tube. The samples were centrifuged at 100 g for 2 min, the supernatant was removed, and the protoplasts resuspended in 1 ml WI buffer (4 mM MES pH 5.7, 0.5 M mannitol, 20 mM KCl). The transfected protoplasts were transferred into a well-plate and incubated at room temperature over night in the dark. Subsequent analysis by confocal microscopy was performed using the following setting: Leica, TCS SP5; objective lens: HCX PL APO CS, magnification: 636x, numerical aperture: 1.3; imaging medium: glycerol.

3.5.3. Protoplast isolation from *Nicotiana benthamiana*

The following buffers were used for isolation of protoplasts from tobacco:

2 M NH_4 succinate: 2 M succinic acid, 2 M NH_4Cl, adjusted to pH 5.8 with KOH

Macro MS (modified): 10 mM KNO_3, 3 mM $CaCl_2$ x 2 H_2O, 1.5 mM $MgSO_4$ x 7 H_2O, 1.25 mM KH_2PO_4, 0.02 M NH_4 succinate, 2 mM MES

Micro MS (1000x): 4.5 mM KI, 109 mM EDTA-Fe(III) sodium salt, 48.5 mM H_3BO_3, 59.16 mM $MnSO_4$ x H_2O, 7 mM $ZnSO_4$ x 7 H_2O, 753 µM Na_2MoO_4 x 7 H_2O, 100 µM $CuSo_4$ x 5 H_2O, 105 µM $CoCl_2$ x 6 H_2O

F-PIN: Macro MS (modified), 1x Micro MS, adjusted to 550 mOsm with sucrose

F-PCN: Macro MS, 1x Micro MS, adjusted to 550 mOsm with glucose, adjusted to pH 5.8 with KOH

W5 buffer: 150 mM NaCl, 125 mM $CaCl_2$, 5 mM KCl, 2 mM MES pH 5.7

The tobacco leaf was immersed in enzyme solution (1% cellulase R10, 0.3% macerozyme R10, 0.1% BSA in F-PIN buffer) and cut in pieces of approximately 1 x 1 cm using a razor blade. Leaf pieces were infiltrated with the enzyme solution by applying vacuum for 30 s. The infiltrated leaf pieces were incubated in the dark under gentle shaking for 90 min. The protoplasts were released by shaking at 80 rpm for 1 min and filtrated through a nylon mesh into a centrifuge tube. The protoplast suspension was overlayed with 2 ml F-PCN and centrifuged at 70 g (low brakes) for 10 min. Intact protoplasts accumulated at the interface between enzyme solution and F-PCN and were transferred into a fresh tube. Protoplasts were washed with 10 ml W5 buffer by centrifugation at 50 g for 10 min. The protoplast pellet was carefully resuspended in 500 µl W5 buffer. Subsequent analysis by confocal microscopy was performed using the following setting: Leica, TCS SP5; objective lens: HCX PL APO CS, magnification: 636x, numerical aperture: 1.3; imaging medium: glycerol.

4. Results

4.1. *In silico* analysis and structure prediction

DJC31 (TPR16, AT5G12430) and DJC62 (TPR15, AT2G41520) were first identified in an *in silico* screening for carboxylate clamp type TPR proteins in *Arabidopsis* by Prasad et al., as two of 24 newly identified carboxylate clamp-type TPR proteins and therefore potential co-chaperones of HSP70 and HSP90. Using different localization prediction software tools, DJC31 and DJC62 were predicted to be located either in the chloroplast or in the nucleus (Prasad et al., 2010). Based on this study, Chiu et al. included DJC31 and DJC62 in their experiments regarding evolution and function of chloroplast HSP70 and its putative co-chaperones. In this study, they have performed chloroplast import experiments to verify the predicted plastidal localization of 19 J-proteins. For DJC31 and DJC62, the import rates of the full-length proteins into the chloroplast were rather low, but using a truncated form, they could demonstrate, that both fragments were imported and processed in the chloroplast, whereas more than one mature form was visible after the import (Chiu et al., 2013).

4.1.1. Domain composition and structure

DJC31 is composed of 1165 amino acids, with a calculated molecular weight of 129 kDa. DJC62 is 1108 amino acids in length and has a calculated molecular weight of 123 kDa. Furthermore, there are two predicted splice variants for DJC62. DJC31 and DJC62 share 34% identity and 50% similarity, with a high degree of conservation especially in the C-terminal part (Figure 5).

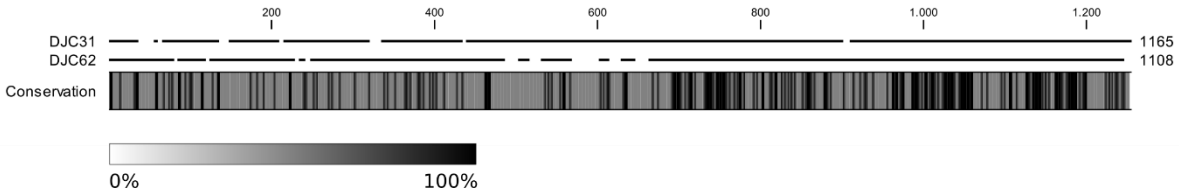

Figure 5: Alignment of DJC31 and DJC62.

Protein sequences of DJC31 and DJC62 were aligned. The graph below indicates the degree of conservation as given in the black/white scale.

The NCBI conserved domains search tool was used to get an overview of predicted structural motifs (Lu et al., 2020). For DJC31, seven TPR repeats could be detected in the C-terminal half of the protein. Additionally, it contains a J-domain at the very C-terminal end, ranging from amino acid 1024 to 1106. For DJC62, six TPR repeats and a J-domain from amino acid 979 to 1059 could be identified in the C-terminal part. The TPR repeats of DJC31 and DJC62 cluster into two regions of three TPR repeats each, which form two TPR domains, spanning the region from amino acid 608 - 714 and 882 - 976 for DJC31. In DJC62 the two domains can be found in the region of amino acid 553 - 659 and 835 – 932

(Figure 6). The two TPR domains of DJC31 and DJC62, respectively, were aligned with the TPR domains of the closest homolog in humans TPR2, which has been proven to be a co-chaperone of HSP70 and HSP90 (Brychzy et al., 2003). The alignment shows the presence of the conserved consensus residues K_5N_9-N_6-K_2R_6, responsible for the interaction with the MEEVD motif of cytosolic HSP90s, which is consistent with the findings of Prasad et al (Prasad et al., 2010; Scheufler et al., 2000). Besides the K_5N_9-N_6-K_2R_6 motif, the TPR domains additionally share some highly conserved residues, which are important for their structural integrity. Among them A/G_8, A_{20} and A_{27}, which are also present in the TPR domains of DJC31 and DJC62 (Zeytuni & Zarivach, 2012) (Figure 7). This indicates, that DJC31 and DJC62 could act like TPR2 as potential co-chaperones of HSP70 and HSP90.

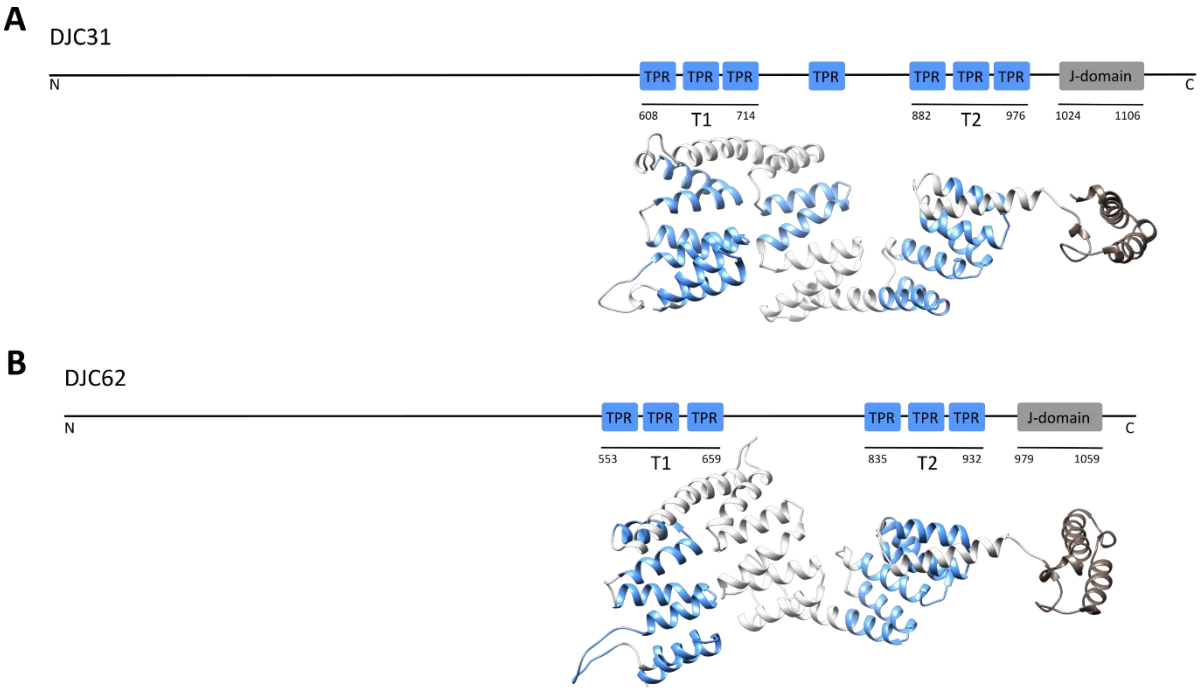

Figure 6: Domain composition.

DJC31 (A) and DJC62 (B) are composed of seven and six TPR repeats (blue), respectively, and a C-terminal J-domain (gray). Both proteins contain a long N-terminal part of unknown structure. Structural models were generated using Phyre2, based on the structure of the human co-chaperone p58IPK. Predicted DJC31 and DJC62 domains are highlighted in blue (TPR repeat) and gray (J-domain).

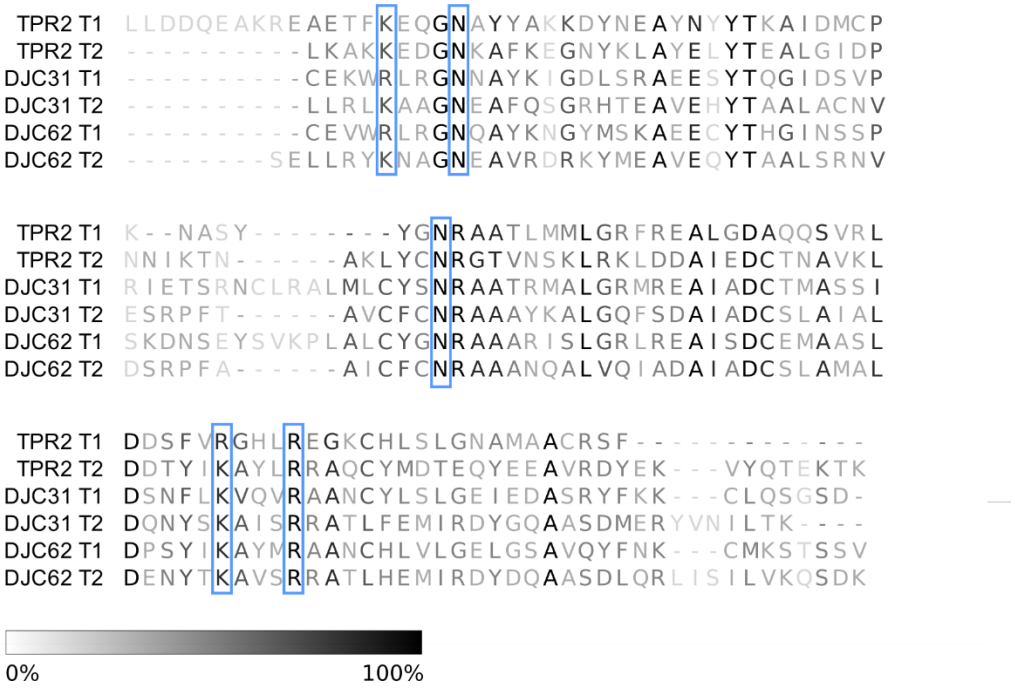

Figure 7: Alignment of potential TPR-carboxylate clamp domains of DJC31 and DJC62 with the TPR domains of the human TPR2.

The sequences of the predicted TPR domains of DJC31 and DJC62 were aligned with the TPR domains of the human HSP70/HSP90 co-chaperone TPR2. Conserved residues of the K_5N_9-N_6-K_2R_6 motif, involved in formation of the carboxylate clamp, are highlighted with blue boxes. The black/white scale indicates the degree of conservation.

The J-domain of DnaJ from *E.coli*, the founding member of the HSP40 protein family, was used to confirm the presence of a J-domain in DJC31 and DJC62. The J-domain sequence alignment of the in general well conserved J-domains shows 35% identity between DnaJ and DJC31, and 30% identity between DnaJ and DJC62. Also the functionally essential HPD motif, responsible for activation of the HSP70 ATPase domain, can be found in all sequences analyzed (Kampinga & Craig, 2010).

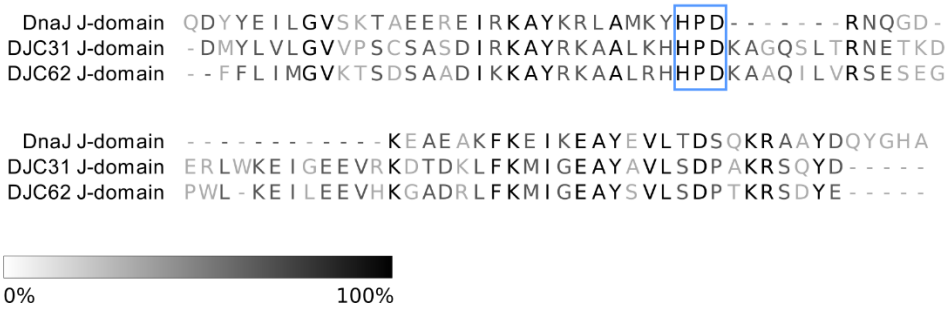

Figure 8: Alignment of the DJC31 and DJC62 J-domains with the J-domain of *E.coli* DnaJ.

Sequences of the predicted J-domains of DJC31 and DJC62 were aligned with the J-domain of *E.coli* DnaJ. The conserved HPD motif, which activates the HSP70 ATPase domain, is highlighted with a blue box. The black/white scale indicates the degree of conservation.

Both DJC31 and DJC62 contain a long N-terminal part of unknown structure, which encompasses approximately half of the proteins. IUPred2A was used to gain more information about the folding state of the N-terminus. This tool is based on an energy estimation model, which uses a low-resolution statistical potential to estimate the tendency of amino acids to form contacts, as observed in proteins of globular structure (Mészáros et al., 2018). The resulting plot indicates a high degree of disorder in the N-terminal part of DJC31 and DJC62, whereas the C-terminal part of the protein, where the predicted domains are located in, is predicted to be predominantly well structured (Figure 9).

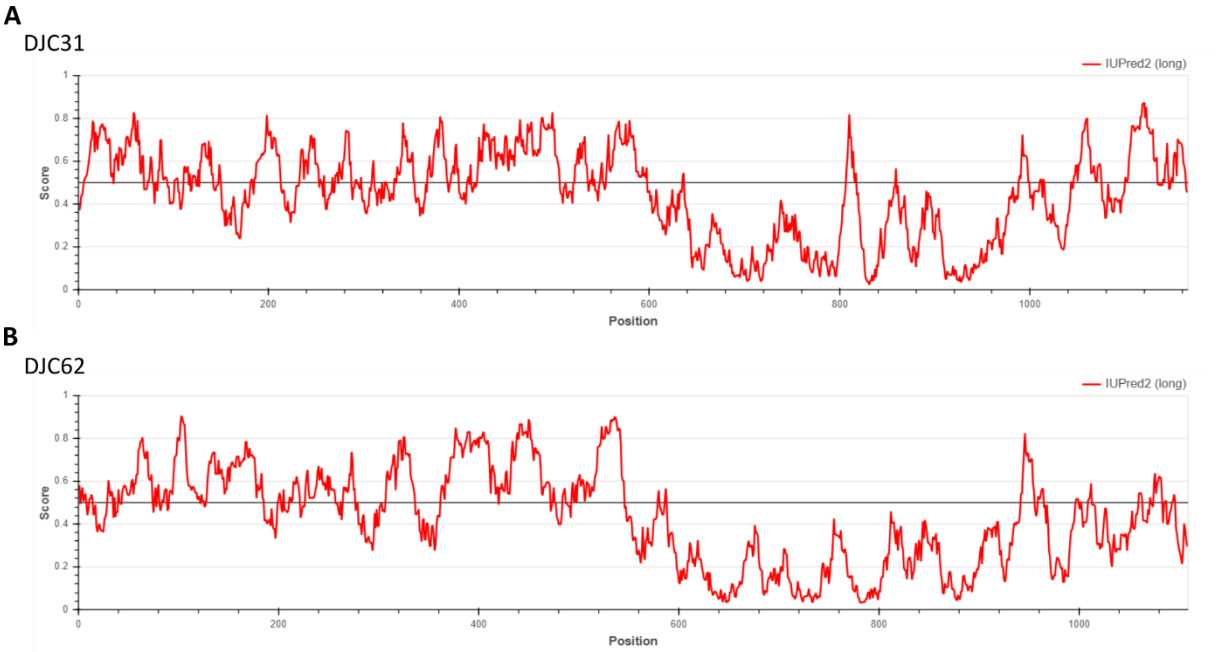

Figure 9: Disorder prediction.

IUPred2 was used to predict disordered regions of DJC31 (A) and DJC62 (B). Both proteins exhibit a high degree of disorder within the N-terminal half of the proteins, whereas the values of the C-terminal half, containing the predicted domains, indicate a predominantly folded state.

Using the Kyte-Doolittle hydrophobicity scale, the hydrophobicity of the proteins and thus the probability of existing transmembrane segments, was analyzed. In this scale, regions composed of hydrophobic amino acids, exhibit a positive value in the graph. Using a window size of 21, regions with a calculated value of >1.6 are likely to be transmembrane segments, which was not reached for neither of the two proteins (Kyte & Doolittle, 1982) (Figure 10). Also the overall hydrophobicity is rather low, which indicates DJC31 and DJC62 to be soluble proteins.

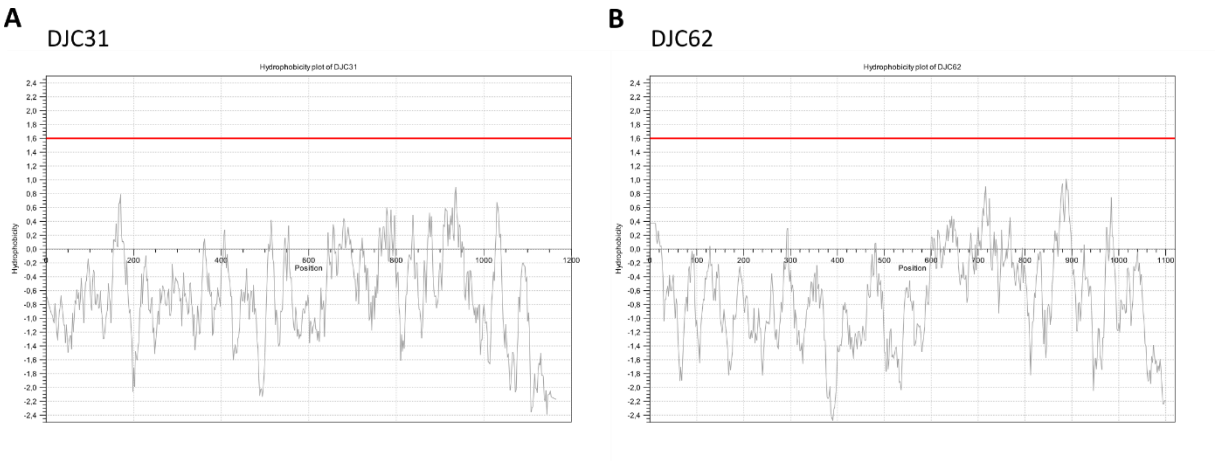

Figure 10: Hydrophobicity plot according to the Kyte-Doolittle scale.

The Kyte-Doolittle scale of hydrophobicity was used to analyze the hydrophobicity of DJC31 (A) and DC62 (B). The threshold value of 1.6 for the presence of transmembrane domains is marked with a red line. The graphs do not provide evidence for the presence of transmembrane segments.

4.1.2. Gene expression profile

To obtain information about the expression levels of *DJC31* and *DJC62* in different organs and tissues, the AtGenExpress eFP viewer was used from the Bio-Analytic Resource for Plant Biology (BAR). This tool uses publicly available gene expression data generated with an Affymetrix ATH1 array, normalized by the GeneChip Operating Software (GCOS) method and a target intensity (TGT) value of 100. Most tissues were sampled in triplicates (Nakabayashi et al., 2005; Schmid et al., 2005; Waese et al., 2017). The overview schemes for *DJC31* and *DJC62* indicate that both genes are expressed in almost all organs, tissues and developmental stages with slight differences regarding expression levels between the two genes (Figure 11). *DJC31* seems to be more expressed in leaves, with maximum expression levels in pollen, whereas *DJC62* seems to be predominantly expressed in the shoot apex and flower stage 9-11. The highest expression levels for *DJC62* can be found in dry seeds.

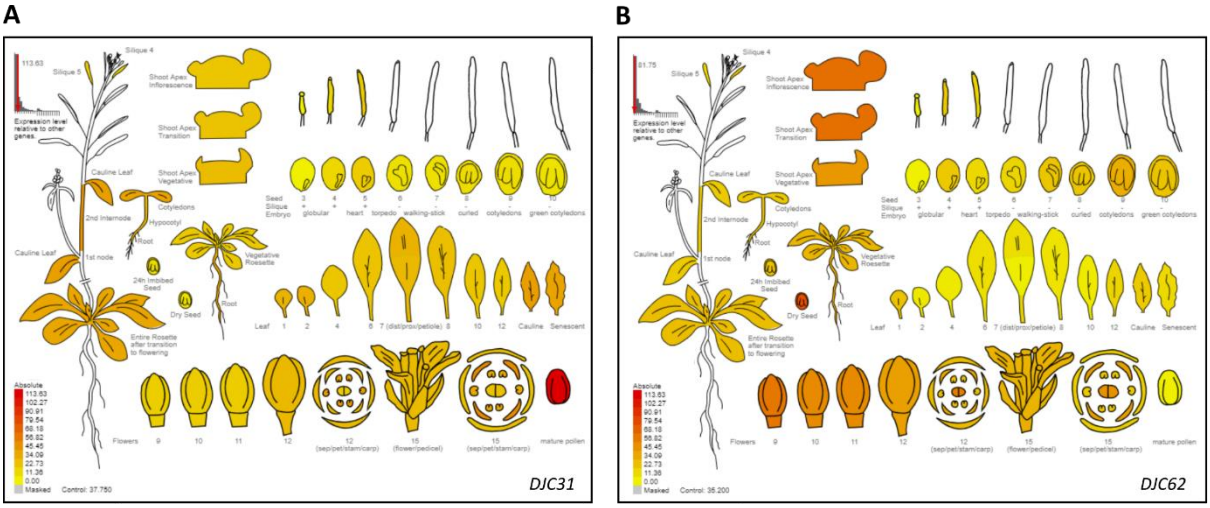

Figure 11: Expression profile of *DJC31* and *DJC62*.

Overview of gene expression in different organs, tissues and developmental stages. *DJC31* (A) and *DJC62* (B) are expressed in almost all organs and developmental stages. Images were generated with the AtGenExpress eFP Viewer.

4.1.3. Prediction of the subcellular localization

In a previous study, conducted by Prasad et al, different bioinformatic tools for the prediction of subcellular localizations were used for *in silico* characterization of newly identified TPR proteins. They found DJC31 and DJC62 to be located in the chloroplast or the nucleus (Prasad et al., 2010). To confirm this result, TargetP was used. Version 1.1 is a neural network-based tool, which analyzes the N-terminal amino acid sequence for presence of targeting signals leading proteins to the chloroplast, mitochondria and the secretory pathway (Almagro Armenteros et al., 2019; Emanuelsson et al., 2000). Using the plant network without a cutoff value, TargetP 1.1 predicted both proteins to be located in the chloroplast with a transit peptide of 48 amino acids in length for DJC31, supported by a strong reliability class of 1, and a very short chloroplast transit peptide of four amino acids in length, with a weak reliability class of 4 for DJC62.

A new version of TargetP was released in 2019. Using TargetP 2.0, no targeting signals could be predicted for neither DJC31, nor DJC62.

A

	Length	cTP	mTP	SP	other	Loc	RC	TPlen
DJC31	1165	0.980	0.031	0.004	0.063	C	1	48
DJC62	1108	0.725	0.027	0.040	0.367	C	4	4

B

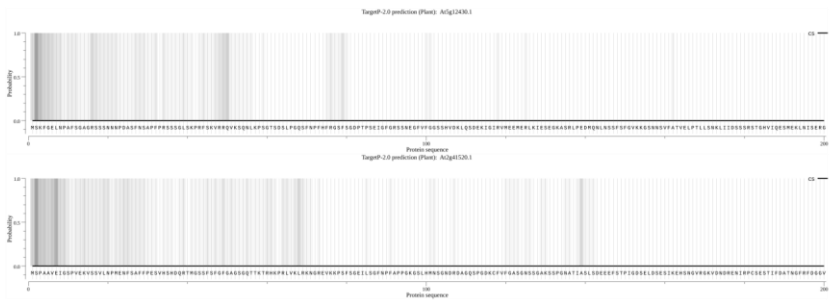

C

	Other	Signalpeptide	Mitochondria	Chloroplast	Thylakoid
DJC31	0.9988	0	0.0001	0.0011	0
DJC62	0.9998	0	0	0.0001	0

Figure 12: Prediction of the subcellular localization of DJC31 and DJC62 using TargetP 1.1 and 2.0.

A) Localization of DJC31 and DJC62 was analyzed using Target P 1.1 regarding the presence of chloroplast transit peptides (cTP), mitochondrial transit peptides (mTP) or signal peptides for proteins of the secretory pathway (SP), to predict the subcellular localization (Loc), considering the reliability class (RC) and the length of the transit peptide (TPlen). The predicted localization of DJC31 and DJC62 was chloroplast.

B – C) Subcellular localization prediction with TargetP 2.0. According to the graphical output for DJC31 (B, upper panel) and DJC62 (B, lower panel) and the calculated values in C, no targeting signal could be detected.

4.2. Characterization of single and double knockout mutant lines

4.2.1. Phenotypic characterization

To analyze the function of DJC31 and DJC62, two knockout lines with Col-0 background were used, carrying T-DNA insertions within the first exon of *DJC31* (*djc31*) or the second exon of *DJC62* (*djc62*), respectively (Figure 13).

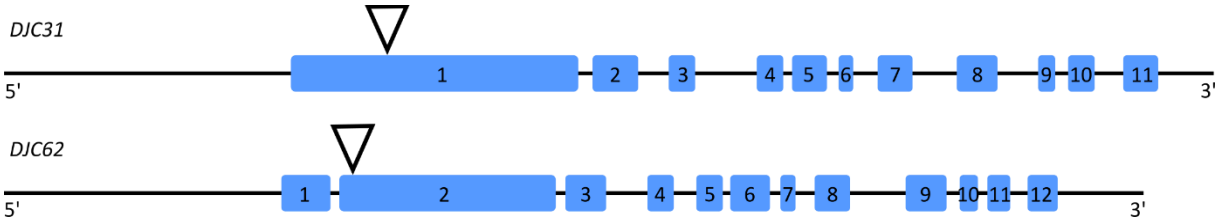

Figure 13: Gene models of *DJC31* and *DJC62*.

Exons are illustrated as blue boxes. The sites of the T-DNA insertions are marked with black triangles

Knockout of only one gene resulted in a very mild phenotype, which is overall comparable to wild type. Therefore, a double mutant was generated by crossing of *djc31* with *djc62*. The resulting double mutant *djc31 djc62* shows a severe phenotype with strong defects in growth and development. To confirm, that these defects are exclusively caused by the knockout of the two genes, the double mutant was complemented with either *DJC31* or *DJC62* under control of a 35S promoter. All mutant lines were checked for homozygosity of the T-DNA insertion, as well as for presence and absence of the respective genes or complementation constructs by genotyping. For that, gDNA was isolated from leaf material and tested by PCR using appropriate primers. For verification of T-DNA presence, primers binding within the gene and within the T-DNA insertion were chosen. To confirm homozygosity of the T-DNA, a primer pair spanning the region before and after the site of the T-DNA insertion was used. For testing of the complementation lines, an additional primer pair, with one primer binding within an intron, was designed to discriminate between the endogenous gene and the complementation construct, which was cloned from cDNA. Additionally, all lines were tested on the protein level via western blotting, using specific antibodies against the N-terminal part of DJC31 or DJC62, respectively, to verify absence and presence of the respective gene product (Figure 14).

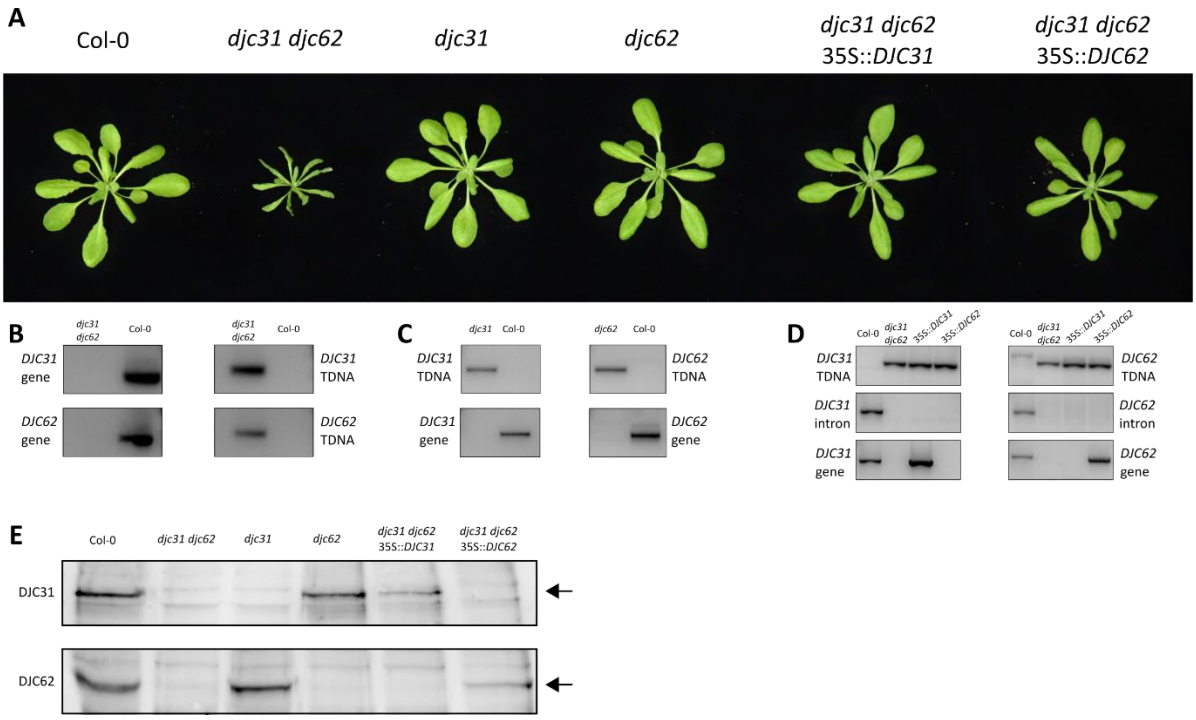

Figure 14: Mutant phenotypes and mutant confirmation by genotyping and western blot.

A) Photographs of four weeks old wild type (Col-0) double mutant (*djc31 djc62*), single mutants (*djc31* and *djc62*) and complementation lines (*djc31 djc62* 35S::*DJC31* and *djc31 djc62* 35S::*DJC62*). The *djc31 djc62* mutant has short, thin, crumpled leaves, whereas the single mutants and complementation lines show a phenotype comparable to wild type.

B-D) Wild type, mutant lines and complementation lines were genotyped to confirm the presence and homozygosity of the T-DNA insertion and successful genomic integration of the complementation construct.

E) Presence and absence of the respective proteins were analyzed via western blot, using antisera against the N-terminus of DJC31 and DJC62, respectively.

The double mutant exhibited a strong leaf phenotype, with extremely shortened petioles and shortened, thin, crumpled leaf blades. The rosette leaf shape of single mutants and complementation lines looked comparable to wild type.

Looking at later growth stages, it became apparent, that the single mutants show a slight growth retardation, whereas the double mutant showed a strong defect in growth and development. In addition to the slow growth, *djc31 djc62* grew bushy with thinner stems and less side branches (Figure 15).

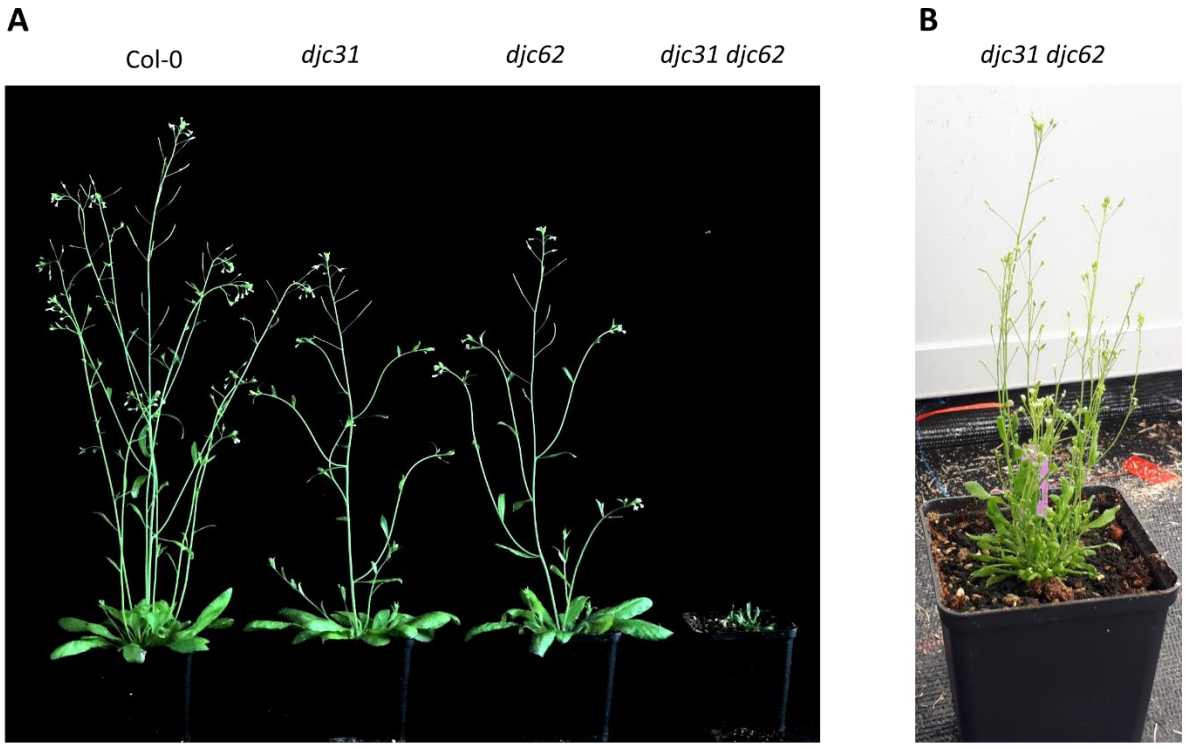

Figure 15: Mutant phenotypes at later growth stages.

A) Six weeks old wild type (Col-0), single mutants (*djc31*, *djc62*) and double mutant (*djc31 djc62*). The single mutants exhibited a slight growth retardation, whereas the double mutant showed a strong growth defect.

B) The double mutant showed bushy growth with thin stems and less branching.

The growth defects of *djc31 djc62* were not only visible in later growth stages, but already at the cotyledon stage. Here, mainly four different cotyledon morphologies could be observed. In most cases, the cotyledons of *djc31 djc62* looked similar to wild type with minor differences. In some cases, heart-shaped cotyledons, triple cotyledons or fused cotyledons could be observed (Figure 16). These altered morphologies were mostly observed on only one side of the cotyledons. Quantification of these altered cotyledon morphologies by counting more than 100 seedlings of Col-0, *djc31*, *djc62* and *djc31 djc62* revealed, that 12% of the *djc31 djc62* seedlings exhibited this defect, whereas for wild type and single mutants differences in cotyledon shape and number could not be observed (Table 7).

Figure 16: *djc31 djc62* showed an altered cotyledon morphology.

Photographs of eight days old seedlings of wild type (Col-0), double mutant (*djc31 djc62*) and single mutants (*djc31* and *djc62*). The double mutant showed various cotyledon defects.

Table 7: Quantification of cotyledon defect occurrence. More than 100 seedlings per genotype were scored. 12% of the *djc31 djc62* seedlings showed an altered cotyledon morphology.

	Total	Altered morphology	%
Col-0	131	0	0%
djc31 djc62	178	22	12%
djc31	104	0	0%
djc62	117	0	0%

Another striking feature of the double mutant was the strong decrease in seed yield. Plants were grown in parallel and were bagged, when most of the siliques were ready to be harvested. After harvesting, seed yield was scored according to the weight of the individual seed batches. The seed yield of *djc31 djc62* was strongly decreased by 89%, whereas *djc31* and *djc62* were decreased by 29% and 25% compared to wild type, respectively (Figure 17). The reduction in seed yield of the single mutants was not significant compared to wild type but indicates a clear trend.

The siliques of *djc31 djc62* showed an altered morphology. They were much shorter compared to wild type and many siliques had a bent or curled appearance. Siliques of the single mutants were slightly shorter than wild type siliques, which fits to the slightly decreased seed yield, but overall they looked normal (Figure 17).

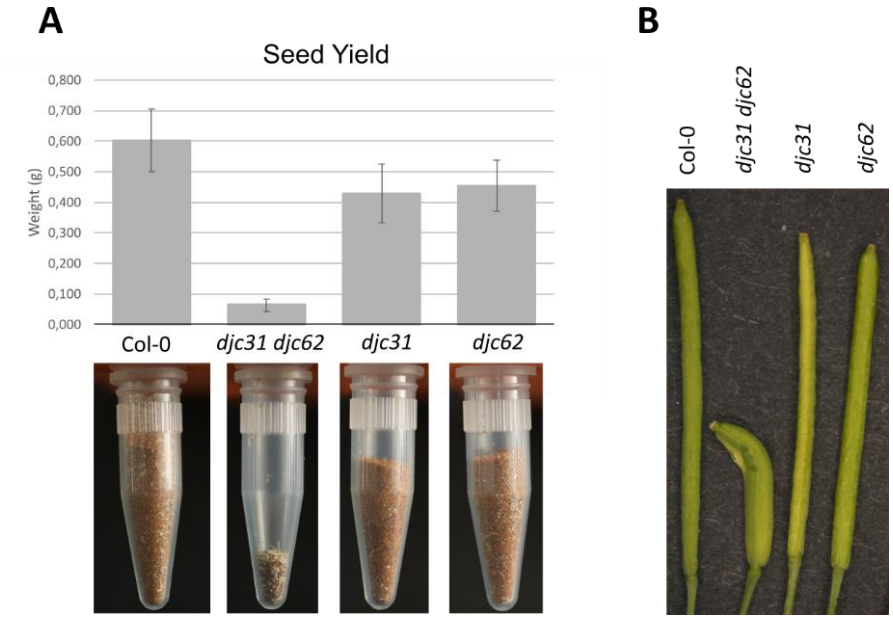

Figure 17: Mutants showed a decrease in seed yield and an altered silique morphology.

A) The amount of seeds in the *djc31 djc62* mutant was tremendously decreased, whereas the *djc31* and *djc62* mutants were not significantly decreased in seed yield (Col-0 n=10, *djc31 djc62* n=7, *djc31* n=9, *djc62* n= 10). Error bars represent the standard deviation

B) Siliques of the *djc31 djc62* mutant were shortened and in some cases bent or curled

Reasons for a decrease in seed yield can be an impaired flower development or defective pollen, and since, according to public gene expression data, *DJC31* shows highest expression in pollen, DJC31 might be of special importance for reproduction and pollen viability. Therefore, flowers and pollen were inspected in more detail. Flowers of the single mutants *djc31* and *djc62* were normal in size and shape compared to wild type. However, flowers of the double mutant showed several different defects. The number of petals, which is typically four for Brassicaceae, was increased or decreased, with petals showing abnormal shapes and fissions. In some flowers, petals were absent completely. Sepals were also affected and showed differences in size and shape. Furthermore, they did not enclose the flower, as it can be seen in the wild type, but rather stuck out to different directions. Stamina were shortened or even absent at all. Pistils were bent or had a spiral shape (Figure 18).

Figure 18: The *djc31 djc62* mutant showed an abnormal flower development.

A) The *djc31 djc62* mutant showed vast defects in flower development. Number and shape of petals were altered or absent. Stamina were shortened or absent. Pistils were bent or curled. Flower morphology of *djc31* and *djc62* was comparable to wild type (Col-0).

B) For analysis of pollen viability, flowers were dabbed onto solid pollen germination medium. After six hours, the samples were scored for pollen tube development. Although flower development was impaired in *djc31 djc62*, the pollen was viable.

These severe defects in flower morphology raised the question, whether pollen is actually generated within the anthers. Analysis of pollen content in the anther by staining was not possible, since the deformations made identification of the right flower stage for staining and sample preparation impossible. Instead, pollen tube formation was analyzed. For that, open flowers from Col-0 and *djc31 djc62* were dapped onto solid pollen germination medium on a microscope slide and placed into an incubation chamber made of an empty tip-box with a wet tissue to prevent the samples to dry out. After six hours at room temperature, germinated pollen was imaged under the microscope. Since

pollen germination depends on density of the pollen grains, regions of approximately equal density were used to compare pollen tube formation between wild type and double mutant (Boavida & McCormick, 2007). In both samples, pollen was viable and comparable regarding pollen tube number and length (Figure 18).

Besides leaves, flowers and siliques, also the roots were affected by the lack of DJC31 and DJC62. Roots of *djc31 djc62* were extremely shortened and barely showed lateral root growth. The single mutants *djc31* and *djc62* were not significantly reduced in root growth, showed a normal morphology and lateral root formation.

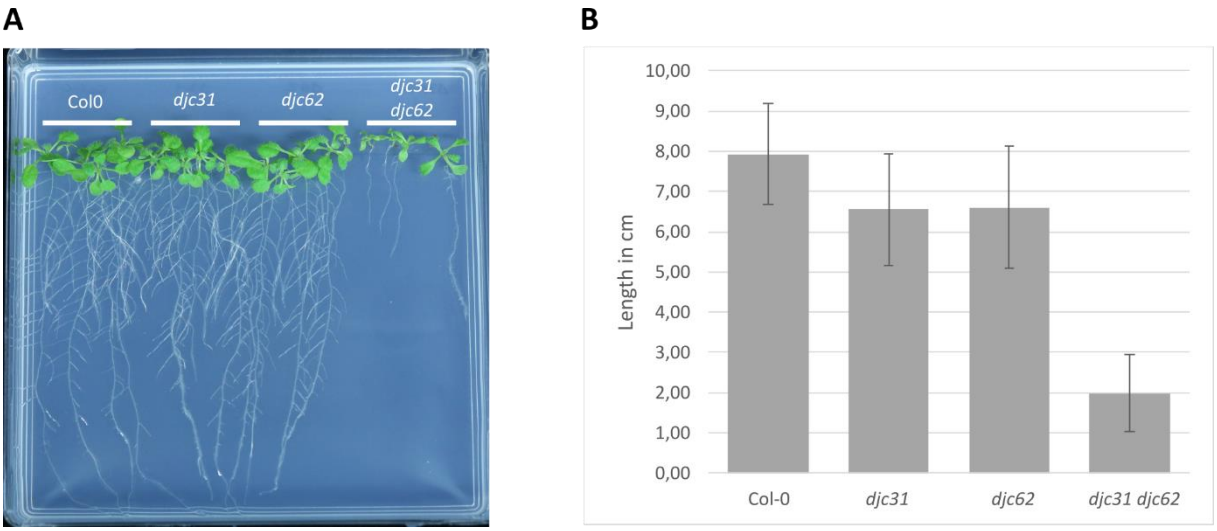

Figure 19: Root morphology and length.

A) The root morphology of *djc31* and *djc62* was comparable to wild type (Col-0), whereas roots of the *djc31 djc62* mutant were extremely shortened and barely showed lateral root growth.

B) Quantification of the root length. The root length of *djc31* and *djc62* did not significantly differ from wild type. Roots of *djc31 djc62* showed a strong decrease in length. Col-0 n=18, *djc31 djc62* n= 17, *djc31* and *djc62* n=19. Error bars represent the standard deviation.

4.2.2. qPCR Analysis of *djc31* and *djc62*

According to their structure and domain composition, it was conceivable that DJC31 and DJC62 have overlapping functions. Phenotypic analysis of single and double mutant lines revealed that *djc31* and *djc62* are barely affected by the knockout of one gene. This has raised the question, whether upregulation of *DJC31* in *djc62* and *DJC62* in *djc31* occurs to compensate for the loss of one gene. To answer this question, RNA was isolated from seven days old seedlings, reverse transcribed into cDNA and analyzed via qPCR, using *OEP24* as reference gene. A significant change in gene expression could neither be observed for *DJC31* in *djc62* or *DJC62* in *djc31* in comparison to wild type (Figure 20).

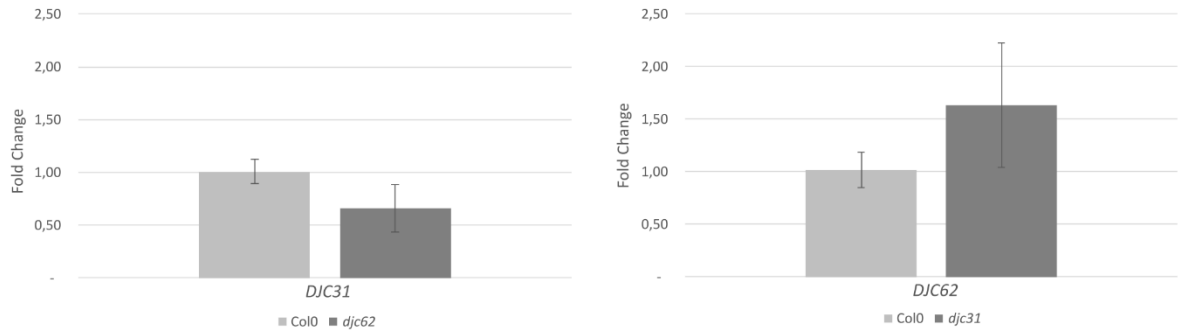

Figure 20: Single mutant analysis via qPCR.

To analyze whether *DJC31* or *DJC62* are upregulated in *djc31* and *djc62*, respectively, to compensate for the loss of the other gene, RNA was isolated from seven days old wild type and single mutant seedlings. A qPCR was performed using *OEP24* as reference gene. No significant up- or downregulation could be observed for *DJC62* in *djc31* and *DJC31* in *djc62*. Error bars represent the standard deviation.

4.2.3. Growth and development of single and double mutants

Since the double mutant exhibited several defects, and the single mutants showed a tendency to slightly retarded growth, development of wild type and mutant lines was tracked in detail, using the plate-based and soil-based phenotyping approach by Boyes et al (Boyes et al., 2001). This method uses the BASF, Bayer, Ciba-Geigy, Hoechst (BBCH) scale to define different *Arabidopsis* growth stages throughout the whole life span, from seed imbibition to seed maturation. The plate-based approach has a focus on early development, encompassing germination and the early vegetative phase. 100 seeds per genotype of Col-0, *djc31*, *djc62* and *djc31 djc62* were put out on ½ MS plates and scored regarding reaching the growth stages of seed imbibition, radicle emergence, hypocotyl and cotyledon emergence, cotyledons fully opened, two rosette leaves >1 mm and four rosette leaves >1 mm. Because of the strong root phenotype of the double mutant, root development was excluded from the analysis. The plates were discarded on day 21, since Col-0, *djc31*, and *djc62* had reached all growth stages to be analyzed and no progression of growth could be observed anymore for *djc31 djc62*.

Table 8: Plate-based phenotyping. Mean values indicate the average duration of reaching the indicated growth stage, with standard deviations (SD)

	Seed imbibition		**Radicle emergence**		**Hypocotyl and Cotyledon emergence**		**Cotyledons fully open**		**2 Rosette leaves**		**4 Rosette leaves**	
	Mean	**SD**	**Mean**	**SD**	**Mean**	**SD**	**Mean**	**SD**	**Mean**	**SD**	**Mean**	**SD**
Col-0	1.00	0.00	2.92	0.54	3.97	0.49	5.12	0.56	10.03	0.86	13.35	1.23
djc31 djc62	1.00	0.00	3.24	1.18	4.49	1.21	8.45	3.04	12.37	2.11	15.55	2.13
djc31	1.00	0.00	2.57	0.49	3.65	0.48	5.18	1.18	10.13	0.63	13.62	0.78
djc62	1.00	0.00	2.77	0.42	3.84	0.37	5.13	0.70	10.34	0.85	14.18	1.22

Based on the plate-based phenotyping, the single mutants grew comparable to wild type. However, growth of the *djc31 djc62* seedlings was severely retarded and showed a high degree of variability (Table 8). Inspection of the plates on day 21 showed a uniform appearance for wild type and single mutants, whereas the *djc31 djc62* mutant grew very heterogenous and exhibited seedlings in different growth stages (Figure 21). Therefore, seedlings were quantified regarding reaching the different growth stages. For Col-0, *djc31* and *djc62* more than 90% of the seedlings reached all growth stages analyzed. For *djc31 djc62*, a growth arrest after opening of the cotyledons was observed and only 68% of the *djc31 djc62* seedlings continued to grow and 64% reached the four rosette leaves stage in this experiment (Figure 21).

The soil-based phenotyping covers later growth stages from leaf development, over flowering to seed maturation (Boyes et al., 2001). For this experiment the growth stages four rosette leaves >1 mm, six rosette leaves >1 mm, ten rosette leaves >1 mm, first flower buds visible, first flower open and flowering complete were chosen and 25 plants per genotype were analyzed individually. Additionally to Col-0, single and double mutants, also the complementation lines 35S::*DJC31* and 35S::*DJC62* were included in this experiment, to verify full complementation of the phenotype. Plants were discarded when most of the siliques were ready to be harvested. *djc31 djc62* exhibited slower growth in all analyzed growth stages. Especially the flowering period was tremendously elongated with high variability between the different plants (Table 9). Rosette leaves growth of *djc31* and *djc62* was comparable to wild type. Appearance of the first flower buds was slightly delayed, but further flower development, silique formation and ripening were comparable to wild type. Furthermore, the complementation lines did not show a strong growth retardation or any defects in development. That confirms that transformation of *djc31 djc62* with either *djc31* or *djc62* did not only complement the morphological phenotype, but also restored normal growth and development (Figure 21).

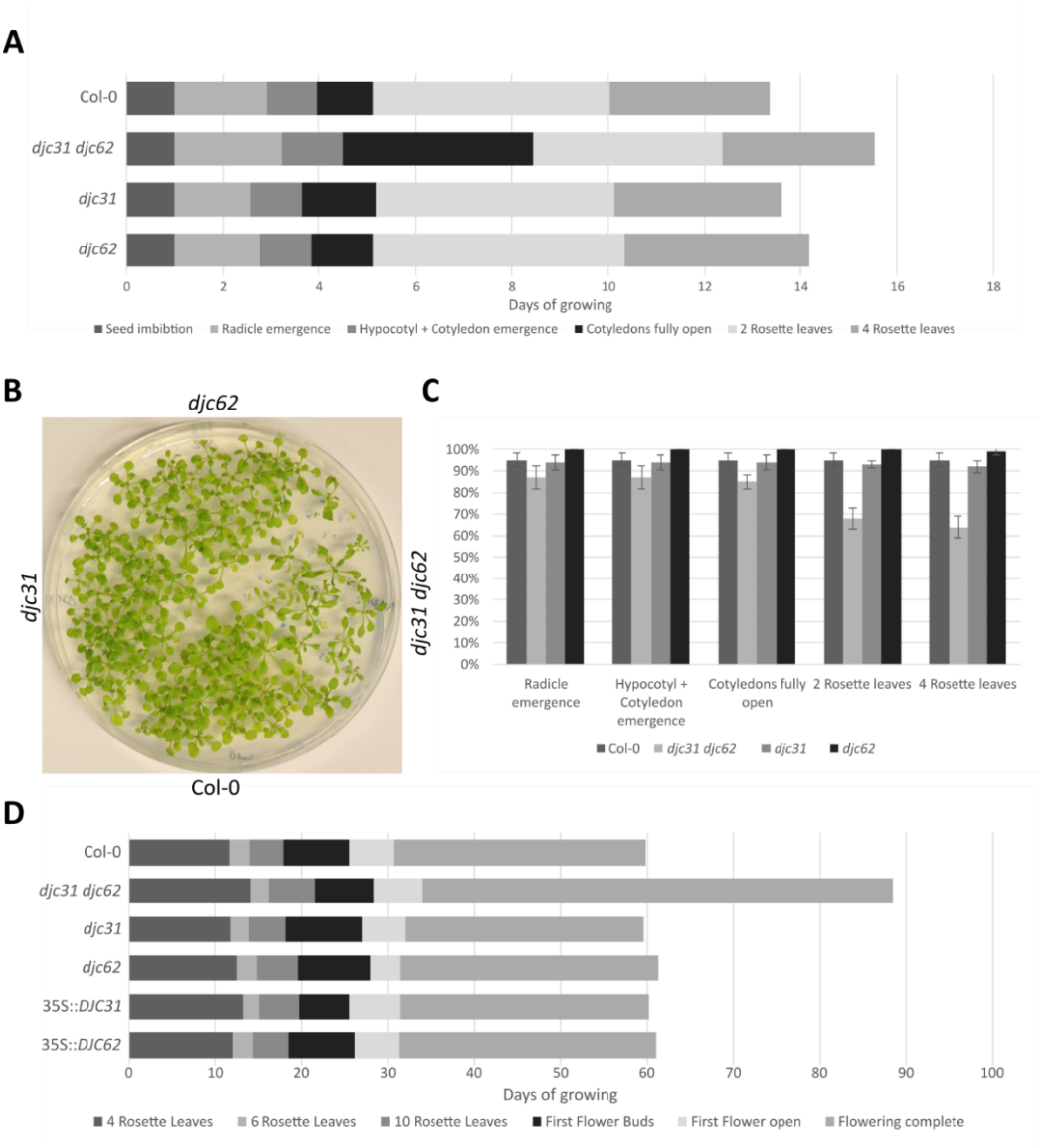

Figure 21: Plate-based and soil-based phenotyping.

A) Plate based phenotyping for observation of early development from seed imbibition to early leaf development of wild type (Col-0) double mutant (*djc31 djc62*) and single mutants (*djc31* and *djc62*); n=100/genotype. The analyzed growth stages were chosen as suggested by Boyes et al.2001. The experiment was stopped at day 21. Progression of development was comparable between wild type and the single mutants. The double mutant showed a developmental delay in all growth stages.

B) Photograph of the seedlings used for plate-based phenotyping at day 21. Col-0, *djc31* and *djc62* showed synchronous growth, whereas for *djc31 djc62* seedlings in different growth stages could be observed.

C) Quantification of seedlings which have reached the respective growth stages. Most seedlings of Col-0, *djc31* and *djc62* have reached all growth stages observed within the experimental period. For *djc31 djc62*, approximately 20% of the seedlings showed a growth arrest at the cotyledon stage. Error bars represent the standard deviation.

D) Soil based phenotyping encompassing leaf development, flower development and silique ripening for wild type (Col-0) double mutant (*djc31 djc62*), single mutants (*djc31* and *djc62*) and complementation lines (35S::*DJC31*, 35S::*DJC62*). Growth stages were chosen according to Boyes et al 2001. The experiment was stopped when the siliques were ready to be harvested. Wild type, single mutants and complementation lines showed an overall comparable development. *djc31 djc62* plants showed a developmental delay in all growth stages and a tremendously elongated flowering period

Table 9: Soil-based phenotyping. Mean values indicate the average duration of reaching the indicated growth stage, with standard deviations (SD)

	4 Rosette leaves		6 Rosette leaves		10 Rosette leaves		First flower buds		First flower open		Flowering complete	
	Mean	**SD**	**Mean**	**SD**	**Mean**	**SD**	**Mean**	**SD**	**Mean**	**SD**	**Mean**	**SD**
Col-0	11.56	0.57	13.96	0.82	17.96	0.66	25.56	1.20	30.68	1.38	59.92	2.00
djc31 djc62	14.04	1.20	16.17	1.09	21.57	1.91	28.30	5.67	33.91	5.95	88.50	2.60
djc31	11.68	0.79	13.76	0.86	18.12	0.91	26.96	1.14	31.92	1.57	59.60	1.96
djc62	12.44	1.20	14.80	1.55	19.56	2.42	28.00	2.02	31.35	2.06	61.36	1.47
35S::*DJC31*	13.15	1.19	15.05	1.36	19.70	1.58	25.50	1.43	31.35	1.74	60.20	1.99
35S::*DJC62*	12.00	0.69	14.29	0.88	18.48	1.10	26.14	1.46	31.24	1.23	61.05	1.70

4.3. Determination of the subcellular localization

4.3.1. Analysis of potential targeting signals

Targeting of newly synthesized proteins to their destined place of action is crucial for proper function of different cellular processes. To find the right destination, proteins of the endoplasmic reticulum, chloroplasts and mitochondria carry special targeting sequences at the N-terminus to facilitate transport to the right organelle and translocation across the membrane (Kunze & Berger, 2015).

In a previous *in silico* study on *Arabidopsis* TPR proteins, in which different prediction tools were used, DJC31 and DJC62 have been predicted to localize either to the nucleus or the chloroplast (Prasad et al., 2010). This result has been experimentally verified by chloroplast import experiments, whereas import rates for the full-length proteins were rather low. Truncated forms of DJC31 and DJC62 could be successfully imported but yielded more than one mature form (Chiu et al., 2013). TargetP 1.1 predicted DJC31 and DJC62 to be located in the chloroplast, with a transit peptide of 48 amino acids in length for DJC31 and a transit peptide of only four amino acids for DJC62. However, the most recent version of TargetP does not detect any signal sequences in neither of the two proteins. To validate the presence of a chloroplast transit peptide, the first 80 amino acids of DJC31 (DJC31-TP-GFP) and DJC62 (DJC62-TP-GFP) were fused to GFP and were transiently expressed in tobacco via agrobacteria mediated transformation. Protoplasts were isolated from transformed leaves and imaged by confocal fluorescent microscopy. For both constructs, localization to the chloroplasts could not be observed. DJC31-TP-GFP was visible as spots in the cytosol and the nucleus. DJC62-TP-GFP localized mainly to the nucleus (Figure 22). Therefore, it can be concluded, that DJC31 and DJC62 do not contain a chloroplast transit peptide.

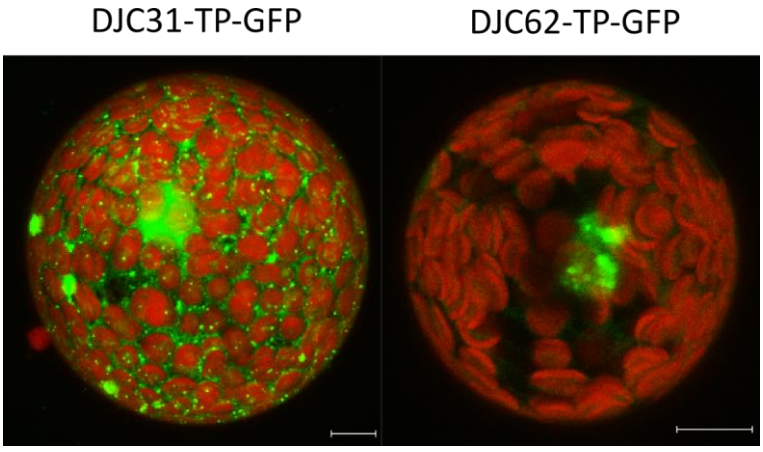

Figure 22: DJC31 and DJC62 do not contain a chloroplast transit peptide.

The first 80 amino acids of DJC31 and DJC62 were C-terminally tagged with GFP and transiently expressed in tobacco. GFP was imaged in protoplasts. DJC31-TP-GFP was observed to be distributed in the cytosol and the nucleus, whereas DJC62-TP-GFP was mainly visible in the nucleus. Scale bar = 10 µm

4.3.2. DJC31 and DJC62 localize to the endoplasmic reticulum

Since the presence of a chloroplast transit peptide could not be confirmed, GFP localization studies were again performed with DJC31 and DJC62 to determine the precise subcellular localization. Unfortunately, a fusion construct of either DJC31 or DJC62 with GFP at the C-terminus, could not be expressed in tobacco leaves or *Arabidopsis* protoplasts. Therefore, only the N-terminal half of either DJC31 (DJC31Int-GFP) and DJC62 (DJC62Int-GFP) was C-terminally fused to GFP. In a first test expression, GFP was mainly observed surrounding the nucleus with net-like structures extending towards the plasma membrane (data not shown). Since this pattern indicated localization to the secretory pathway, DJC31Int-GFP and DJC62Int-GFP were co-expressed with compartment markers for the endoplasmic reticulum and the Golgi apparatus in *Arabidopsis* protoplasts by transient protoplast transfection. The ER marker consists of the signal peptide of the *Arabidopsis* WALL-ASSOCIATED KINASE 2 fused to mCherry, carrying a C-terminal HDEL ER retention signal. The Golgi marker is composed of the first 49 amino acids of the soybean α-1,2 mannosidase I fused to mCherry (Nelson et al., 2007; Saint-Jore-Dupas et al., 2006). For analyzing co-localization with chloroplasts, the chlorophyll autofluorescence was used.

An overlay between the GFP signal of DJC31Int-GFP or DJC62Int-GFP and the chlorophyll autofluorescence could not be observed, confirming the previous result, that DJC31 and DJC62 do not contain a chloroplast transit peptide. Comparing the localization pattern of the ER marker with the GFP signal of DJC31Int-GFP and DJC62Int-GFP showed, that both fluorescent signals match each other, indicating that DJC31 and DJC62 localize to the endoplasmic reticulum (Figure 23). However, comparing the Golgi marker with DJC31Int-GFP and DJC62Int-GFP did not show an overlay of the GFP and mCherry signals. From that, it can be concluded that DJC31 and DJC62 localize to the endoplasmic reticulum but are not further transported along the secretory pathway to e.g. the Golgi apparatus.

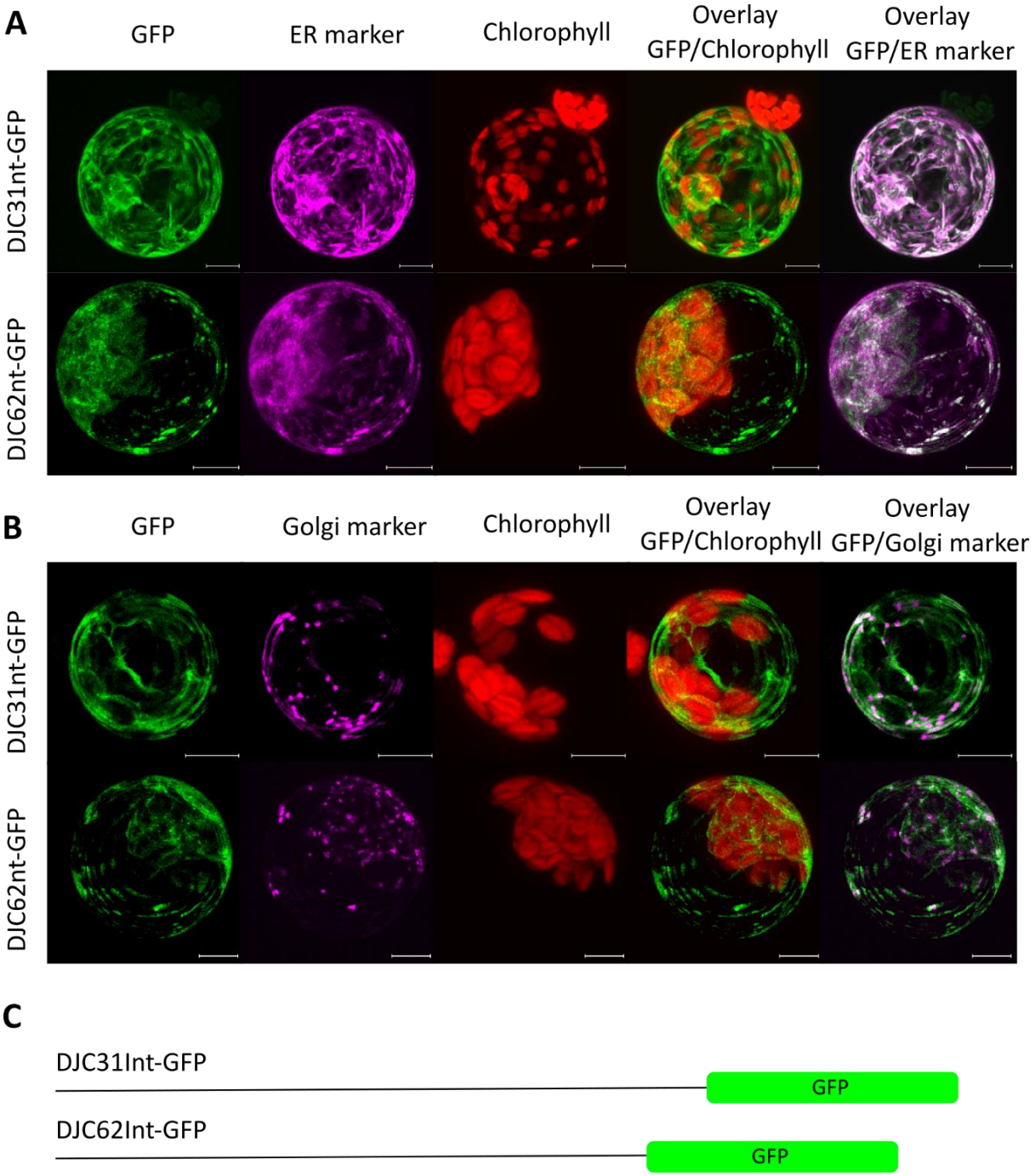

Figure 23: DJC31 and DJC62 localize to the endoplasmic reticulum (ER).

A-B) For determination of the subcellular localization, the N-terminal part of DJC31 and DJC62 was C-terminally fused to GFP and co-expressed with either a mCherry based ER marker (A) or Golgi marker (B). The GFP distribution pattern of DJC31Int-GFP and DJC62Int-GFP was comparable with the pattern of the ER marker. Scale bar = 10 µm.

C) Schematic overview of the constructs used for determination of subcellular localization.

To biochemically confirm this observation, a western blot was performed with isolated chloroplasts and microsomal membranes. The samples were separated via SDS-PAGE and after western blotting probed with antibodies directed against the N-terminus of DJC31 or DJC62. The ER resident HSP70 family protein BiP was used as ER control and FNR, located in the chloroplast stroma and at the thylakoid membranes, was used as chloroplast control. As it can be seen from the FNR bands, microsomes contained contaminations from plastidal membranes but DJC31 and DJC62 were exclusively detected in microsomal membranes and not in the chloroplast sample, which fits to previous results (Figure 24). Therefore, localization to the chloroplast can finally be excluded.

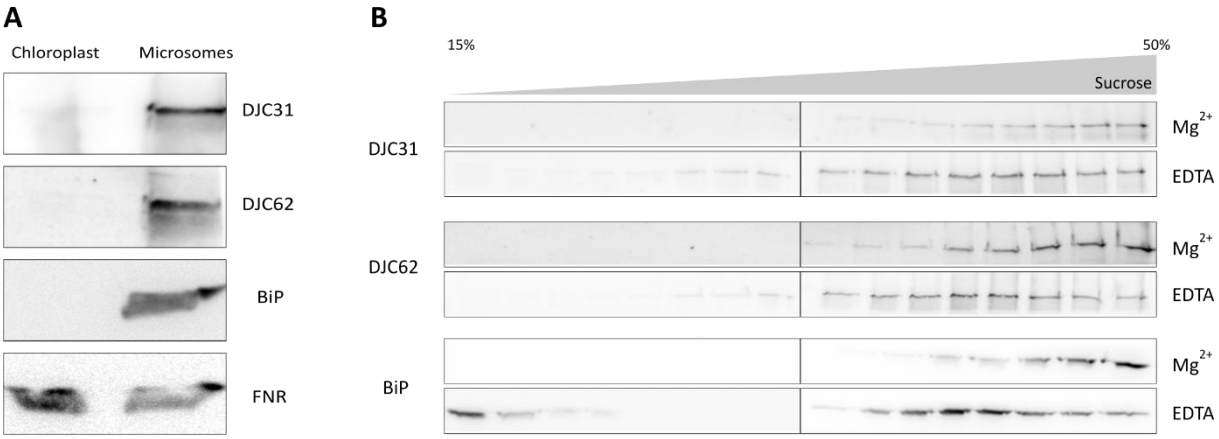

Figure 24: Biochemical confirmation of the ER localization.

A) Isolated chloroplasts and microsomal membranes were probed with antibodies against DJC31 and DJC62 to exclude a plastidal localization and confirm the localization to the endoplasmic reticulum. BiP was used as microsomal control and FNR as chloroplast control.

B) Microsomal membranes were isolated with either Mg^{2+} or EDTA. Subsequently, microsomes were loaded onto a linear 15-50% sucrose gradient. Fractions were loaded onto an 8% SDS-gel and after western blotting probed with specific antibodies against DJC31, DJC62 and BiP as endoplasmic reticulum control. The lack of Mg^{2+} in the buffer leads to a shift of the ER membranes to lighter fractions due to removal of ER associated ribosomes. This shift is an indicator for ER resident proteins and was observed for both DJC31 and DJC62.

Microsomal membranes do not only contain membranes derived from the endoplasmic reticulum, but also from the Golgi apparatus, plasma membrane and the outer mitochondrial membrane (Fujiki et al., 1982). To distinguish between ER membranes and other membranes, a microsomal shift assay can be performed. This experiment is based on the biological feature, that ribosomes are attached to the ER membrane in presence of Mg^{2+}. If the membranes are treated with EDTA, to remove Mg^{2+}, ribosomes detach from the ER and isolated membranes exhibit a shift to lighter density fractions within a linear sucrose gradient (Schweiger et al., 2012). To analyze DJC31 and DJC62 regarding a shift in a sucrose gradient, to validate the ER localization, microsomal membranes were isolated with buffer either containing Mg^{2+} or EDTA. Isolated microsomes were loaded onto a linear sucrose gradient containing either Mg^{2+} or EDTA, with a sucrose concentration ranging from 15-50%. After ultracentrifugation, the

gradient was divided in different fractions. The fractions were loaded onto SDS-gels, blotted and probed with specific antibodies against DJC31, DJC62 and BiP as ER luminal control. BiP exhibited a pattern, typical for ER resident proteins. Accumulation in dense fractions was observed in presence of Mg^{2+}, and a shift to lighter density fractions upon treatment with EDTA. A similar behavior was observed for both DJC31 and DJC62, which were detected in higher density fractions if isolated with Mg^{2+} and a shift to lighter fractions in presence of EDTA (Figure 24). This result clearly confirms a localization of DJC31 and DJC62 to the endoplasmic reticulum.

Usually, proteins located in the endoplasmic reticulum carry an N-terminal signal peptide which directs them to the right organelle, enables translocation across the membrane and is cleaved off in the ER lumen (Kunze & Berger, 2015). Additionally, many soluble ER resident proteins contain a C-terminal K/HDEL retention motif, which prevents them from being secreted (Robinson & Aniento, 2020). Neither a predictable signal peptide, nor an ER retention motif could be found in the amino acid sequences of DJC31 and DJC62, which raises the question, whether these proteins are located inside the ER lumen or localize to the endoplasmic reticulum from the cytosolic side. To answer this question, a split-GFP approach was chosen, based on the split-GFP vector system developed by Xie et al., which was originally designed for topology studies on membrane proteins. GFP consists of eleven β-sheets. If the first ten β-sheets (GFP1-10) and β-sheet eleven (GFP11) are separated and co-expressed, they are able to self-assemble into a functional fluorescent protein. This biochemical feature of GFP is used in this experiment with modified constructs of GFP1-10, which localize to different cellular compartments. GFP1-10 without modifications is located in the cytosol. The ER luminal GFP 1-10 (SP-GFP1-10-HDEL) contains the signal peptide of PATHOGENESIS-RELATED GENE 1 (PR-1) at the N-terminus and the HDEL retention motif at the C-terminus (Xie et al., 2017). Co-expression with a protein fused to GFP11 should only show a GFP signal, if GFP1-10 or SP-GFP1-10-HDEL and the protein of interest are present in the same compartment. To validate this experiment, GFP1-10 and SP-GFP1-10-HDEL were transiently co-expressed in tobacco leaves with either GFP11-HSP70.1, one of the cytosolic HSP70 family proteins, or BiP2-GFP11, a HSP70 family protein located in the ER lumen. As expected, only co-expression of cytosolic GFP1-10 with GFP11-HSP70.1 and luminal SP-GFP1-10-HDEL with BiP2-GFP11 showed a green fluorescent signal, confirming that the system is suitable to distinguish between cytosol and ER lumen. In a next step GFP1-10 and SP-GFP1-10-HDEL were co-expressed in tobacco leaves with the N-terminal half of either DJC31 or DJC62, carrying GFP11 at the C-terminus (DJC31Int-GFP11, DJC62Int-GFP11). A GFP signal was exclusively observed, if DJC31Int-GFP11 or DJC62Int-GFP11 were co-expressed with the cytosolic GFP1-10, indicating that DJC31 and DJC62 localize to the cytosolic side of the ER membrane (Figure 25).

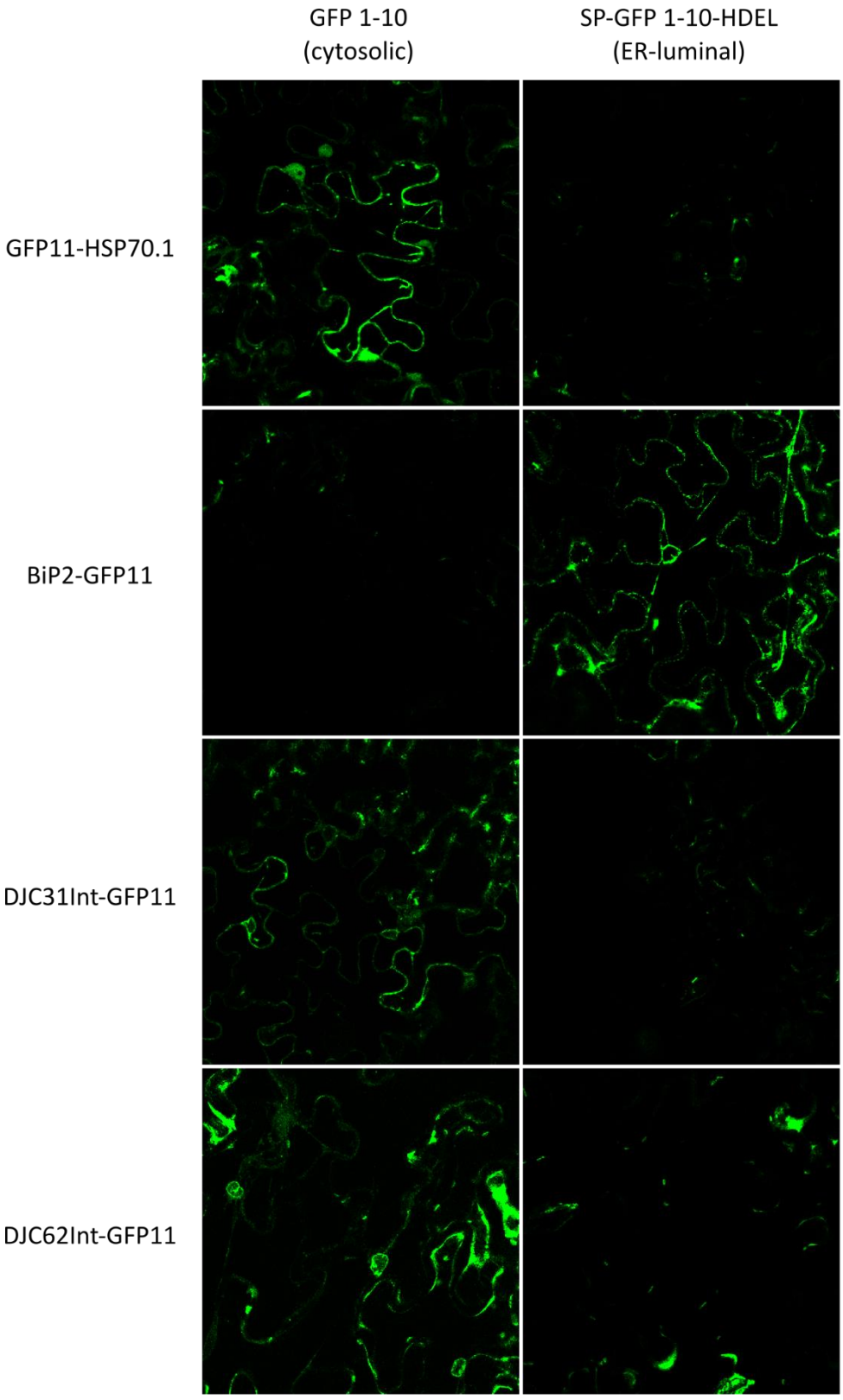

Figure 25: DJC31 and DJC62 are located on the cytosolic side of the ER membrane

For discrimination between cytosol and ER lumen, DJC31Int and DJC62Int were C-terminally fused to GFP11 and co-expressed in tobacco leaves either with GFP1-10 (cytosolic) or SP-GFP1-10-HDEL (ER-luminal). Cytosolic HSP70.1 and luminal BiP fused to GFP11 were used as controls

4.3.3. DJC31 and DJC62 are associated to the ER membrane

Previous predictions of hydrophobicity using the Kyte-Doolittle scale have indicated, that DJC31 and DJC62 do not contain transmembrane domains or hydrophobic regions that might mediate peripheral attachment to membranes. However, DJC31 and DJC62 could only be detected via western blot in isolated microsomal membranes. Together with the subcellular distribution pattern, which looks identical to the localization of the ER marker, this finding hints to attachment of DJC31 and DJC62 to the ER membrane. To analyze this in more detail isolated microsomes were treated with different buffers for 30 min on ice. Na_2CO_3 for alkaline pH conditions, 1 M NaCl for high salt conditions, 6 M urea for denaturing conditions, 1% SDS to extract integral membrane proteins and Tris buffer as control. The samples were separated into pellet and soluble fraction via ultracentrifugation and analyzed via western blot.

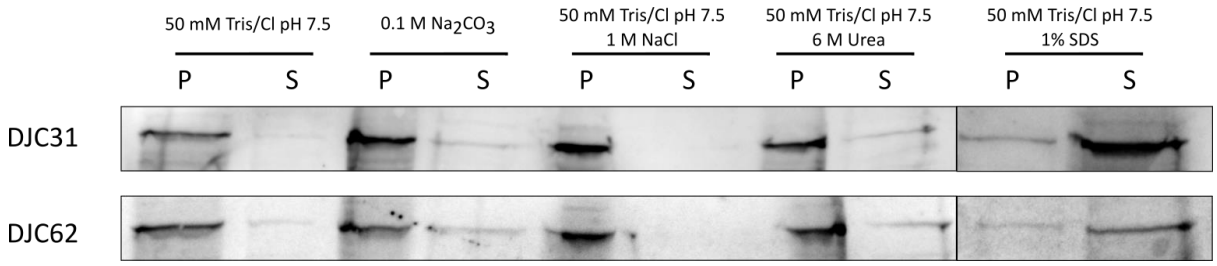

Figure 26: DJC31 and DJC62 are attached to the ER membrane.

Isolated microsomal membranes were incubated in buffer, 0.1 M Na_2CO_3, 1 M NaCl, 6 M Urea and 1% SDS for 30 min on ice. After ultracentrifugation, pellet (P) and soluble (S) fractions were loaded onto an SDS-gel and after western blotting probed with antibodies against DJC31 and DJC62. Both proteins could be washed off the membrane under alkaline and denaturing conditions.

Isolated microsomes treated with carbonate are known to transform from vesicles into open membrane sheets, releasing proteins which are contained in the vesicle lumen. Furthermore, it was observed that carbonate can be used to remove ribosomes from rough ER membranes, indicating that peripherally attached proteins can also be removed using carbonate (Fujiki et al., 1982). Carbonate treatment of microsomes showed, that both DJC31 and DJC62 can partially be removed from the ER membrane and can be found in the supernatant after ultracentrifugation. A similar result could be obtained under denaturing conditions after treatment with 6 M urea. Applying 1% SDS, a strong detergent, solubilized the membranes and released most of DJC31 and DJC62 into the soluble fraction (Figure 26). From this result it can be concluded, that DJC31 and DJC62 attach to the ER membrane.

Since for the determination of subcellular localization only the N-terminal halves of DJC31 and DJC62 were used, the localization experiment was repeated using the C-terminal halves of DJC31 (GFP-31TPR+J) and DJC62 (GFP-62TPR+J), which contain the TPR and J-domains, to see, whether the N-terminus alone determines localization to the ER membrane. The N-terminus was replaced by GFP

and the constructs were co-expressed with an ER-marker in *Arabidopsis* protoplasts via transient protoplast transfection. Compared to the previous experiment, in which the DJC31/DJC62 N-terminus fused to GFP perfectly matched the pattern of the ER marker, the C-terminal part of DJC31 or DJC62, with a GFP on its N-terminal side, appeared to be more distributed in the cytosol, confirming that mainly the N-terminal part of the proteins is responsible for targeting and tethering of DJC31 and DJC62 to the ER membrane (Figure 27).

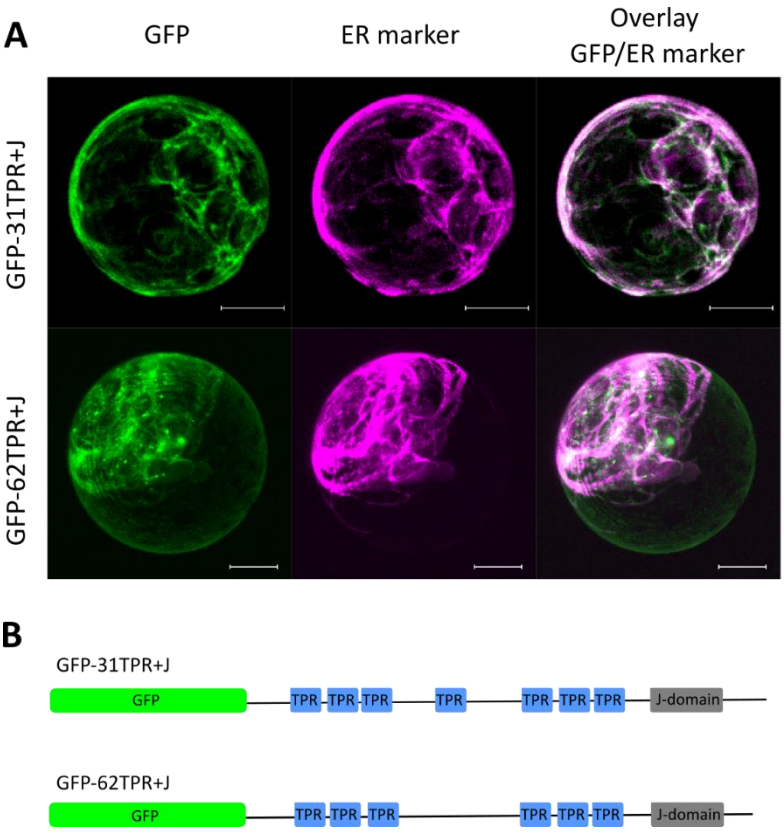

Figure 27: Attachment to the ER membrane is mediated by the N-terminus.

A) The C-terminal part of DJC31 and DJC62, containing the TPR repeats and the J-domain, was N-terminally fused to GFP and co-expressed with an ER marker in *Arabidopsis* protoplasts. The GFP signal did not overlap properly with the ER marker and showed a more distributed pattern in the cytosol.

B) Schematic overview of the constructs used. Scale bar = 10 µm.

In addition to the experiments using truncated versions of DJC31 and DJC62, the localization experiments should be repeated with the full-length proteins, but previous experiments, fusing GFP to the C-terminus of DJC31 and DJC62 did not show expression of the fusion constructs in tobacco leaves. Since the cytosolic localization was clearly demonstrated, the risk of proteolytic cleavage at the N-terminus due to the removal of a signal peptide could be excluded. Therefore, a N-terminal GFP fusion to the full length DJC31 and DJC62 was generated to confirm the cytosolic localization to the ER membrane. Surprisingly, expression of GFP-DJC31 and GFP-DJC62 in *Arabidopsis* protoplast by transfection, exhibited a similar result as observed for GFP-31TPR+J and GFP-62TPR+J. The GFP pattern

did not properly overlap with the ER marker and GFP-DJC31 and GFP-DJC62 seemed to be more spread in the cytosol (Figure 28). This result indicates, that the GFP at the N-terminus disturbs attachment to the ER membrane.

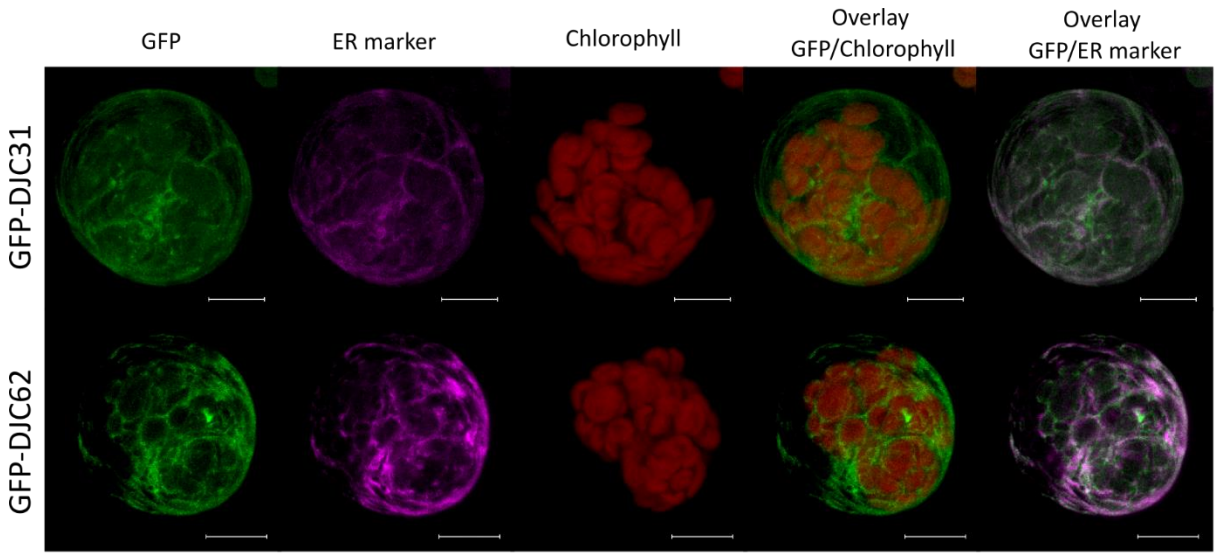

Figure 28: N-terminal GFP disturbs membrane attachment.

DJC31 and DJC62 were fused N-terminally to GFP and were co-expressed with an ER marker in *Arabidopsis* protoplasts. The GFP signal did not perfectly match with the pattern of the ER marker, indicating that the N-terminal GFP might disturb membrane attachment. Scale bar = 10 µm

To analyze, whether attachment to the membrane is crucial for protein function, 35S::*GFP-DJC31* or 35S::*GFP-DJC62* was transformed into *djc31 djc62* via stable agrobacteria mediated transformation. After selection, successful transformation was tested via RT-PCR. Furthermore, microsomes were isolated from seedlings to confirm the presence of the GFP-tagged proteins by western blotting, using antibodies against DJC31, DJC62 and BiP as a loading control (Figure 29). Although the whole protein sequence was present, GFP-DJC31 and GFP-DJC62 could not rescue the mutant phenotype, which indicates that the N-terminal GFP interferes with functional processes, e.g. membrane attachment, as it could already be seen in the fluorescence microscopic analysis of transfected protoplasts, expressing GFP-DJC31 or GFP-DJC62.

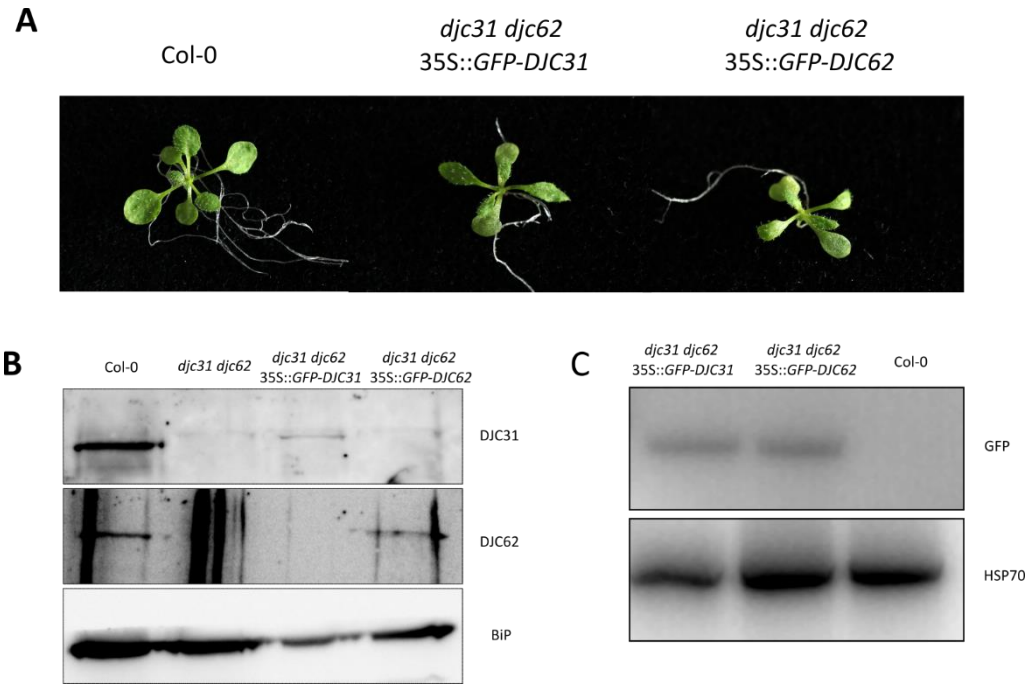

Figure 29: Stable transformation of *djc31 djc62* with GFP-DJC31 or GFP-DJC62.

A) *djc31 djc62* plants were stably transformed with either GFP-DJC31 or GFP-DJC62. The GFP-fusion constructs could not rescue the mutant phenotype.

B) A western blot using microsomal membranes isolated from Col-0, *djc31 djc62*, *djc31 djc62* 35S::*GFP-DJC31* and *djc31 djc62* 35S::*GFP-DJC62* was used to confirm the presence of the GFP-tagged proteins. BiP was used as loading control.

C) To confirm successful stable transformation of *djc31 djc62* with 35S::*GFP-DJC31* or 35S::*GFP-DJC62*, RT-PCR was performed using a primer pair against the GFP-tag and *HSP70* as control.

4.4. DJC31 and DJC62 are potential cytosolic co-chaperones

DJC31 and DJC62 were predicted to contain several TPR repeats, which form two carboxylate clamp type TPR domains. Additionally, both proteins possess a J-domain at the C-terminus, which acts as the activator of the HSP70 ATPase (Kampinga & Craig, 2010). From these two features it can be assumed that DJC31 and DJC62 may act as cytosolic co-chaperones of either HSP70 and/or HSP90. *Arabidopsis* contains 18 HSP70 proteins, located in different cellular compartments, from which 14 belong to the DnaK-type HSP70 proteins. Five of them could be detected in the cytosol (Lin et al., 2001). For HSP90, seven proteins can be found in the *Arabidopsis* genome, of which four HSP90 proteins are located in the cytosol (Krishna & Gloor, 2001).

4.4.1. DJC31 and DJC62 interact with HSP70 and HSP90

To find out, whether DJC31 and DJC62 interact with cytosolic chaperones, bimolecular fluorescence complementation (BiFC) was performed with HSP70.1 and HSP90.2. This method is based on the assembly of two separately expressed N- and C-terminal fragments of different fluorescent proteins, which are fused to the proteins to be tested for interaction. The two fluorescent protein fragments are

not functional and not able to spontaneously assemble into a functional fluorophore. If the proteins of interest interact, the contact between the two fluorophore fragments is close enough to assemble and refold into a functional fluorescent protein (Gehl et al., 2009).

DJC31 and DJC62 were N-terminally fused to the C-terminal part of the cyan fluorescent protein SCFP3a (SCFP^{C}-DJC31, SCFP^{C}-DJC62); HSP70.1 and HSP90.2 were fused to the N-terminal part of the yellow fluorescent protein Venus (VYNE^{N}-HSP70.1, VYNE^{N}-HSP90.2). SCFP^{C}-DJC31 or SCFP^{C}-DJC62 were co-transfected in *Arabidopsis* protoplasts with either VYNE^{N}-HSP70.1 or VYNE^{N}-HSP90.2, respectively. DJC31 as well as DJC62 were observed to interact with HSP70.1 and HSP90.2, which supports, that DJC31 and DJC62 might act as co-chaperones in cooperation with different cytosolic members of the HSP70 and HSP90 protein families (Figure 30).

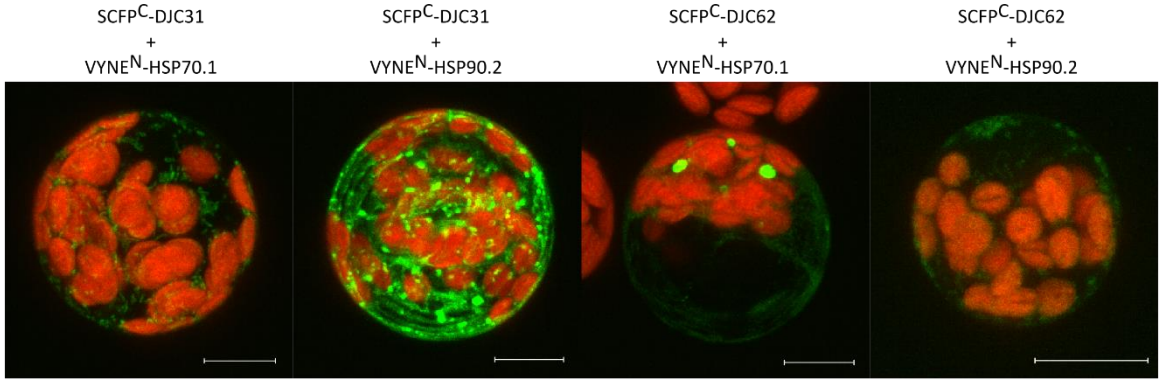

Figure 30: DJC31 and DJC62 interact with cytosolic HSP70 and HSP90.

DJC31 and DJC62 were fused to the C-terminal part of SCFP. HSP70.1 and HSP90.2 were fused to the N-terminal half of VYNE. DJC31 and DJC62 BiFC-constructs were co-expressed in Arabidopsis protoplasts with either the HSP70 or HSP90 BiFC construct respectively. Scale bar = 10 µm

4.4.2. Activation of the HSP70 ATPase domain is essential for the function of DJC31 and DJC62

The main function of the J-domain is activating the ATPase domain of HSP70, thus inducing the chaperone to bind a client protein. Essential for activation is the highly conserved HPD motif, which is located between helix II and III of the J-domain (Kampinga & Craig, 2010). Mutating this motif inhibits ATPase activation and creates an inactive co-chaperone. Besides their function as co-chaperones of HSP70, J-proteins can have additional functions, which are independent of the J-domain and the interaction with HSP70 but mediated by additional domains or regions outside the J-domain (Ajit Tamadaddi & Sahi, 2016). Considering that DJC31 and DJC62 contain several TPR repeats and were shown to interact with HSP90, it might be possible that their main function might be dependent on the interaction with HSP90. To analyze, whether the activation of HSP70 is important for the function of DJC31 and DJC62, loss of function mutants were generated by exchanging the histidine of the HPD motif, to glutamine (DJC31 H1052Q, DJC62 H1006Q). Subsequently, *djc31 djc62* plants were stably

transformed with either 35S::*DJC31 H1052Q* or 35S::*DJC62 H1006Q*. The loss of function variants of DJC31 and DJC62 could not complement the mutant phenotype of *djc31 djc62*, confirming that DJC31 and DJC62 act as co-chaperones of HSP70 and activation of the HSP70 ATPase domain is essential for the yet unknown process they are involved in. To confirm the presence of the mutant proteins a western blot was performed with isolated microsomes, using antibodies against DJC31 or DJC62 and BiP as loading control (Figure 31).

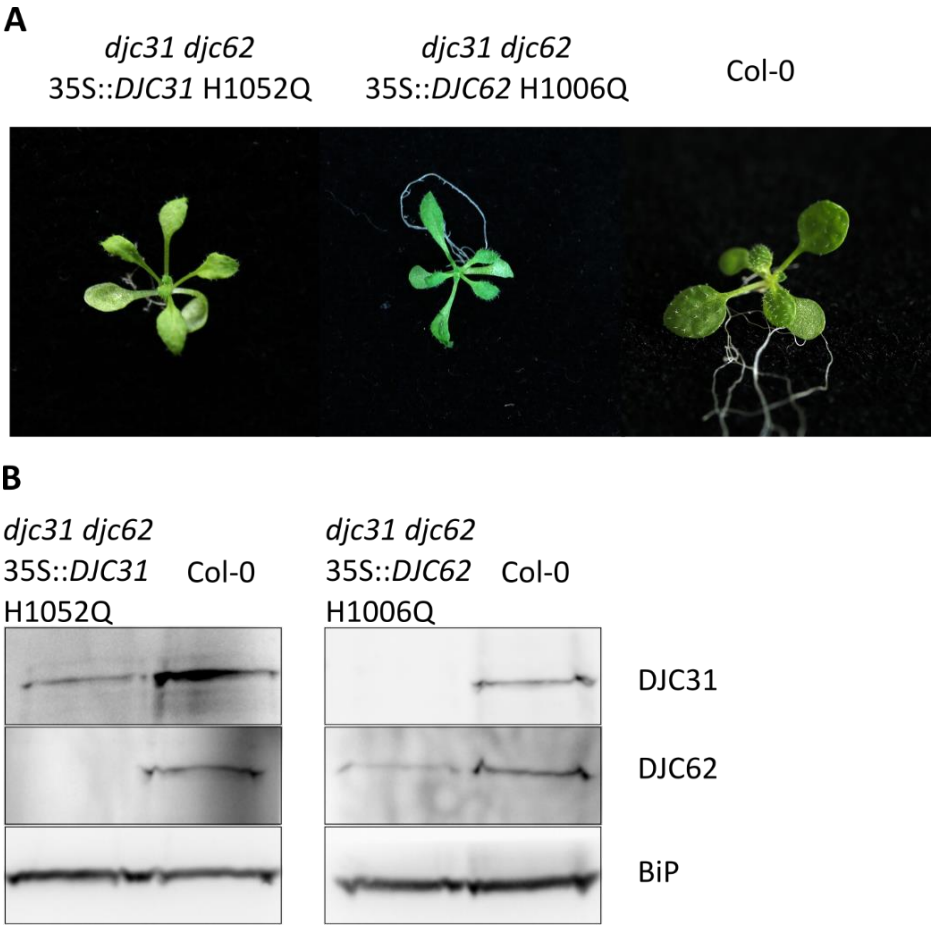

Figure 31: Interaction with HSP70 is essential for the function of DJC31 and DJC62.

A) The conserved HPD motif of DJC31 and DJC62 was mutated to QPD to inhibit activation of the HSP70 ATPase domain. Transformation of *djc31 djc62* with HPD mutant constructs could not complement the mutant phenotype.

B) Presence of the HPD mutant proteins was confirmed via western blot. Microsomal membranes isolated from 14 days old Col-0 and *djc31 djc62* 35S::*DJC31* H1052Q or *djc31 djc62* 35S::*DJC62* H1006Q were separated on an SDS gel and probed with antibodies against DJC31 and DJC62. BiP was used as loading control.

4.5. Yeast Two-Hybrid library screening

J-proteins are known for being mediators between client proteins and HSP70, thereby assisting in protein folding and preventing aggregation by binding to the respective client. Additionally, J-proteins are also involved in protein degradation and remodeling. Different J-proteins can have different client spectra, which can be broad or very specialized, depending on the J-protein structure and domain composition in addition to the J-domain (Kampinga & Craig, 2010). To find out more about potential clients and other interacting factors of DJC31 and DJC62, a yeast two-hybrid (Y2H) library screening was performed, using a normalized *Arabidopsis*, fragmented cDNA library.

The method is based on a bait protein, fused to the DNA binding domain of GAL4 (GAL4-BD), and a library consisting of prey proteins fused to the GAL4 activation domain (GAL4-AD). If bait and prey proteins interact, the GAL4 binding and activation domains are brought in proximity and activate the transcription of different reporter genes (Fields & Song, 1989). The Clontech yeast two-hybrid system uses four reporter genes under control of three unrelated promoters.

- *AUR1-C* under control of a M1 promoter encodes a mutant version of the *AUR1* gene, which encodes an inositol phosphoryl ceramide synthase, that confers resistance to Aureobasidin A.
- *His3* under control of a G1 promoter enables biosynthesis of histidine and promotes growth of yeast cells on medium lacking histidine.
- *ADE2* under control of a G2 promoter enables growth on medium lacking adenine
- *MEL1* is controlled by a M1 promoter and encodes an α-galactosidase, which is secreted and turns colonies blue in the presence of X-α-Gal in the medium.

4.5.1. Test experiments

To generate the Y2H bait constructs, the two genes *DJC31* and *DJC62* were cloned into the vector pGBKT7, which adds the amino acids 1-147 of the GAL4 DNA binding domain N-terminally to DJC31 (GAL4-BD-DJC31) or DJC62 (GAL4-BD-DJC62), respectively. Afterwards, the respective constructs were transformed into competent Y2HGold cells. To get a reliable screening result, the constructs were tested beforehand, regarding toxicity to the yeast strain, autoactivation of the reporter genes and expression of the fusion constructs.

In order to test expression and stability of the GAL4-BD fusion proteins, whole cell lysates, isolated from transformed yeast cells, were loaded in three different amounts onto an SDS gel. After western blotting, the membrane was probed with a c-myc antibody, which targets a c-myc epitope located between the GAL4-BD and the protein of interest. As a control, yeast cells transformed with an empty pGBKT7 were used. Additionally, the blot was stained with Coomassie to ensure equal loading. GAL4-BD-DJC31 as well as GAL4-BD-DJC62 were both expressed in yeast, but the band intensity for

GAL4-BD-DJC62 was much weaker, compared to GAL4-BD-DJC31. As it can be judged from Coomassie staining, amounts of total protein loaded was comparable between the different samples (Figure 32). Therefore, GAL4-BD-DJC62 seems to be not stable in yeast.

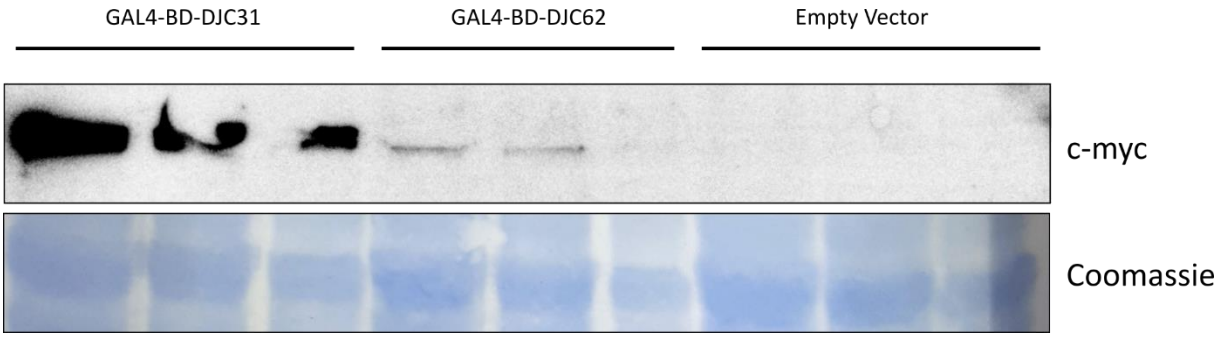

Figure 32: Expression and stability of the bait constructs was tested via western blot.

Total protein was isolated from transformed yeast cells and separated on an SDS gel. After western blotting, the membranes were probed with a c-myc antibody to confirm the presence of the GAL4-BD fusion proteins. As a negative control, yeast cells transformed with an empty vector were used. Both bait constructs could be detected, but GAL4-BD-DJC62 was strongly decreased. Coomassie staining was performed to ensure equal loading of the different samples.

To exclude toxicity of the bait constructs to the yeast cells, GAL4-BD-DJC31, GAL4-BD-DJC62 and an empty vector as control were transformed in Y2HGold cells and plated onto SD-Trp medium in a 1:10 dilution. After incubation for three days at 30°C, cells were evaluated regarding colony number and size. The number of colonies for GAL4-BD-DJC31 and GAL4-BD-DJC62 was comparable to the empty vector control. Also the diameter of the individual colonies was approximately equal (Figure 33). Accordingly, the bait constructs do not inhibit growth or decrease viability of the yeast cells.

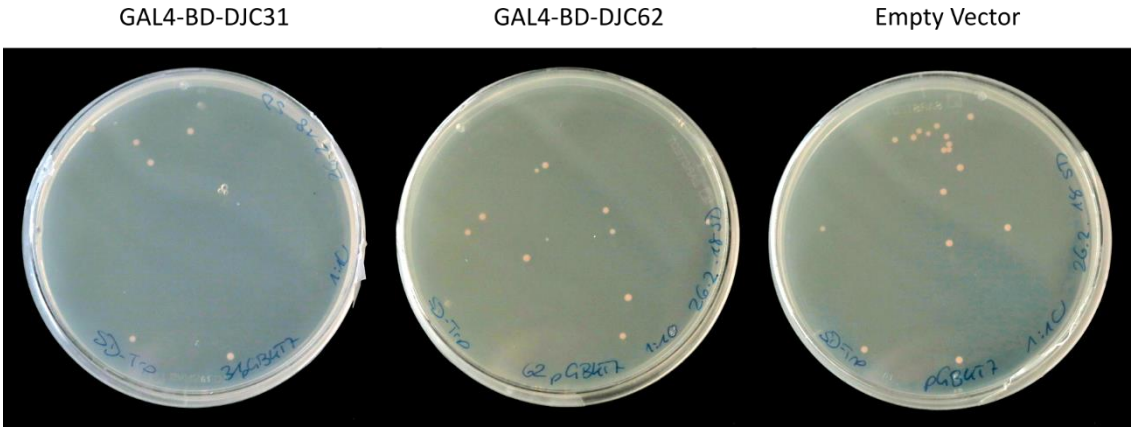

Figure 33: Test for toxicity to yeast cells.

To exclude interference of the bait constructs with cellular processes, which might lower the cell's viability, Y2HGold cells were transformed with GAL4-BD-DJC31, GAL4-BD-DJC62 and an empty pGBKT7 as control. Colony number and size, of yeast cells expressing the bait construct, was comparable to the empty vector control.

Next, a control mating was performed to check the different selection media and to adjust the concentrations for the selection markers Aureobasidin A and X-α-Gal. For the mating, the control vectors provided by the Y2H kit were transformed in either competent Y2HGold (bait strain) or Y187 cells (prey strain). The mating was set up as follows:

Positive control mating:	pGBKT7-53 in Y2HGold	x	pGADT7-T in Y187
Negative control mating:	pGBKT7-53 in Y2HGold	x	pGADT7-Lam in Y187

The mated culture was spread on different selection media in a 1:100 dilution: SD-Trp to test viability of the bait strain, SD-Leu to test viability of the prey strain, SD-Trp-Leu to select for diploid yeast cells after successful mating and SD-Trp-Leu +Aureobasidin A + X-α-Gal to select for the interaction between bait and prey proteins. For both positive and negative control mating, the bait and prey strains could be detected on SD-Trp and SD-Leu plates, respectively. Successful mating could be confirmed by colony growth on SD-Trp-Leu plates for the positive and the negative control. As expected for the negative control mating, no colonies could be observed on the SD-Trp-Leu plates containing Aureobasidin A and X-α-Gal, proving that the Aureobasidin A concentration is sufficient to suppress growth of yeast cells without interaction of the bait and prey proteins. On the positive control mating plates, growth of blue colonies was observable on the selection media, confirming that expression of the reporter genes and the respective gene products are working (Figure 34). From this pre-test it can be concluded that the media, additives and reporter gene products are fully functional and suitable for the planed library screening.

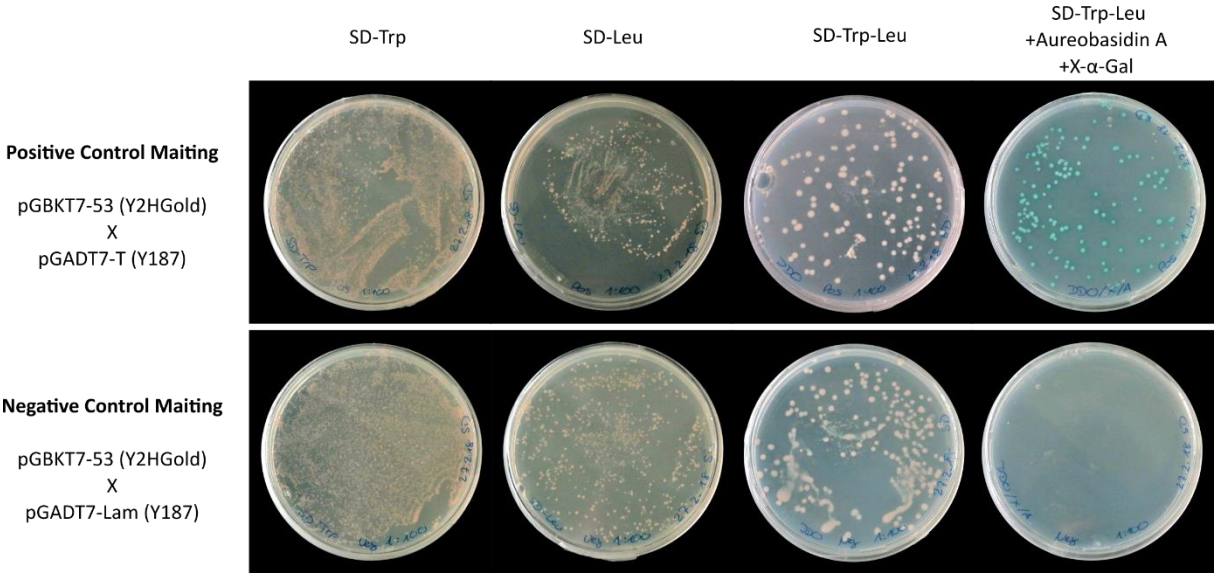

Figure 34: Control mating for media and experimental set up validation.

Yeast cells carrying the positive and negative control vectors were mated and spread on different selection media to test bait and prey strain viability, mating success and proper activation of reporter genes or selection markers.

Besides testing the media for proper selection, also the bait constructs GAL4-BD-DJC31 and GAL4-BD-DJC62 were tested before the library screening, to exclude autoactivation of the reporter genes. Y2HGold cells transformed with one of the two constructs, were plated in a 1:10 dilution on SD-Trp medium as a positive control, SD-Trp + X-α-Gal to check expression of the α-galactosidase and SD-Trp + Aureobasidin A to test for unspecific expression of the resistance gene. For Gal4-BD-DJC31, no blue colonies could be found on SD-Trp + X-α-Gal, demonstrating that the α-galactosidase is not unspecifically expressed in absence of a Gal4-AD. However, colonies of yeast cells containing Gal4-BD-DJC62 turned slightly blue on SD-Trp + X-α-Gal, indicating that the reporter gene is unspecifically activated. On SD-Trp +Aureobasidin A plates no colonies could be detected for both constructs (Figure 35). Therefore, the slight activation of the α-galactosidase gene by GAL4-BD-DJC62 could be neglected, since the two reporter genes are expressed under different promoters.

From the pre-experiments it could be concluded, that the constructs and media used were suitable for the screening and that selection of positive interactions could be considered to be safe, especially because positive colonies in the library screening were streaked out on higher stringency medium to reduce the occurrence of false positives.

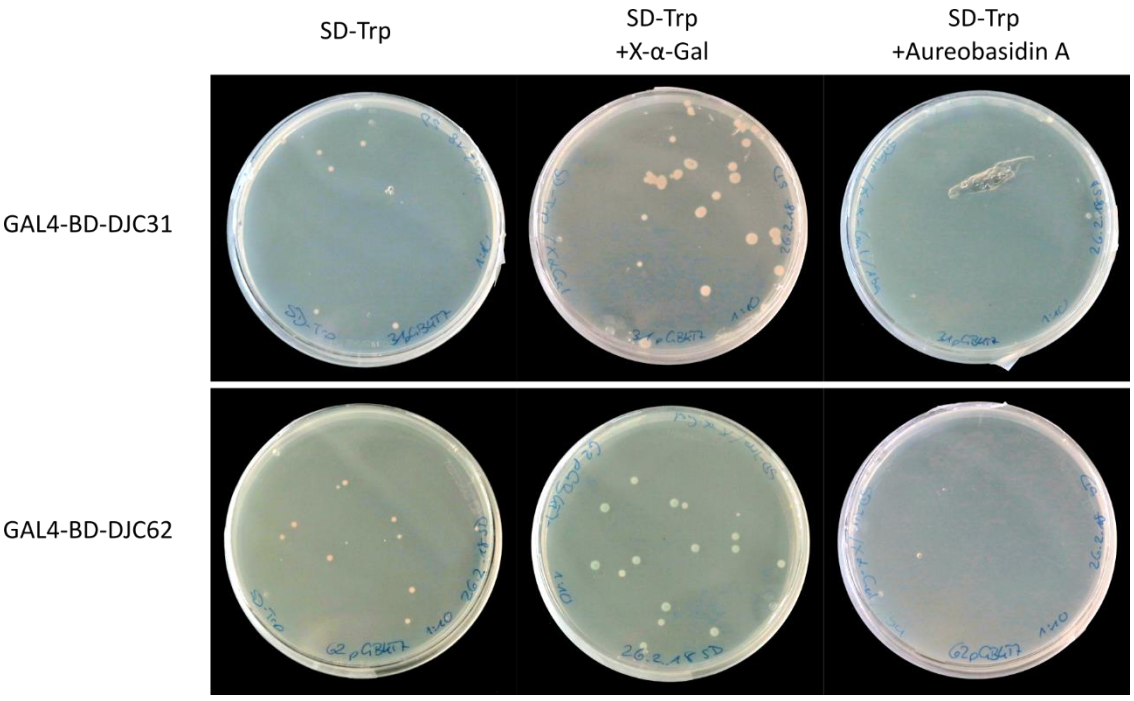

Figure 35: Test for reporter gene autoactivation.

DJC31 and DJC62 fused to Gal4-BD were transformed into Y2HGold cells and plated on SD-Trp +X-α-Gal or SD-Trp +Aureobasidin A to exclude activation of the reporter genes in absence of an interaction partner.

4.5.2. Yeast Two-Hybrid library screening

Y2HGold cells expressing either GAL4-BD-DJC31 or GAL4-BD-DJC62 were mated over night with the library strain. On the next day, the culture was checked under the microscope for the presence of zygotes as indicators of successful mating. Subsequently, the mating culture was spread in different dilutions on SD-Trp, SD-Leu and SD-Trp-Leu plates as controls for viability of the bait and prey strains and of the diploids after mating. The residual culture was plated on SD-Trp-Leu + Aureobasidin A + X-α-Gal plates and incubated at 30°C. After three days blue colonies from SD-Trp-Leu + Aureobasidin A + X-α-Gal plates were streaked out onto higher stringency SD-Trp-Leu-His-Ade + Aureobasidin A + X-α-Gal plates to eliminate false positives that have escaped the first round of selection. After five days the plates from the mating were checked again and remaining blue colonies were also transferred onto SD-Trp-Leu-His-Ade + Aureobasidin A + X-α-Gal plates. Surviving blue colonies on SD-Trp-Leu-His-Ade +Aureobasidin A + X-α-Gal plates were used for further analysis. For identification of the library fragment, a yeast colony PCR was performed, to amplify the library fragment for sequencing. The interaction partner was identified from the sequencing data using BLAST.

For DJC31, around 400 colonies were analyzed by sequencing. Removal of interaction partners occurring more than once resulted in a list of 115 potential candidates. To further analyze these proteins, they were grouped according to their subcellular localization and processes they are involved in. For determination of the subcellular localization SUBA4 was used. The majority of the proteins was assigned to the nucleus with 19.47%, followed by 16.81% cytosolic and 15.93% plastidal proteins. Only 4.42% were predicted to be ER resident and 12.39% to be secreted or present in the plasma membrane, respectively. Residual candidates were predicted to be in the mitochondria (8.85%), Golgi apparatus (6.19%), Vacuole (2.65%) and the peroxisome (0.88%). An overview is given in Figure 36.

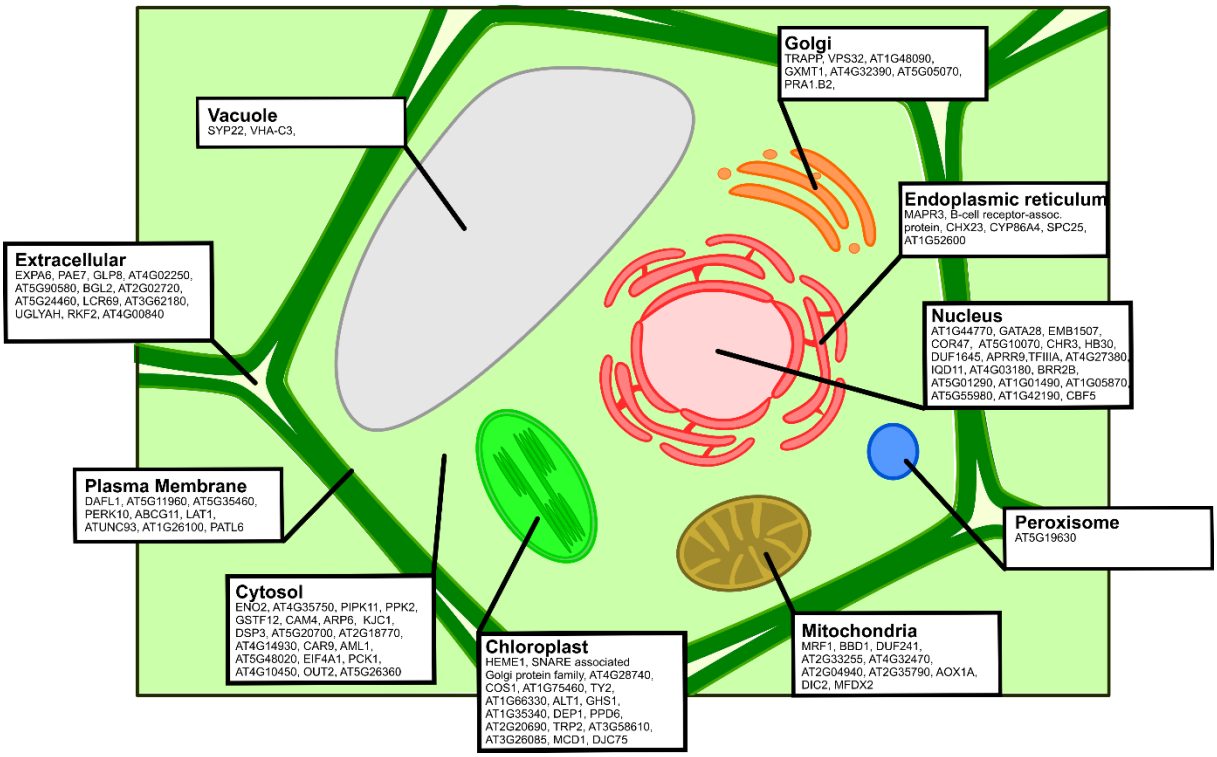

Figure 36: Prediction of the subcellular localization of potential interaction partners of DJC31.

SUBA4 was used to assign the interaction candidates identified in the library screening to their respective compartment.

In a next step, the interaction candidates were sorted according to their assigned function, using MapMan BINs. Potential interaction partners of DJC31 could predominantly be assigned to protein synthesis and homeostasis, as well as different processes related to transcriptional regulation. Furthermore, some proteins were found to be involved in stress response and cellular signaling. Other processes, candidates were found to be involved in, mostly encompassed synthesis of different primary and secondary metabolites. An overview is given in Figure 37.

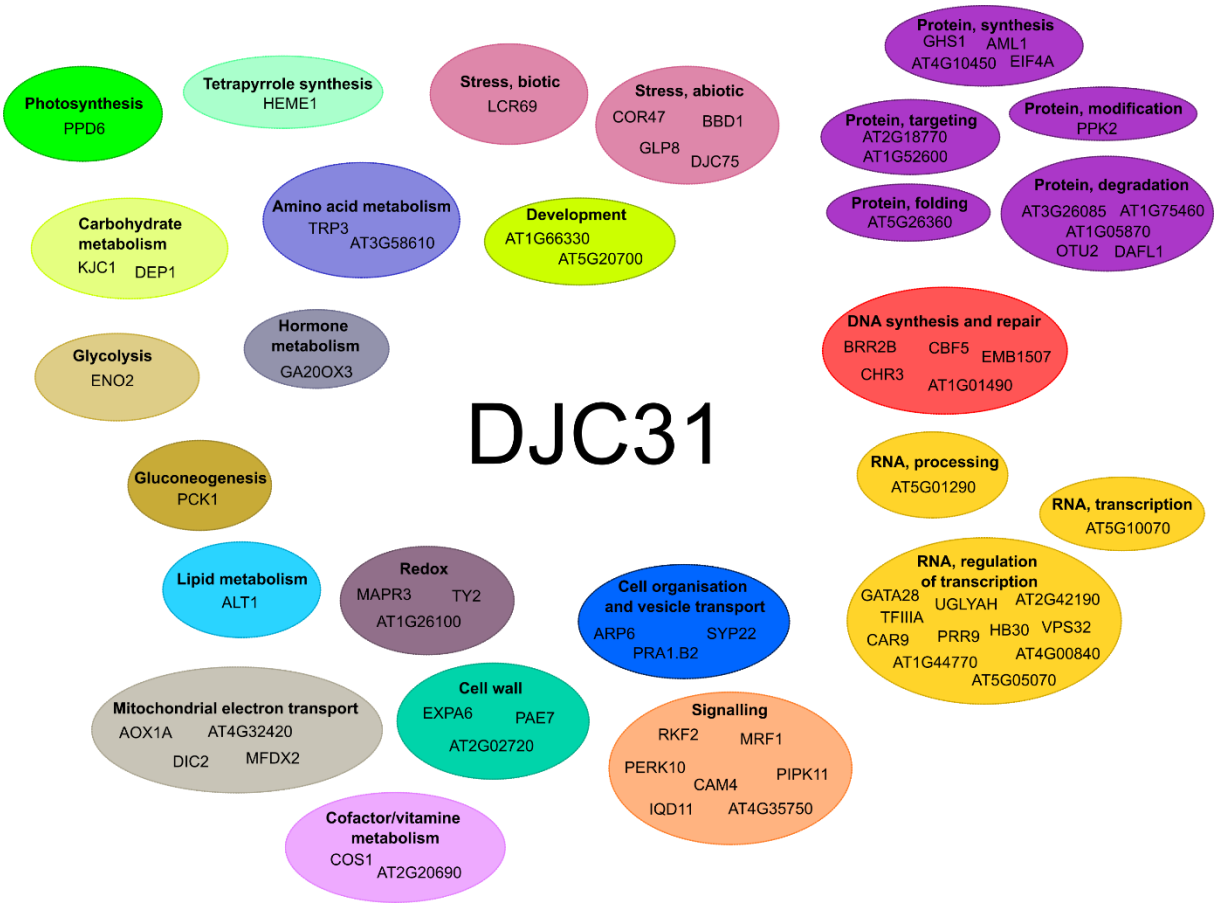

Figure 37: Potential interaction partners identified in the Y2H screening are involved in different cellular processes

Potential interaction partners of DJC31, identified in the yeast two-hybrid library screening, were grouped according to the processes they are involved in by using the MapMan BINs.

For DJC62, the library screening has been performed twice as described for DJC31, however no blue colonies could be detected on the SD-Trp-Leu + Aureobasidin A + X-α-Gal plates after several days of incubation. Considering the low protein levels of DJC62, detected in the western blot during the test experiments, it might be, that DJC62 interfered with cellular processes of the yeast cells and was therefore degraded. Since DJC31 and DJC62 share a high degree of similarity, it can be assumed that the two proteins have overlapping client spectra.

4.6. Transcriptome analysis by RNA sequencing

Because of the broad range of different functions, potential interaction partners of DJC31 are involved in, it seemed to be likely that this might have a strong influence on regulatory processes. In addition, DJC31 and DJC62 interact with HSP90, a chaperone, which is known for being involved in signal transduction and regulation of different transcription factors (di Donato & Geisler, 2019). Therefore, transcriptome analysis of Col-0, *djc31*, *djc62* and *djc31 djc62* was performed via RNA sequencing (RNAseq). Plants grown on soil at the four-leaves stage were ground in liquid nitrogen. Subsequently, RNA was extracted and sequenced.

Functional annotation was performed using the Database for Annotation, Visualization an Integrated Discovery Version 6.8 (DAVID 6.8), only considering genes, which were up- or downregulated at least two-fold with an adjusted p-value of <0.05 (Huang da et al., 2009). A gene ontology (GO) term analysis was performed regarding biological process, molecular function and cellular component. A GO term enrichment of at least two-fold and a Benjamini corrected value of <0.05 were used as cutoff values.

For *djc31*, especially genes associated with hormone signaling, abiotic and biotic stress response were up and down regulated. For the upregulated genes an enrichment of genes associated with ADP binding was enriched as a molecular function (Figure 38). This group contains several disease resistance genes of the CC-NBS-LLR and the TIR-NBS-LLR class. For the downregulated genes, especially genes with DNA binding functions were enriched. A similar result was obtained for *djc62* (Figure 39). Again, genes involved in different signaling cascades as well as biotic and abiotic stress response were both up and downregulated. Among the upregulated genes, carbohydrate binding and ADP binding was enriched, whereas for the downregulated genes, sequence-specific DNA binding and xyloglucan related processes were enriched. Likewise, for the double mutant *djc31 djc62,* up- and downregulation of different stress and signaling related genes was observed with an enrichment of ADP binding factors among the upregulated genes and genes associated with DNA binding and transcription for the downregulated genes. Additionally, among the upregulated genes, genes encoding proteins with heme binding function, like different peroxidases and cytochrome p450 family proteins, and transport function were enriched (Figure 40).

For the category cellular component, an enrichment of different compartments could be observed for upregulated genes of *djc31* and *djc62*. However, a clear pattern, pointing towards a certain function or a compartment of special importance could not be determined.

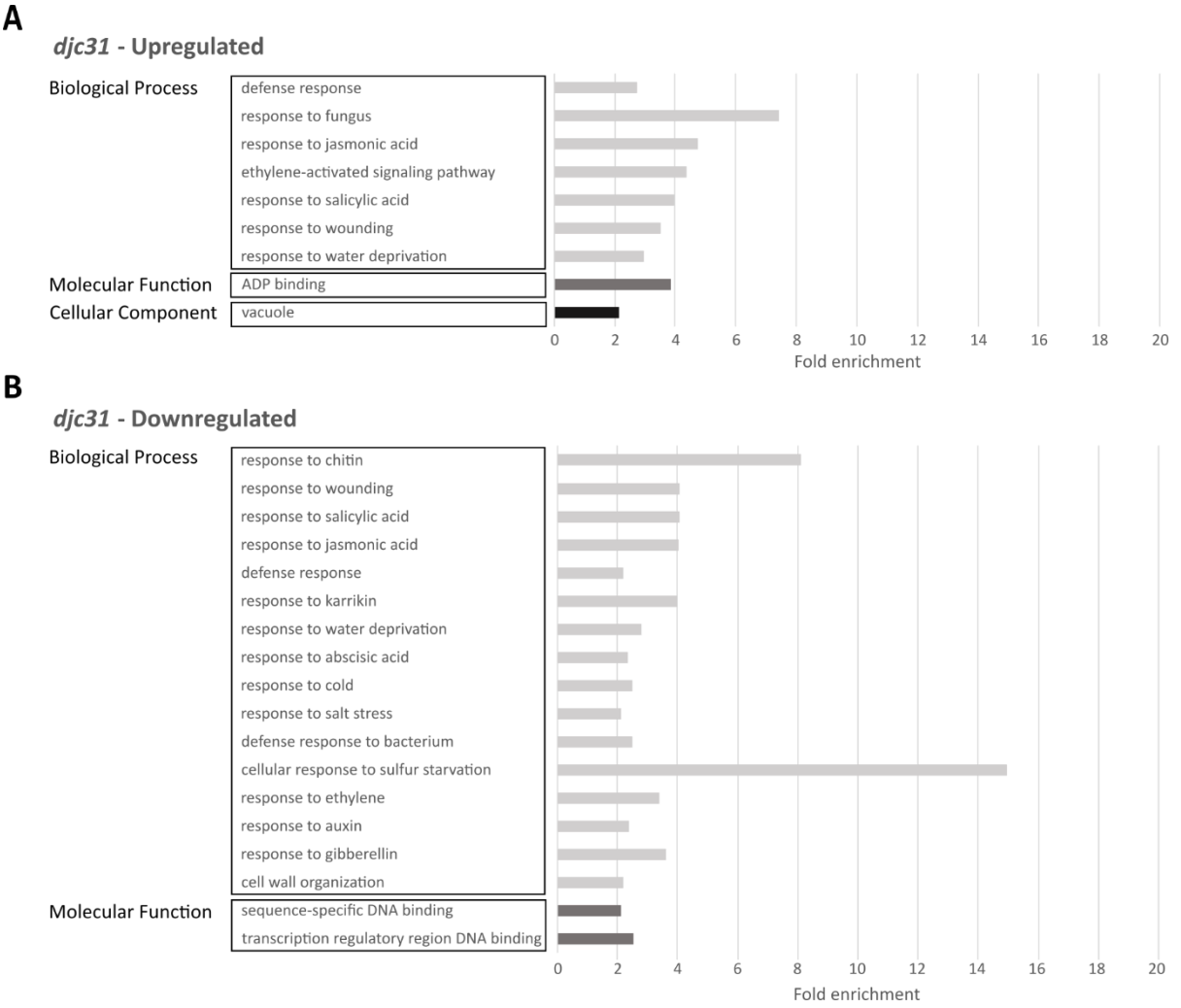

Figure 38: GO term analysis of up-and downregulated genes in *djc31*.

The at least two-fold upregulated genes (A) and downregulated genes (B) in *djc31* were analyzed using the functional annotation tool of DAVID 6.8. GO terms with an at least two-fold enrichment score and a Benjamini corrected value of <0.05 are depicted in the diagram, showing values for enriched biological processes in light gray, molecular function in dark gray and cellular components in black.

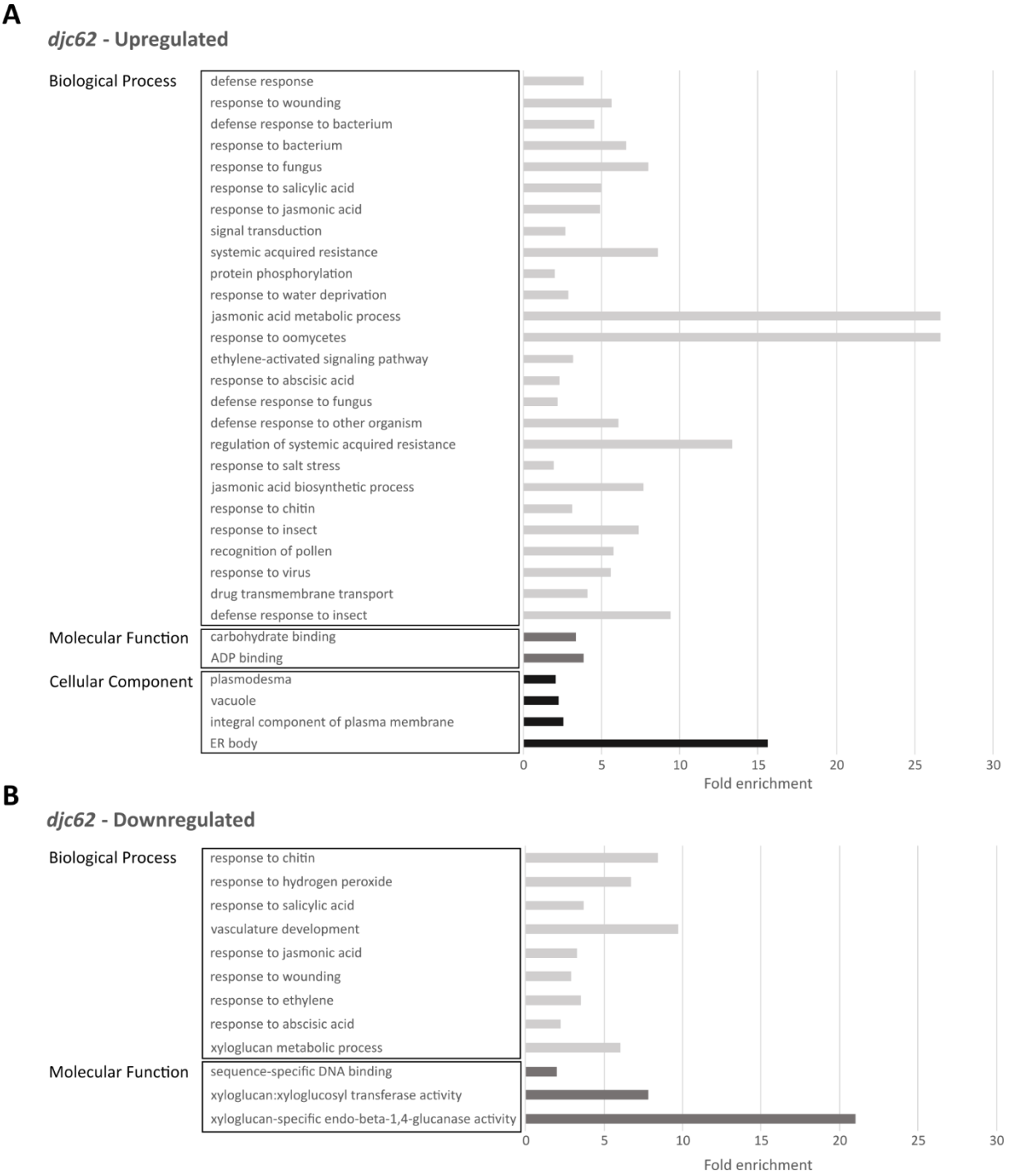

Figure 39: GO term analysis of up-and downregulated genes in *djc62*.

The at least two-fold upregulated genes (A) and downregulated genes (B) in *djc62* were analyzed using the functional annotation tool of DAVID 6.8. GO terms with an at least two-fold enrichment score and a Benjamini corrected value of <0.05 are depicted in the diagram, showing values for enriched biological processes in light gray, molecular function in dark gray and cellular components in black.

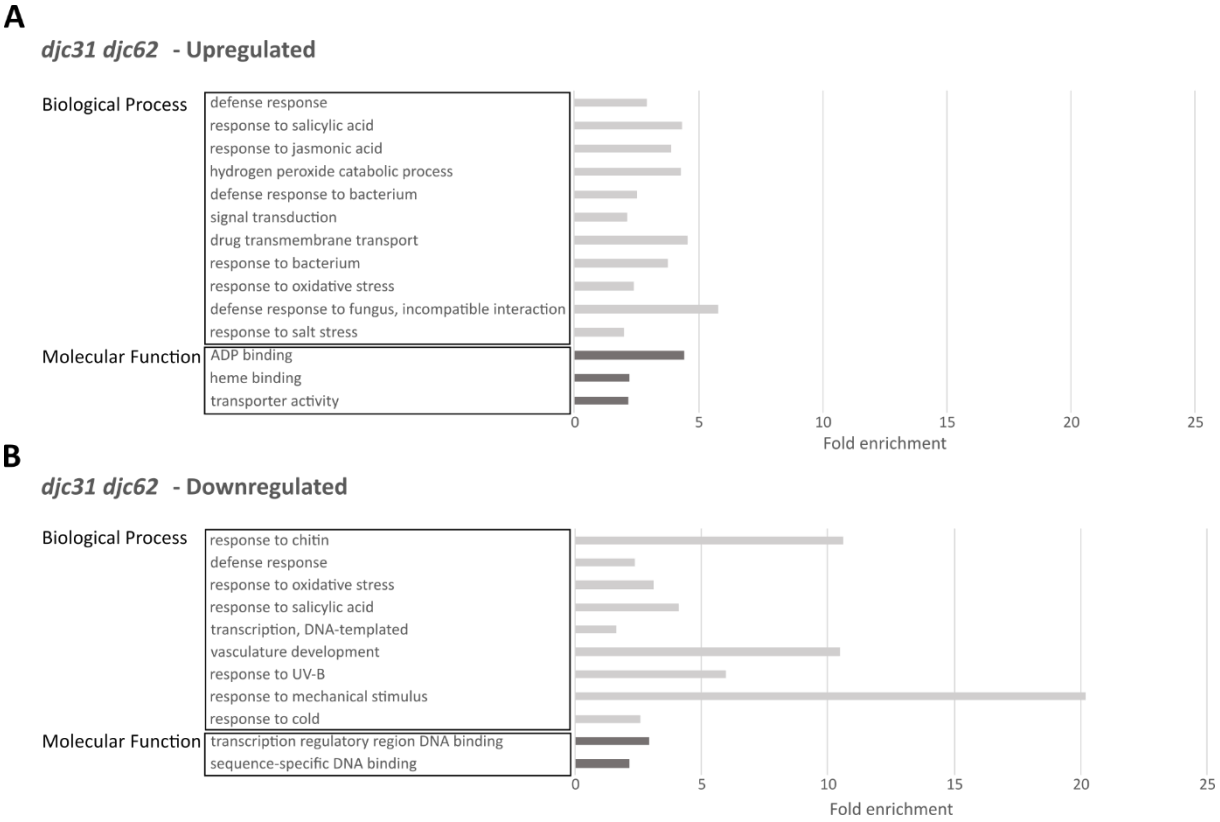

Figure 40: GO term analysis of up-and downregulated genes in *djc31 djc62*.

The at least two-fold upregulated genes (A) and downregulated genes (B) in *djc31 djc62* were analyzed using the functional annotation tool of DAVID 6.8. GO terms with an at least two-fold enrichment score and a Benjamini corrected value of <0.05 are depicted in the diagram, showing values for enriched biological processes in light gray and for molecular function in dark gray.

Additionally, Venn diagrams were generated using MapMan for at least two-fold up and downregulated genes of *djc31*, *djc62* and *djc31 djc62* with an adjusted p-value of <0.05. The Venn diagram for up- and downregulated genes, respectively, shows large overlaps between single mutants and the double mutant, which confirms the above finding of the GO term analysis (Figure 41). However, this cannot explain why only the double mutant exhibits a strong phenotype, whereas *djc31* and *djc62* behave almost wild type-like. Therefore, only the genes, which are exclusively up- or downregulated in *djc31*, *djc62* or *djc31 djc62* were again subjected to GO term analysis regarding biological processes using DAVID 6.8.

At least two-fold enriched GO terms of transcripts, which were exclusively upregulated in *djc31 djc62* encompassed processes like response to osmotic, salt, oxidative and cold stress, as well as glucosinolate catabolic processes and different transport processes. Among the downregulated genes, the GO terms related to leaf senescence, redox processes and methylation were enriched. For genes exclusively upregulated in *djc31* only autophagosome assembly was enriched, whereas the downregulated genes included different biotic stress response processes, response to different hormones, regulation of transcription and protein phosphorylation. In contrast to that, genes related

to the GO terms biotic and abiotic stress response, response to jasmonic acid, lipid regulatory processes and ADP/ATP transport processes were upregulated in *djc62*. Among the downregulated genes, GO terms related to regulation of the cell wall were enriched. It needs to be considered, that none of the GO terms were significantly enriched, as measured according to the Benjamini corrected value. Thus, these enrichments can provide only a careful point of reference (Table 10).

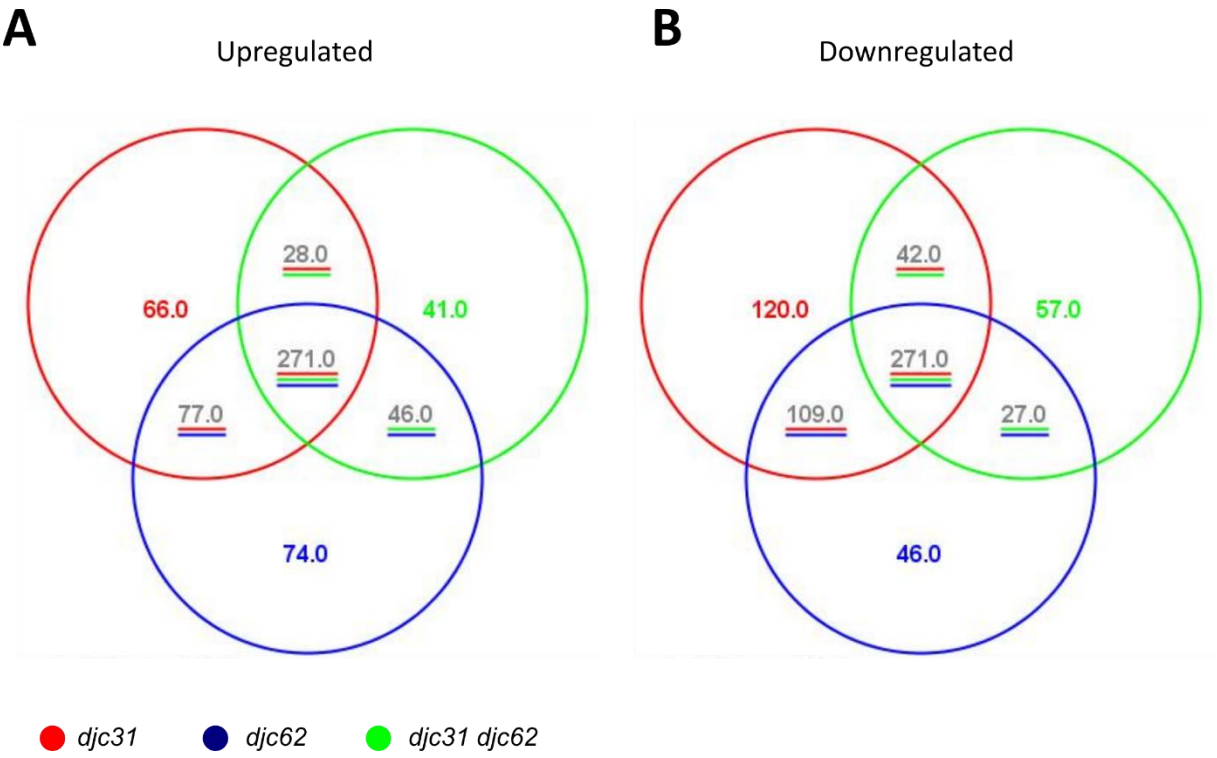

Figure 41: Venn diagram of upregulated (A) and downregulated (B) genes in *djc31*, *djc62* and *djc31 djc62*.

Transcripts, which were up- or downregulated at least two-fold with an adjusted p-value of <0.05 were used for analysis.

Table 10: Genes up- or downregulated exclusively in *djc31*, *djc62* or *djc31 djc62*.

Genes which were exclusively up- or downregulated in *djc31*, *djc62* or *djc31 djc62* at least two-fold with an adjusted p-value of <0.05 were analyzed regarding their biological process using DAVID. Biological processes with an at least two-fold enrichment are listed below. It must be noted that none of the GO terms reached a Benjamini corrected value of <0.05.

djc31 djc62		*djc31*		*djc62*	
Upregulated	**Downregulated**	**Upregulated**	**Downregulated**	**Upregulated**	**Downregulated**
response to osmotic stress	leaf senescence	autophagosome assembly	defense response to bacterium	response to wounding	xyloglucan metabolic process
response to salt stress	oxidation-reduction process		plant-type hypersensitive response	oxylipin biosynthetic process	cell wall biogenesis
glucosinolate catabolic process	response to oxidative stress		response to jasmonic acid	jasmonic acid biosynthetic process	cell wall organization
response to oxidative stress	removal of superoxide radicals		abscisic acid-activated signaling pathway	defense response	
response to cold	methylation		response to wounding	response to jasmonic acid	
transport			defense response	response to salt stress	
drug transmembrane transport			response to salicylic acid	lipid oxidation	
			response to abscisic acid	ATP transport	
			protein phosphorylation	jasmonic acid metabolic process	
			response to gibberellin	ADP transport	
			positive regulation of transcription	glutamate metabolic process	
			response to bacterium	mRNA catabolic process	
			response to molecule of bacterial origin	response to osmotic stress	
				protein phosphorylation	
				response to water deprivation	
				fatty acid biosynthetic process	
				response to cadmium ion	

Besides GO term analysis, a KEGG pathway analysis was performed with g:Profiler using genes, which were at least two-fold up- or downregulated with an adjusted p-value of <0.05 (Raudvere et al., 2019). The differentially expressed genes in *djc31 djc62* could be assigned to pathways related to biosynthesis of secondary metabolites, phenylpropanoid biosynthesis, MAPK signaling and zeatin biosynthesis. For *djc31* an enrichment for genes involved in biosynthesis of secondary metabolites, plant-pathogen interactions and α-linolenic acid metabolism could be observed. For *djc62*, factors of pathways for biosynthesis of secondary metabolites, MAPK signaling, plant-pathogen interaction and circadian rhythm were enriched (Figure 42).

KEGG		djc31	djc62	djc31djc62
Term Name	Term ID	p_adj	p_adj	p_adj
Biosynthesis of secondary metabolites	KEGG:01110	3.390×10^{-2}	1.617×10^{-3}	4.315×10^{-5}
Phenylpropanoid biosynthesis	KEGG:00940	~~1.000~~	~~1.000~~	5.805×10^{-5}
MAPK signaling pathway - plant	KEGG:04016	1.407×10^{-2}	~~1.000~~	5.240×10^{-4}
Plant-pathogen interaction	KEGG:04626	2.564×10^{-3}	1.526×10^{-2}	~~4.766×10^{-1}~~
Zeatin biosynthesis	KEGG:00908	~~1.000~~	~~1.000~~	3.207×10^{-2}
Circadian rhythm - plant	KEGG:04712	3.301×10^{-2}	~~1.000~~	~~1.000~~
alpha-Linolenic acid metabolism	KEGG:00592	~~7.547×10^{-2}~~	4.741×10^{-2}	~~8.332×10^{-1}~~

Figure 42: KEGG pathway analysis.

The at least two-fold up- or downregulated genes with an adjusted p-value of <0.05 were analyzed with g:Profiler regarding an enrichment of different pathways. Values, which are not significant are crossed out.

As a second approach, the at least two-fold up- and downregulated transcripts, with an adjusted p-value of <0.05, of *djc31*, *djc62* and *djc31 djc62* were analyzed using MapMan. Since DJC31 and DJC62 seem to be involved in regulatory processes, genes with a two-fold up- and downregulation and an adjusted p-value of <0.05 were mapped to the Regulation_Overview pathways (Figure 43).

All samples showed differences in expression levels, especially for transcription factors and factors involved in protein modification and degradation. *djc31 djc62* exhibited slightly more upregulation in these categories compared to the single mutants. Furthermore, an effect was visible in pathways related to signal transduction. Here, especially receptor kinases and calcium mediated signaling processes were affected. Whereas *djc31* showed rather downregulation of receptor kinases, in *djc31 djc62* and *djc62* receptor kinases were rather upregulated. Regarding hormonal signaling, especially expression levels of genes involved in auxin, ethylene and jasmonate signaling were altered.

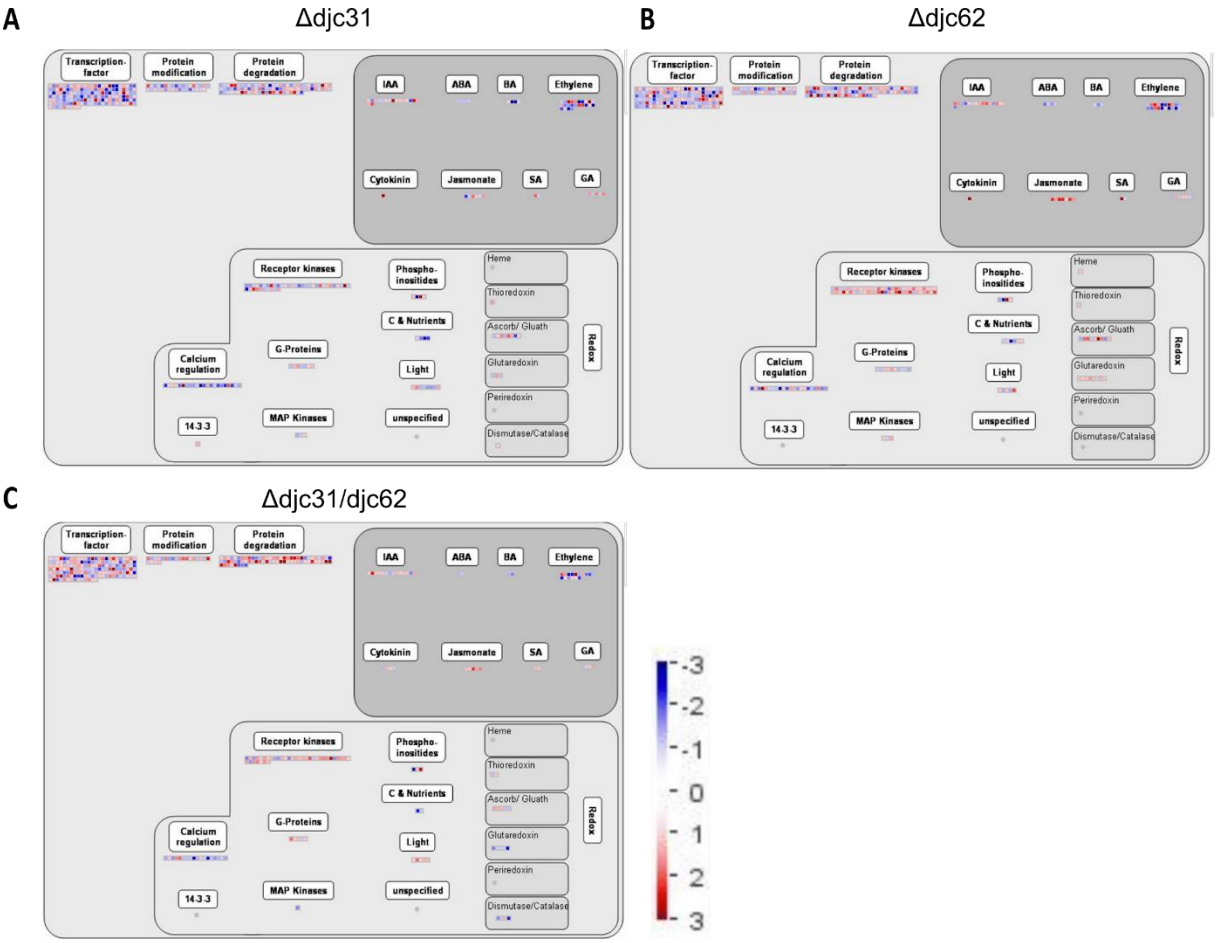

Figure 43: Overview of regulatory pathways.

RNAseq data of djc31 (A), djc62 (B) and djc31 djc62 (C), showing an at least two-fold up- or downregulation with an adjusted p-value of <0.05, were analyzed regarding their influence on regulatory processes within the cell. The color scale indicates downregulated genes in blue shades and upregulated genes in red shades.

4.7. DJC31 and DJC62 are involved in abiotic stress response

The differential expression of genes involved in abiotic and biotic stress response in the RNAseq experiment, as well as the involvement of cytosolic chaperones in response to stress, indicated DJC31 and DJC62 to play a role in regulation of different stress pathways (Jacob et al., 2017). Therefore, the effect of different abiotic stress inducing agents was tested on the phenotypic and molecular level.

4.7.1. Endoplasmic reticulum stress

Considering the localization of DJC31 and DJC62 to the cytosolic side of the ER membrane and the fact, that co-chaperones are known for being involved in stress response, they might be involved in the endoplasmic reticulum associated degradation (ERAD) pathways. Proteins in the ER lumen, which fail to fold properly are retrotranslocated across the ER membrane back to the cytosol, where they are ubiquitinated and degraded via the cytosolic ubiquitin proteasome system (Y. Liu & Li, 2014). So far, the precise mechanism of how proteins are retrotranslocated and ubiquitinated is still unknown. To test, whether DJC31 and DJC62 play a role in this process, Col-0, *djc31*, *djc62* and *djc31 djc62* seedlings were grown on ½ MS medium containing tunicamycin for 14 days. Tunicamycin is an antibiotic, which inhibits glycosylation and consequently induces accumulation of unfolded proteins in the ER lumen (Chen & Brandizzi, 2013). Since *djc31 djc62* seedlings exhibit heterogenous growth and partially a growth arrest at the cotyledon stage already under non-stressed conditions, it was difficult to determine whether the double mutant is more affected by the stress treatment compared to wild type and single mutants. Therefore, plants were evaluated regarding the individual growth stages they have reached after 14 days. For Col-0, *djc31* and *djc62*, almost all seedlings reached the four leaves stage under non-stressed conditions. Treatment with tunicamycin did not affect the germination rate, but the number of seedlings reaching the two leaves stage was reduced to 70-80% and at the four leaves stage reduced to approximately 60%. For the double mutant, the germination rate has been 81% for untreated and tunicamycin-treated seedlings. As already seen in previous experiments, around one third of the seedlings showed a growth arrest at the cotyledon stage and only 49% and 37% of the *djc31 djc62* seedlings reached the two leaves and four leaves stages under non-stressed conditions. Under ER stress conditions, the number of *djc31 djc62* seedlings reaching the two leaves stage was lowered to 29% and at the four leaves stage to 15% (Figure 44). Although by phenotypic inspection the double mutant seemed to be more affected by the tunicamycin treatment, comparison of the differences between the values for treated and untreated at the different growth stages showed, that the growth retardation caused by tunicamycin is comparable between Col-0, *djc31*, *djc62* and *djc31 djc62*. This indicates, that DJC31 and DJC62 do not play a role in processes related to ER stress.

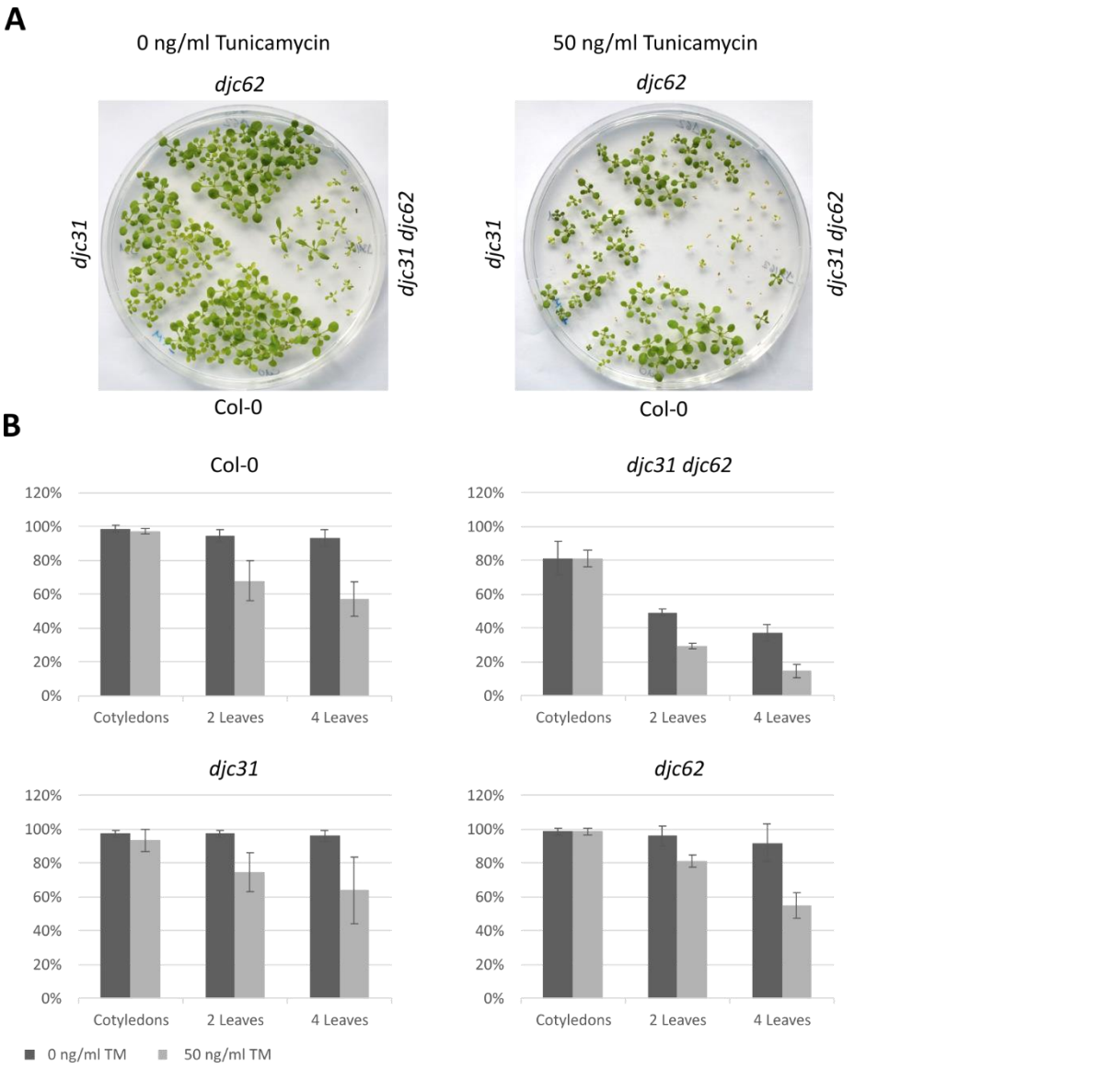

Figure 44: Growth under ER stress induced by tunicamycin

A) Col-0, *djc31*, *djc62* and *djc31 djc62* were grown on ½ MS medium containing 0 ng/ml (DMSO as solvent control) or 50 ng/ml tunicamycin (TM) for 14 days.

B) Quantification of growth stages reached at day 14 by the different genotypes under non-stressed (dark gray) and ER-stress (light gray) conditions. All genotypes were approximately equally affected by the treatment and showed slightly retarded growth. Error bars represent the standard deviation; n=75/genotype.

4.7.2. Salt and osmotic stress

Next, sensitivity to salt stress was analyzed. Sodium chloride (NaCl) is the predominant salt in the soil and has tremendous impact on agriculture and crop yield. Under normal conditions, plants maintain their ionic balance in a way that the high osmotic pressure inside the cell can be used as driving force to take up water and minerals. Under conditions of high salinity, the osmotic pressure of the soil exceeds the osmotic pressure of the cell and disturbs uptake of water and essential minerals, which leads to reduced growth and decreased metabolic activity in the cytosol (Kader & Lindberg, 2010). To

examine the effect of NaCl on Col-0, *djc31*, *djc62* and *djc31 djc62*, seedlings were grown on ½ MS medium with or without 100 mM NaCl and were phenotypically analyzed after 14 days. Again, because of the heterogenous growth of the double mutant, the seedlings were analyzed regarding the growth stages they have reached. Under non-stressed conditions, almost all Col-0, *djc31* and *djc62* seedlings could reach the four leaves stage. Growth under salt stress did not affect the germination rate and also the two leaves stage was reached by almost all seedlings. However, only 45-52% could reach the four leaves stage within 14 days. For the double mutant, a decreased germination rate of 76% was observed under non-stressed conditions, as observed previously. 45% reached the two leaves stage and 28% the four leaves stage. Growth on 100 mM NaCl led to a reduced growth rate of 63% and the following growth stages were only reached by 9% and 1%, respectively (Figure 45). This result indicates DJC31 and DJC62 to be involved in processes linked to the response to salt stress.

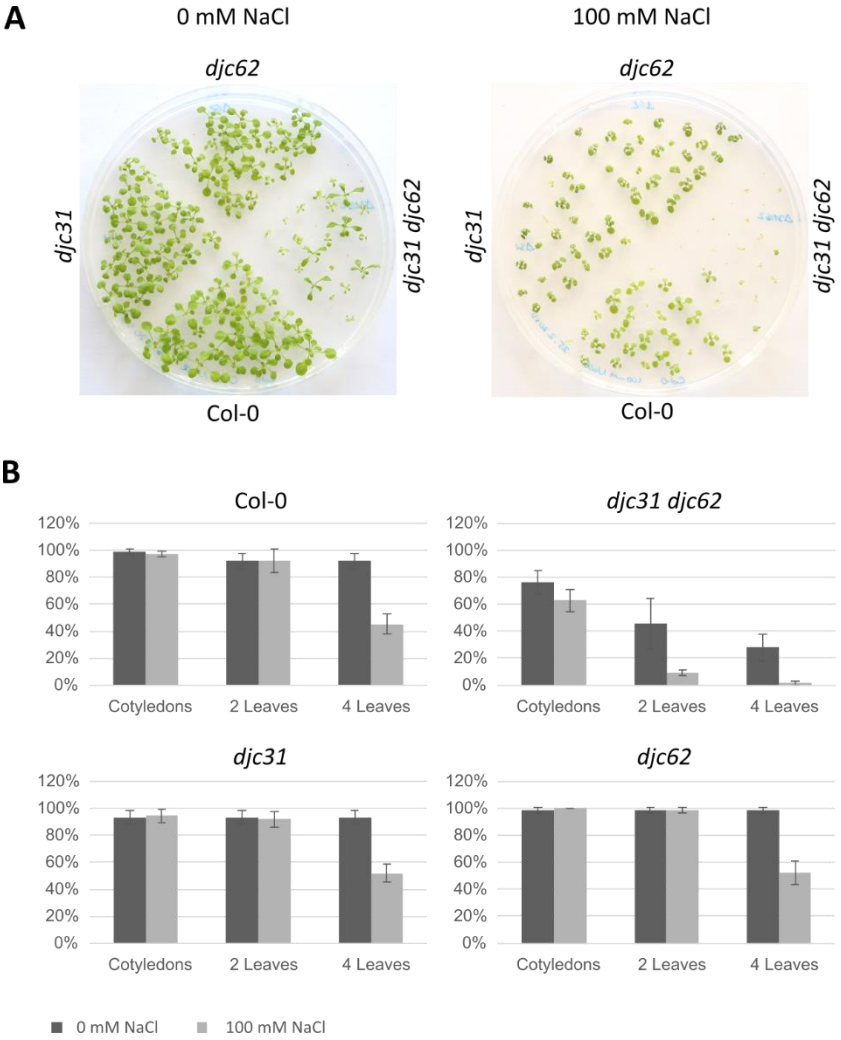

Figure 45: Growth under salt stress

A) Col-0, *djc31*, *djc62* and *djc31 djc62* were grown on ½ MS medium containing 0 mM or 100 mM NaCl for 14 days.

B) Quantification of growth stages reached on day 14 by the different genotypes under non-stressed (dark gray) and salt-stress (light gray) conditions. *djc31 djc62* shows a strong developmental arrest at the cotyledon stage, whereas Col-0 and single mutants developed comparable. Error bars represent the standard deviation, n=75/genotype

Besides osmotic stress, the harmful effect of NaCl is also mediated by ionic toxicity. Sodium ions, which are usually present in low concentrations in the cytosol, can compete with potassium ions for binding to different enzymes, involved in different cytosolic processes (Kader & Lindberg, 2010). To exclude, that the effect is exclusively caused by ionic toxicity, the experiment was repeated, using glucose and mannitol as inducers of osmotic stress. After 14 days, the seedlings were analyzed regarding reaching different growth stages. Under non-stressed conditions, germination and growth rates were comparable between Col-0, *djc31* and *djc62,* and 93-97% of the seedlings reached the four leaves stage. Treatment with 3% glucose did not affect the germination rates and the generation of the first two rosette leaves of Col-0, *djc31* and *djc62*, However, *djc62* was more affected by the glucose treatment and only 49% of the seedlings reached the four leaves stage after 14 days. For *djc31 djc62*, the germination rate under non-stressed conditions has been 80% and was slightly decreased to 68% under 3% glucose treatment. Progression to the two leaves stage was not affected but only 21% have reached the four leaves stage, compared to 34% under non-stressed conditions (Figure 46). In conclusion one can say, that the glucose treatment had a mild effect on the growth rate, especially for *djc31 djc62* and *djc62*.

Treatment with 3% mannitol showed a more severe effect. Whereas Col-0, *djc31* and *djc62* did not show an effect at the cotyledon stage and the two leaves stage, the double mutant showed a strong decrease in germination to 59% and only a few single seedlings were able to proceed to later growth stages. But also wild type and single mutants were affected by the mannitol treatment at the four leaves stage. For Col-0, more than half of the seedlings were able to reach the four leaves stage, but for the two single mutants, only around 25% proceeded growing after the two leaves stage (Figure 46).

This result confirms, that DJC31 and DJC62 are of special importance for mechanisms involved in the osmotic stress response

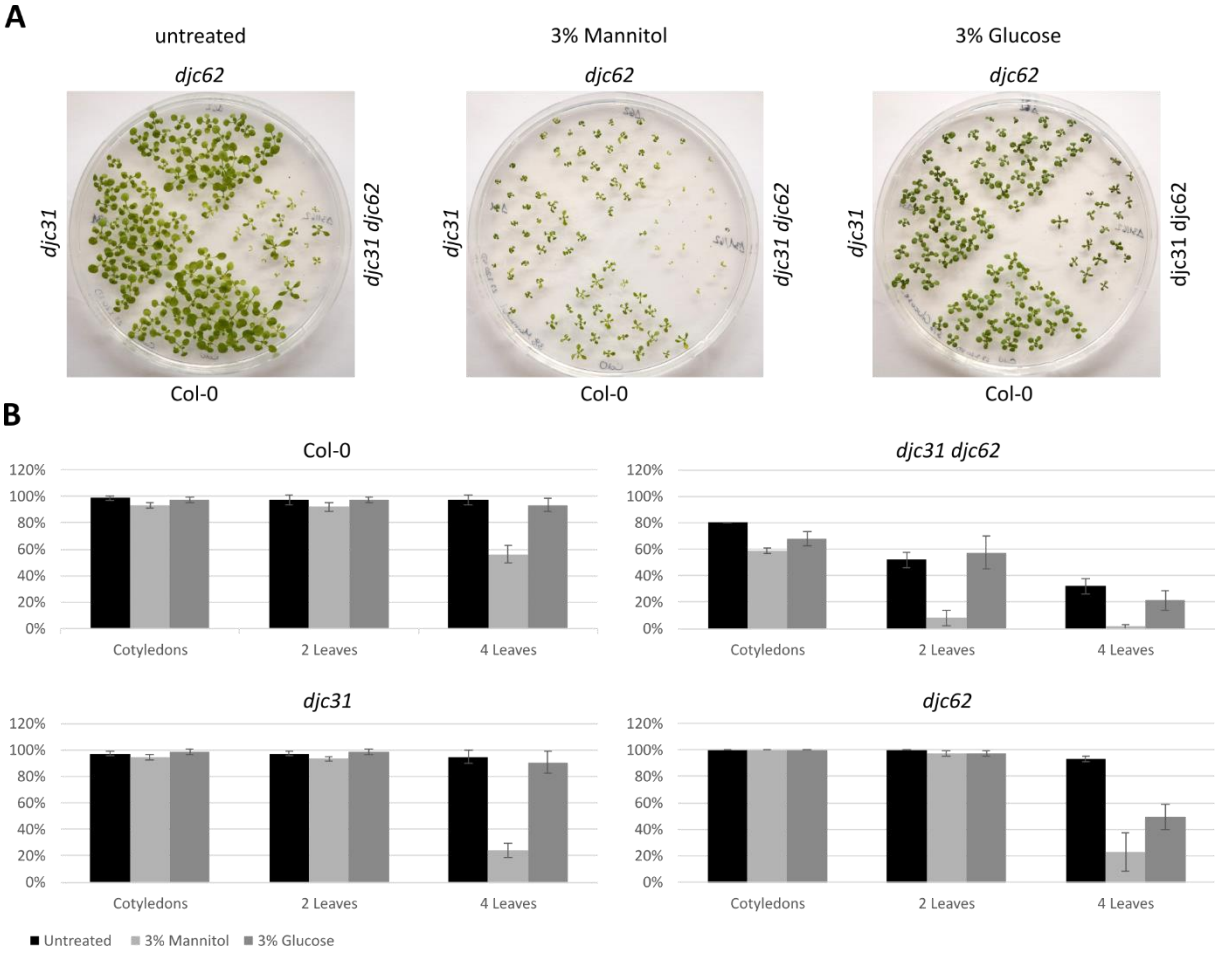

Figure 46: Growth under osmotic stress

A) Col-0, *djc31*, *djc62* and *djc31 djc62* were grown on ½ MS medium containing either 3% mannitol or 3% glucose for 14 days. B) Quantification of growth stages reached by the different genotypes on day 14 under non-stressed (black), mannitol treated (light gray) or glucose treated (dark gray) conditions. Mannitol treatment of *djc31 djc62* showed a strong effect, whereas glucose treatment had only a mild effect on growth. Also the single mutants were more affected by the mannitol treatment than the wild type, but *djc62* was also slightly more affected under glucose treatment than Col-0 and *djc31*. Error bars represent the standard deviation, n=75/genotype

4.7.3. Drought tolerance

Besides high soil salinity, drought is also one of the major threats in agriculture and affects plant growth and development (Harb et al., 2010). Since osmotic and drought stress show some overlapping features, it was likely that DJC31 and DJC62 might also play a role in response to water deprivation. To test this hypothesis, Col-0, *djc31*, *djc62* and *djc31 djc62* plants were grown in medium size pots under standard conditions for 14 days. Subsequently, water was withdrawn for 21 days. After seven days, no signs of dryness could be observed at the leaves. Growth was comparable between wild type and single mutants. The double mutant showed growth and development as observed before under non-stressed conditions. After 21 days, Col-0, *djc31* and *djc62* were completely dry, whereas 75% of the *djc31 djc62* plants were still green. Plants were thoroughly watered and examined after three days again. The re-watering could not rescue Col-0, *djc31* and *djc62*, but surviving *djc31 djc62* plants remained viable and

started to produce flowers (Figure 47). Although the responses to drought and osmotic stress share some pathways, the double mutant turned out to be more drought tolerant than wild type and single mutants. This result indicates that absence of DJC31 and DJC62 might lead to deregulation of cellular processes, which favors survival under drought conditions.

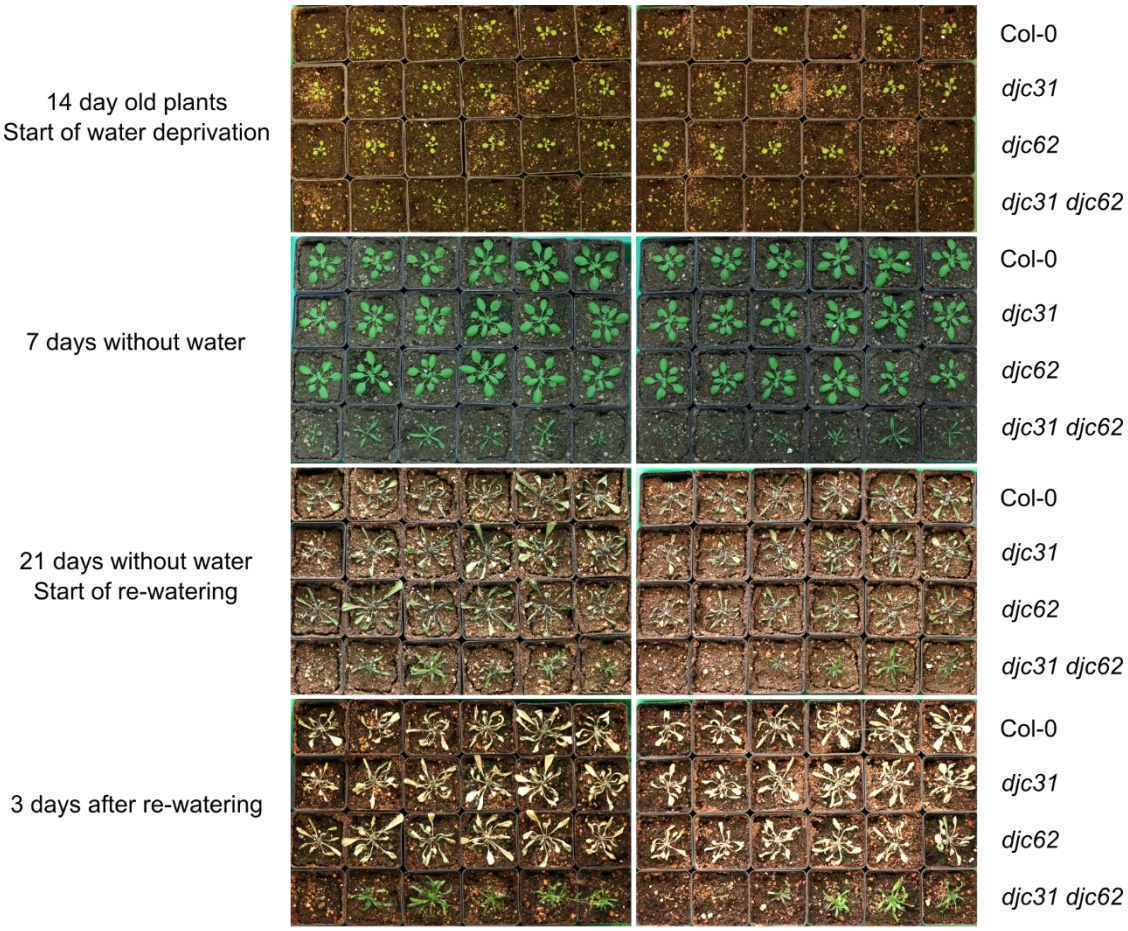

Figure 47: *djc31 djc62* is drought tolerant

Water was withdrawn from 14 days old plants. After seven days no signs of dryness or strong growth retardation could be observed. On day 21, Col-0, *djc31* and *djc62* showed a high degree of dryness, whereas *djc31 djc62* was still green. After 21 days, the plants were watered again. After 3 days of re-watering Col-0, *djc31* and *djc62* were not able to recover from the water withdrawal, in contrast to *djc31 djc62*, for which 75% of the plants survived and remained viable.

To analyze, whether the drought tolerance of *djc31 djc62* is enhanced by less water loss, the transpiration rates of detached wild type and mutant rosettes were determined over the time course of 120 min. However, a significant difference of the transpiration rates between Col-0, *djc31*, *djc62* and *djc31 djc62* could not be determined (Figure 48).

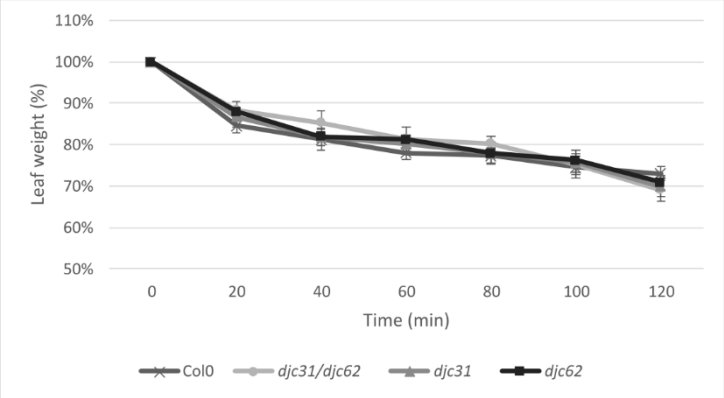

Figure 48: Transpiration rates of Col-0, *djc31*, *djc62* and *djc31 djc62*.

Five leaf rosettes per genotype were placed in petri dishes and loss of water was observed as decreasing leaf weight over time. No significant difference could be observed between wild type and mutants.

4.7.4. Molecular analysis of the stress response via qPCR

The sensitivity to osmotic or salt stress and the enhanced tolerance to drought support that DJC31 and DJC62 might be important for the regulation of cellular stress response mechanisms. To analyze this function in more detail on the molecular level, qPCRs were performed to analyze transcript levels of *DJC31* and *DJC62* after stress treatment. Primers for *DJC31* and *DJC62* were designed using NCBI Primer Blast with the following parameters: PCR product size between 100-200 bp, a melting temperature of 60°C ±3°C, at least one primer must span an exon-exon junction, primers must be separated by at least one intron.

Since DJC31 and DJC62 localize to the endoplasmic reticulum, they might be upregulated in response to ER stress to assist in activation of ER related stress pathways like, the unfolded protein response or endoplasmic reticulum associated degradation (Chen & Brandizzi, 2013; Y. Liu & Li, 2014). Therefore, seven days old Col-0 seedlings, grown vertically on plates, were transferred into liquid ½ MS medium for 24 hours to adapt the plants to the incubation medium. On the next day, the medium was exchanged and supplemented with 5 µg/ml tunicamycin or DMSO as solvent control. After incubation for six hours, RNA was isolated, reverse transcribed and tested via qPCR, using *OEP24* as reference gene. To verify successful induction of ER stress by tunicamycin, the ER luminal chaperones *BiP1/2*, which are known to be upregulated under ER stress, were included as positive controls (Chen & Brandizzi, 2013; Schott et al., 2010). *BIP1/2* was indeed upregulated, confirming that tunicamycin induced ER stress in the seedlings. However, for *DJC31* and *DJC62*, no significant alteration in gene expression levels could be observed (Figure 49).

Furthermore, since chaperones are expressed under heat stress to maintain protein homeostasis, up- or downregulation of *DJC31* and *DJC62* was analyzed after heat treatment. Seven days old wild type seedlings on ½ MS plates were incubated at 38°C for three hours. After RNA isolation and cDNA

synthesis, a qPCR was performed, with *OEP24* as reference gene. As a positive control to confirm successful heat treatment, HSP70-HSP90 organizing protein 3 (*HOP3*) was used. HOP3 is a cytosolic co-chaperone of HSP70 and HSP90, which was observed to be upregulated under heat stress in *Arabidopsis* (Fernández-Bautista et al., 2018). Successful heat treatment was confirmed by upregulation of *HOP3*. However, *DJC31* and *DJC62* were not significantly altered in gene expression (Figure 49).

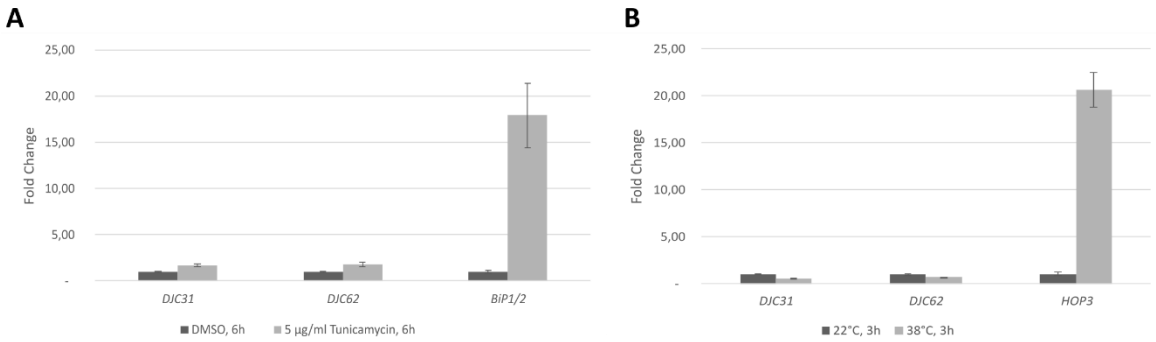

Figure 49: *DJC31* and *DJC62* are not upregulated under ER-stress or heat stress

A) Eight days old Col-0 seedlings were treated with 5 µg/ml tunicamycin or DMSO as control for six hours. After RNA isolation and cDNA synthesis, qPCR analysis was performed with *BiP1/2* as induction control.

B) Seven days old seedlings were incubated at 22°C or 38°C for three hours. After RNA isolation and cDNA synthesis, qPCR analysis was performed with *HOP3* as induction control.

Since *djc31 djc62* seedlings exhibited enhanced sensitivity to salt and osmotic stress on the phenotypic level, salt stress was included in the molecular analysis via qPCR. Besides *DJC31* and *DJC62*, two salt stress induced genes, *ABI5* and *RD29A*, were used as positive controls. Furthermore, expression of the two genes was also tested in the double mutant, to find out more about the influence of DJC31 and DJC62 on regulatory mechanisms under salt stress. ABA INSENSITIVE 5 (ABI5) is a bZIP transcription factor, involved in regulation of abscisic acid (ABA) signaling (Finkelstein & Lynch, 2000; Park & Kim, 2014). RESPONSIVE-TO-DESSICATION 29A (RD29A) is a protein of unknown function, which is induced under salt stress, drought, cold and ABA treatment (Clément et al., 2011; Lee et al., 2016). Seven days old Col-0 and *djc31 djc62* seedlings were transferred into liquid MS medium to adapt the seedlings to the incubation medium. After 24 hours, the medium was exchanged to ½ MS medium containing 150 mM NaCl. ½ MS medium without supplements was used as negative control. After incubation for six hours, RNA was isolated, reverse transcribed and tested via qPCR with *OEP24* as reference gene. As observed already under different stress conditions, *DJC31* and *DJC62* were again not significantly up- or downregulated. Under non-stressed conditions, the *ABI5* expression level was comparable between wild type and double mutant. Under salt stress, *ABI5* was two-fold induced in Col-0, but four-fold induced in *djc31 djc62*. *RD29A* transcripts were present in similar amounts under non-stressed

conditions in Col-0 and *djc31 djc62* and as expected upregulated under salt stress, but the transcript levels under salt stress were comparable between wild type and double mutant (Figure 50).

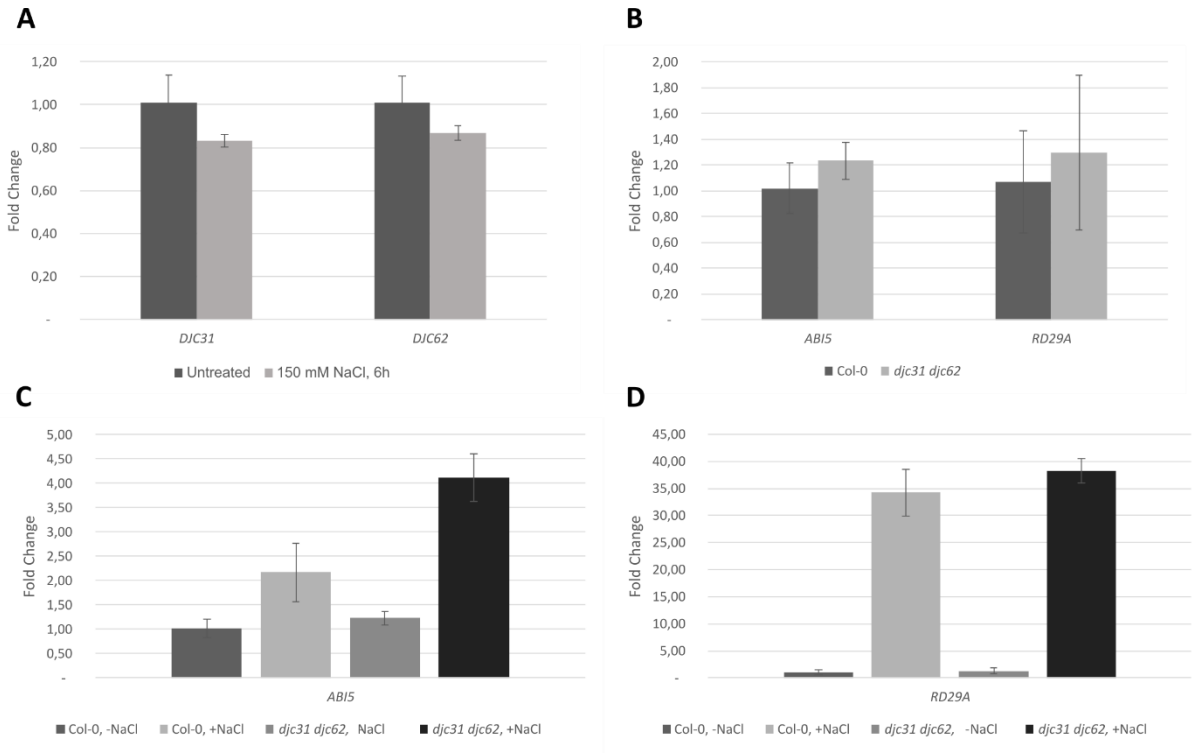

Figure 50: *djc31 djc62* exhibited enhanced ABA signaling under salt stress

A) Eight days old Col-0 seedlings were treated with 150 mM NaCl for six hours. After RNA isolation and cDNA synthesis, qPCR analysis was performed. No significant up- or downregulation could be observed.

B) Expression of *ABI5* and *RD29A* was comparable between Col-0 and *djc31 djc62* under non-stressed conditions in eight days old seedlings.

C-D) Eight days old Col-0 and *djc31 djc62* seedlings were treated with 150 mM NaCl for six hours. After RNA isolation and cDNA synthesis, qPCR analysis was performed with *ABI5* and *RD29A*. *ABI5* showed a stronger upregulation during salt stress in *djc31 djc62*, whereas transcript levels of *RD29A* were comparable between Col-0 and *djc31 djc62* after salt treatment.

4.7.5. DJC31 and DJC62 are released from the membrane upon salt stress

In previous experiments DJC31 and DJC62 were observed to be attached to the ER membrane, which is most likely mediated by the flexible N-terminal parts of the two proteins. Because of the low hydrophobicity of DJC31 and DJC62 permanent integration into the membrane via transmembrane domains or direct interaction with the membrane as a peripheral membrane protein is unlikely. Therefore, DJC31 and DJC62 might be associated to a protein complex or a scaffold protein. Such interactions are often transient, and it is conceivable that DJC31 and DJC62 might change their localization under certain circumstances. Such a behavior was already described for the cytosolic co-chaperones HOP1-3 in *Arabidopsis*. Under heat stress, HOP1, HOP2 and HOP3 localize to cytoplasmic

foci, also known as stress granules, and the nucleus. After a recovery period, they return to a diffuse cytoplasmic localization pattern (Fernández-Bautista et al., 2018).

To examine, whether DJC31 and DJC62 are released from the ER membrane under stress conditions, DJC31Int-GFP, DJC62Int-GFP and GFP only as control were transiently co-expressed with an ER-marker in tobacco leaves. Since GFP-DJC31 and GFP-DJC62 were observed to be impaired in membrane attachment, the N-terminal halves of DJC31 or DJC62, fused to GFP, were chosen for this experiment. After protoplast isolation, the protoplasts were incubated with either 150 mM NaCl in W5 buffer or W5 buffer without supplements as negative control for two hours at room temperature.

Under non-stressed conditions, DJC31Int-GFP and DJC62Int-GFP showed localization to the endoplasmic reticulum, as observed before. Under salt stress, DJC31Int-GFP and DJC62Int-GFP seemed to be released from the membrane and formed spots in the cytosol. The localization pattern of GFP, which could be observed in the cytosol and the nucleus, was comparable between non-stressed and salt-stressed conditions (Figure 51). This result indicates, that DJC31 and DJC62 are regulated via attachment to the ER membrane and are released into the cytosol upon induction of salt stress, presumably to influence stress related mechanisms.

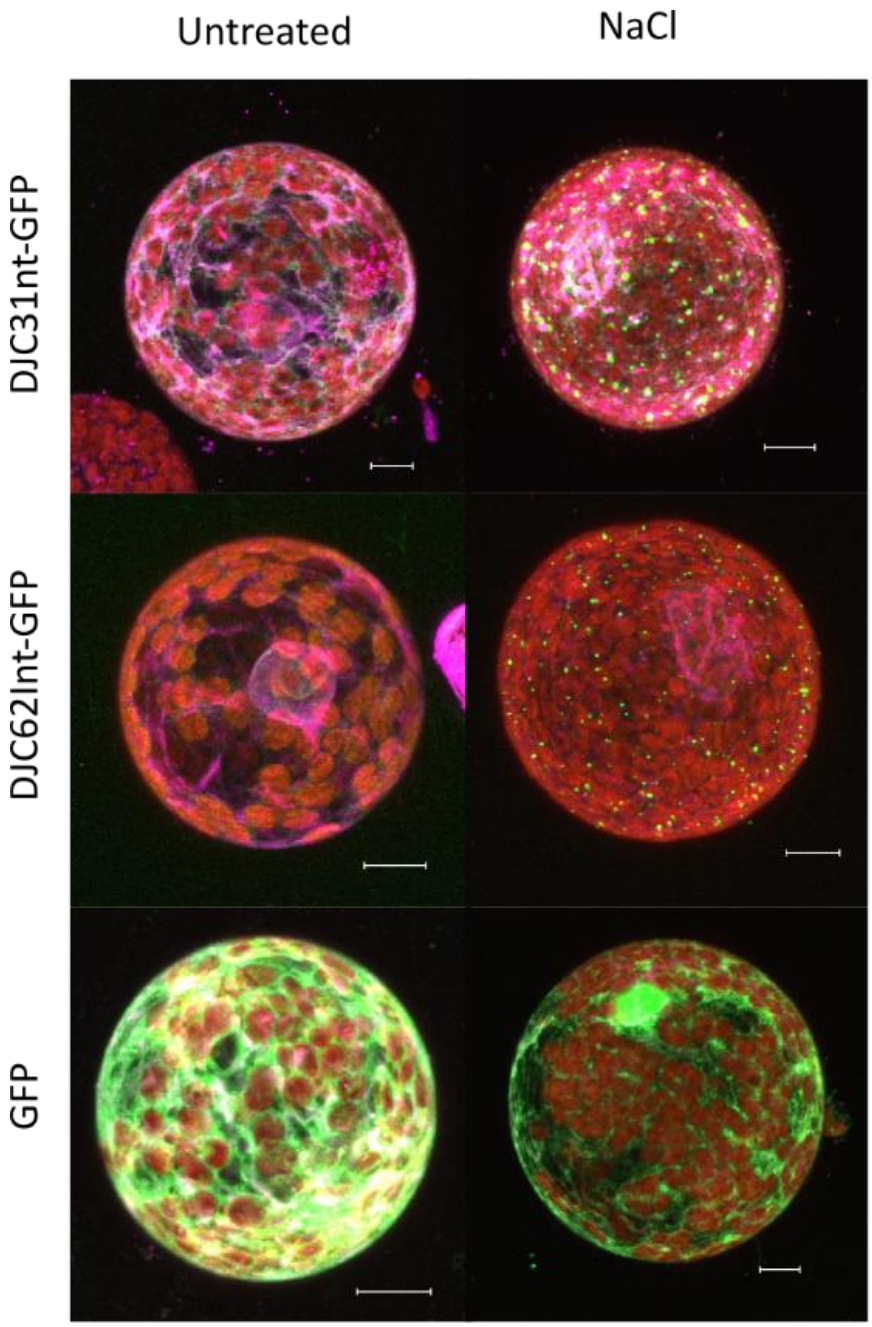

Figure 51: DJC31 and DJC62 change their subcellular localization under salt stress

DJC31Int-GFP, DJC62Int-GFP or GFP were co-expressed with an ER-marker in tobacco. After protoplast isolation, the protoplasts were either incubated with 150 mM NaCl in buffer or only buffer as negative control for two hours at room temperature. Protoplasts expressing DJC31Int-GFP and DJC62Int-GFP showed formation of fluorescent spots in the cytosol upon salt stress, whereas for GFP the distribution remained comparable between stressed and non-stressed.

Scale bar = 10 µm.

4.8. DJC31 and DJC62 do not interact with CaM4 and IQD11 under non-stressed conditions

Calcium (Ca^{2+}) plays an important role during both developmental processes and response to different environmental conditions. Spatial and temporal patterns of Ca^{2+} provide information about external stimuli, which are used by Ca^{2+} sensors to induce appropriate responses that lead to changes in metabolism, gene expression and protein homeostasis. *Arabidopsis* contains three protein families, which act as Ca^{2+} sensors: Calmodulin (CaM) and CaM-like proteins (CML), Ca^{2+}-dependent protein kinases (CPK) and calcineurin B-like proteins (CBL) (La Verde et al., 2018). The RNAseq analysis of *djc31*, *djc62* and *djc31 djc62* revealed, that expression levels of different transcription factors are altered, which are influenced by Ca^{2+} signaling and that especially factors related to Ca^{2+} signaling are predominantly downregulated. In the DJC31 yeast two-hybrid screening different factors involved in Ca^{2+} signaling could be identified as potential interaction partners. Among them a protein of unknown function of the calcium dependent lipid binding family, C2-DOMAIN ABA-RELATED 9 (CAR9) of the calcium-dependent lipid-binding family, Calmodulin 4 (CaM4) and the calmodulin binding protein IQ-DOMAIN 11 (IQD11). To examine a potential role of DJC31 and DJC62 in regulation of Ca^{2+} dependent processes, interaction studies with CaM4 and IQD11 were performed using BiFC. DJC31 or DJC62 ($SCFP^C$-DJC31, $SCFP^C$-DJC62), carrying the C-terminal part of SCFP at their N-terminus, were co-expressed in tobacco with either CaM4 or IQD11, N-terminally fused to the N-terminus of Venus ($VYNE^N$-CaM4, $VYNE^N$-IQD11). Protoplasts were isolated and analyzed by fluorescence microscopy. No fluorescence could be detected for neither DJC31 nor DJC62, when co-expressed with CaM4 or IQD11 (Figure 52).

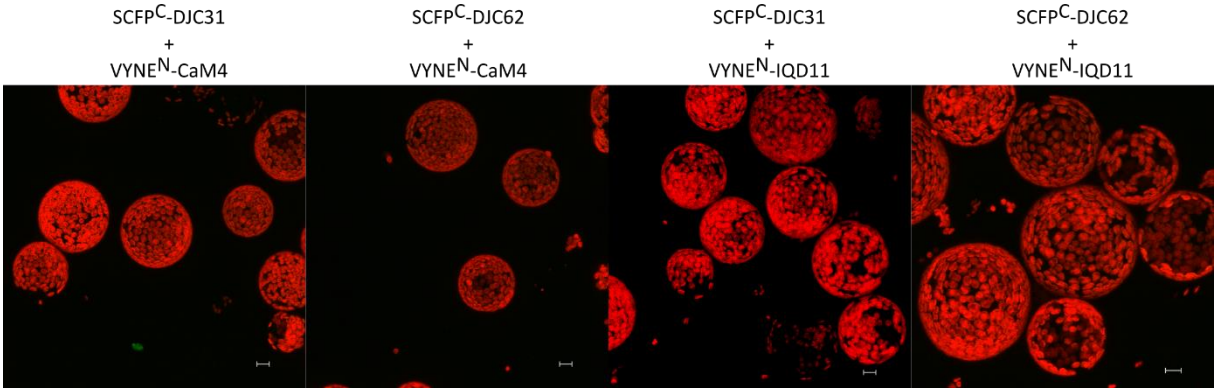

Figure 52: DJC31 and DJC62 do not interact with CaM4 or IQD11

CaM4 and IQD11 were identified as potential interaction partners in the yeast two-hybrid screening. Both proteins were N-terminally fused to the N-terminal part of VYNE. DJC31 and DJC62 were N-terminally fused to the C-terminal part of SCFP. DJC31 and DJC62 were co-expressed with either CaM4 or IQD11 in tobacco. Protoplasts were isolated for imaging. Scale bar = 10 µm.

4.9. DJC31 and DJC62 interact with ENO2

Another potential interaction partner, identified in the yeast two-hybrid screening, is ENOLASE 2 (ENO2). ENO2 catalyzes the dehydration of 2-phosphoglycerate to phosphoenolpyruvate in the glycolytic pathway. Phosphoenolpyruvate is required for ATP production and as precursor for aromatic compounds and secondary metabolites. ENO2 is encoded by the *LOS2* (LOW EXPRESSION OF OSMOTICALLY RESPONSIVE GENES 2) locus, which besides encoding ENO2, also encodes the putative transcription factor AtMBP-1 (*A. thaliana* cMyc binding protein), which is translated from a second start codon. Plants lacking *LOS2* expression show severe developmental defects, like reduced shoot and root growth, defective vascular development and impaired floral organogenesis. These defects can partially be restored by expression of a *LOS2* variant, lacking the alternative start codon for AtMBP-1 translation, which indicates that mainly the absence of ENO2 is responsible for impaired development (Eremina et al., 2015).

DJC31 and DJC62, N-terminally fused to the C-terminal part of SCFP3a (SCFP^{C}-DJC31, SCFP^{C}-DJC62) and ENO2, fused to the N-terminal part of Venus (VYNE^{N}-ENO2), were co-expressed in tobacco by leaf infiltration with agrobacteria. Protoplasts were isolated for imaging via fluorescence microscopy. Interaction between DJC31 and DJC62 with ENO2 was visible as green fluorescent spots in the cytosol (Figure 53).

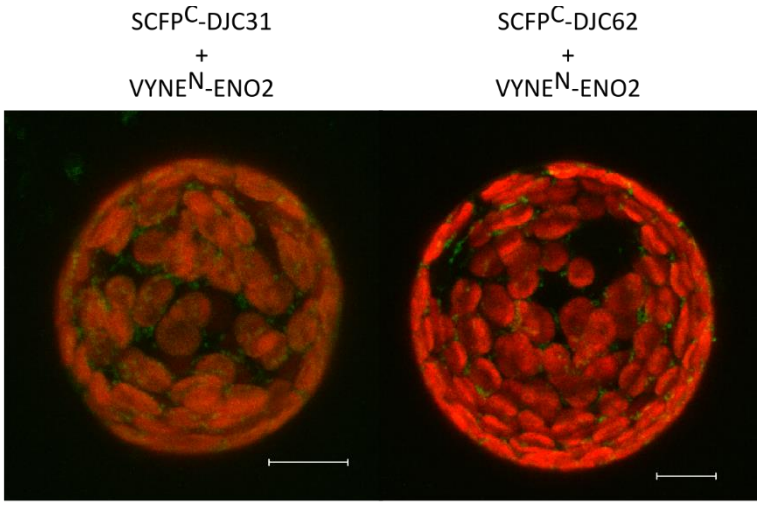

Figure 53: DJC31 and DJC62 interact with ENO2

DJC31 and DJC62 were N-terminally fused to the C-terminal part of SCFP and co-expressed in tobacco with ENO2 N-terminally fused to the N-terminal part of VYNE. Protoplasts were isolated for imaging. Scale bar = 10 µm.

4.10. Influence of hormones on growth and development

In previous experiments, the *djc31 djc62* mutant exhibited a decreased germination rate and retarded growth and development. Furthermore, *djc31 djc62* seedlings were more affected by salt or osmotic stress and under drought stress, they have proven to be more resistant to water deprivation than wild type and single mutants. Furthermore, *ABI5* was more upregulated in *djc31 djc62* under salt stress compared to Col-0. Besides transcriptional regulation, cellular processes like growth and development, as well as response to stress conditions are influenced and regulated by different plant hormones. An influence of co-chaperones on hormone signaling in *Arabidopsis* could already be observed for the mitochondrial J-protein AtJ1. Mutants lacking AtJ1 are sensitive to salt or glucose and exhibited enhanced drought tolerance. In addition, mutant seedlings are hypersensitive to abscisic acid (Park & Kim, 2014). To analyze a potential link between DJC31 and DJC62 and abscisic acid (ABA) signaling, Col-0, *djc31*, *djc62* and *djc31 djc62* seedlings were grown on ½ MS plates containing either 0.5 µM ABA or ethanol as solvent control. After 14 days, growth was compared between the different genotypes by determination of the growth stages, that were reached within this time frame.

Germination was comparable between ABA treated and untreated seedlings for all genotypes. Non-treated seedlings of Col-0, *djc3*1 and, *djc62* developed normally. Seedlings of *djc31 djc62* showed retarded growth under non-treated conditions, as observed in previous experiments. Under ABA treatment, almost all seedlings of Col-0 and *djc31* have reached the two leaves stage, whereas for *djc62* a slight reduction was visible. For *djc31 djc62*, the number of seedlings reaching the two leaves stage was tremendously decreased to 10%, whereas under non-treated conditions 44% of the seedlings could reach the two leaves stage. At the four leaves stage, the number of seedlings of wild type and single mutants was decreased to 66%-74%. For *djc31 djc62*, seedlings reaching the four leaves stage could not be observed under ABA treatment. From this result it can be concluded, that *djc31 djc62* seedlings are hypersensitive to ABA (Figure 54).

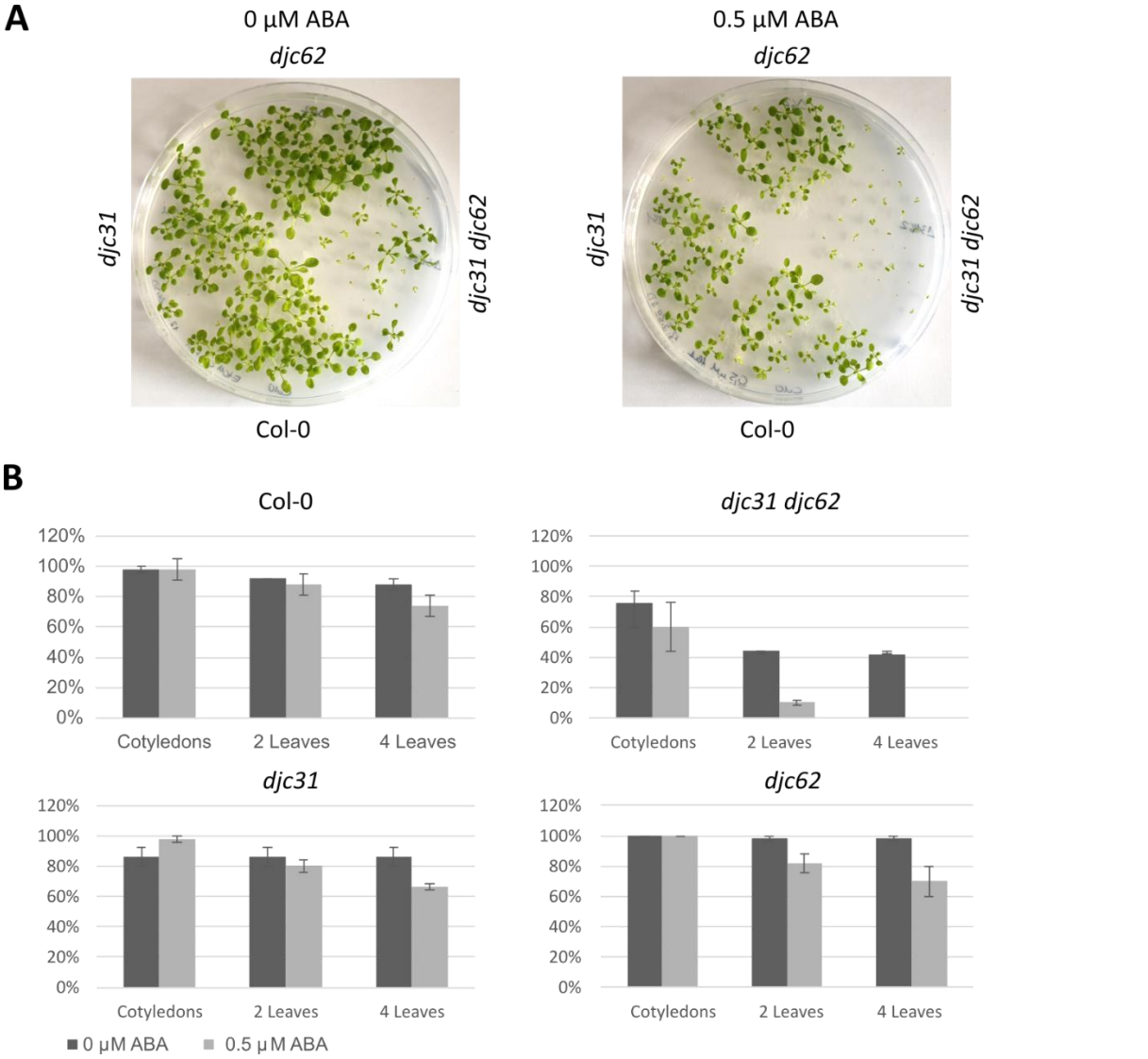

Figure 54: *djc31 djc62* seedlings are sensitive to ABA

A) Col-0, *djc31*, *djc62* and *djc31 djc62* were grown on ½ MS plates containing 0.5 µM ABA or EtOH as negative control for 14 days.

B) Quantification of growth stages reached by the different genotypes on day 14 without ABA treatment (dark gray) or with ABA treatment (light gray). *djc31 djc62* showed a strong growth reduction under treatment with ABA. Error bars represent the standard deviation; n= 50/ genotype

The molecular counterpart to abscisic acid is gibberellin (GA). Gibberellins are a large group of molecules from which the predominant forms, with hormone function, are GA_1 and GA_4. It is involved in various processes throughout the whole developmental cycle, e.g. it induces the transition from seed dormancy to seed germination (Colebrook et al., 2014). Furthermore, a study on the crosstalk between auxin and gibberellin revealed that impaired gibberellin signaling could enhance the occurrence of cotyledon defects in a *pin1* mutant (Björn C. Willige et al., 2011). In the double mutant *djc31 djc62*, lower germination rates, as well as occurrence of morphologically altered cotyledons could be observed. To examine, whether supplementation with gibberellin can enhance the

germination rate and mitigate the strong mutant phenotype of the double mutant, seeds of Col-0, *djc31*, *djc62* and *djc31 djc62* were put out on ½ MS plates containing 10 µM GA or ethanol as solvent control. Col-0, *djc31* and *djc62* were comparable regarding growth. For *djc31 djc62*, germination was slightly higher on plates containing GA, compared to the control plates. Furthermore, progression to subsequent growth stages was enhanced under GA treatment (Figure 55). However, occurrence of altered cotyledon shapes was also observed under treatment with GA but was not quantified or analyzed in more detail.

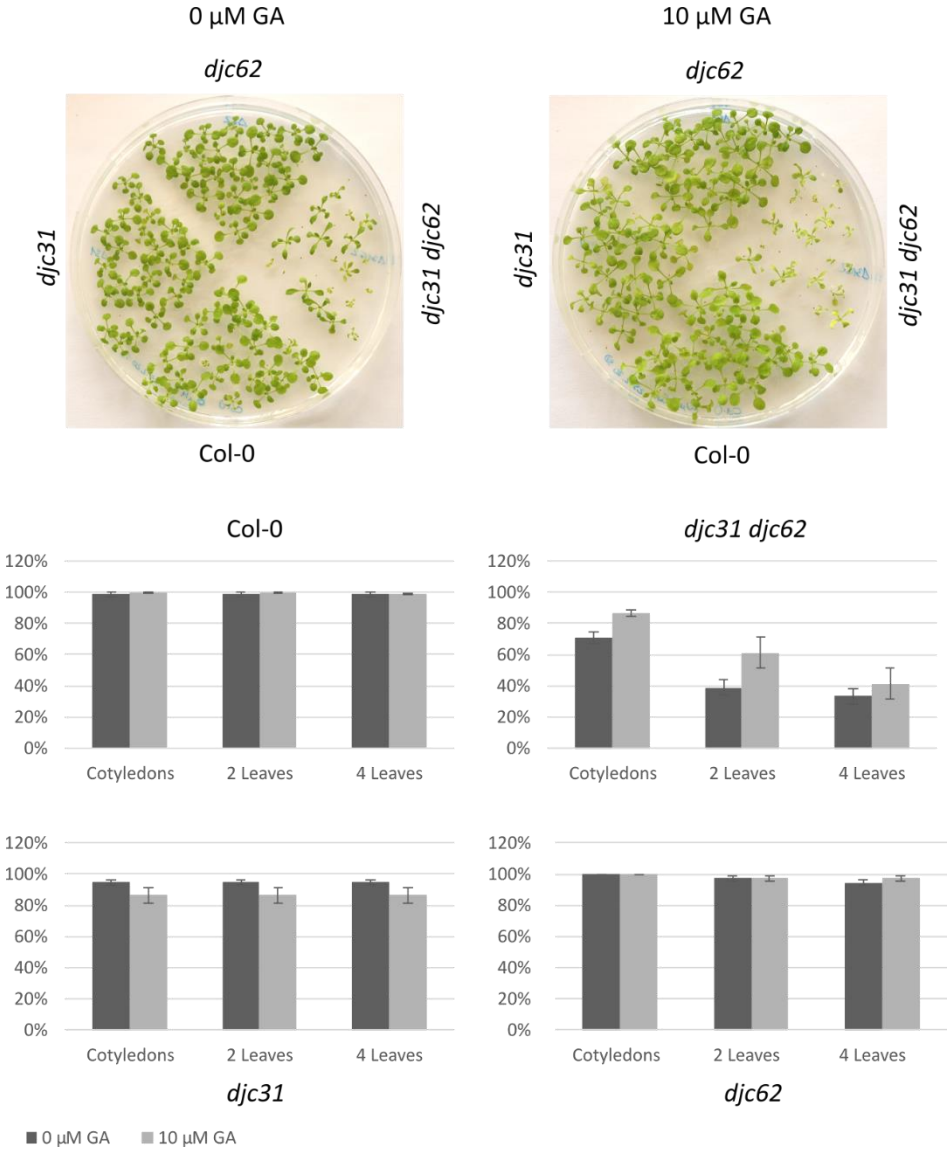

Figure 55: Effect if gibberellin on growth and development

A) Col-0, *djc31*, *djc62* and *djc31 djc62* were grown on ½ MS plates containing 10 µM GA for 14 days. EtOH was used as solvent control.

B) Quantification of growth stages reached by the different genotypes on day 14 without GA treatment (dark gray) or with GA treatment (light gray). Col-0, *djc31* and *djc62* were comparable in growth. Growth of *djc31 djc62* was slightly enhanced. Error bars represent the standard deviation; n= 75/ genotype

To confirm, that GA indeed can enhance germination rates for *djc31 djc62* seeds and partially prevents the growth arrest, which was observed during the phenotyping after the cotyledon stage for some seedlings, 150 seeds of wild type and double mutant were put out on ½ MS plates with 10 µM GA, 30 µM GA and plates containing ethanol as solvent control. After 14 days, the growth stages reached within this time frame were analyzed. Col-0 seedlings developed normally under non-treated and GA-treated conditions. On GA containing plates, ¼ of the Col-0 seedlings were able to reach the six leaves stage. For *djc31 djc62*, the enhanced germination rate, that was observed before upon treatment with GA, could not be confirmed in this experiment for neither supplementation with 10 µM nor 30 µM GA. Also enhanced progression to subsequent growth stages could not be observed again, which indicates, that GA cannot at least partially rescue the mutant phenotype (Figure 56).

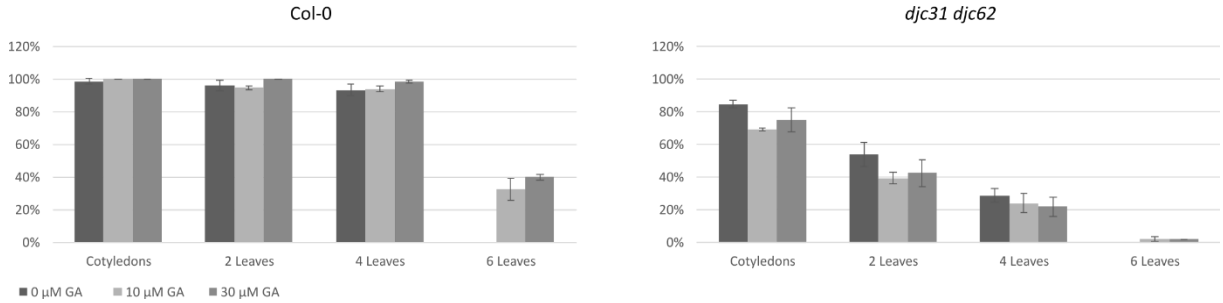

Figure 56: The growth enhancing effect of GA on *djc31 djc62* could not be confirmed

Col-0 and *djc31 djc62* were grown on ½ MS plates containing 10 µM or 30 µM GA for 14 days. The growth enhancing effect of GA on *djc31 djc62* could not be confirmed. Error bars represent the standard deviation; n= 150/ genotype.

5. Discussion

Chaperones have been described to be involved in a multitude of different processes, like folding and refolding of proteins, assembly of protein complexes, protein trafficking and degradation. Additionally, they play a role in response to stress (Rosenzweig et al., 2019). Plants are confronted with many different biotic and abiotic stress factors, like pathogens, soil salinity, drought and varying or extreme temperatures. Since plants are sessile organisms, efficient adaptation strategies are essential in order to survive. With 18 HSP70 proteins, 118 HSP40 proteins, seven HSP90 proteins, their co-chaperones and other factors, *Arabidopsis thaliana* possesses a complex and versatile chaperone machinery with both overlapping and specialized functions (Craig & Marszalek, 2017; di Donato & Geisler, 2019; Lin et al., 2001). Unfortunately, the interplay of this complex chaperone network as well as precise mechanisms of how chaperones and their co-chaperones are involved in different cellular processes are barely understood so far. In this work, two HSP40/J-proteins, DJC31 and DJC62, were investigated to broaden the understanding of the function and importance of co-chaperones for plant viability.

5.1. DJC31 and DJC62 play an important role in growth and development

Knockout of either *DJC31* or *DJC62* led to only a very mild phenotype. Leaves and other organs of the single mutants looked comparable to wild type, but in later stages a slight growth retardation was visible. Crossing of the two single mutants yielded the double mutant *djc31 djc62*, which exhibited a strong growth and developmental phenotype. The plate-based phenotyping approach revealed that *djc31 djc62* was delayed in growth at all stages from seed imbibition to reaching the four-leaves-stage and additionally, a growth arrest for approximately 20% of the seedlings was observed after the cotyledon stage. Also in the soil-based phenotyping, retarded growth of the double mutant was apparent. Especially the flowering period was tremendously elongated. Besides the slow development, the double mutant exhibited several aberrant morphological features. 12% of the seedlings showed cotyledon defects, with heart-shaped, fused or bipartite appearances. Similar cotyledon morphologies could already be observed in mutants defective in auxin transport (Huang et al., 2010). Another study could show, that

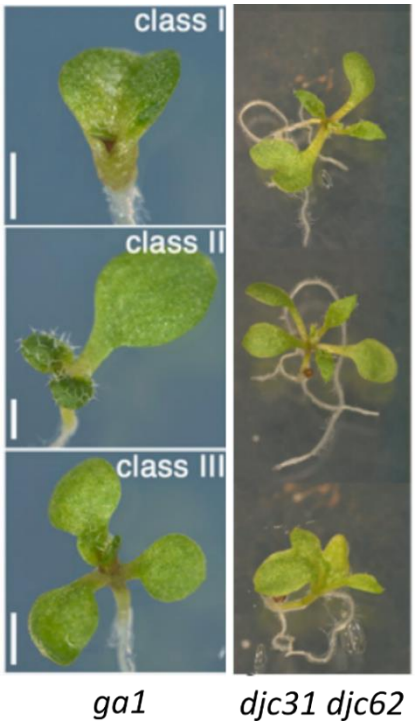

Figure 57: Comparison of the cotyledon mutant morphologies of *ga1* and *djc31 djc62*.
Cotyledons of the *ga1* mutant show fused cotyledons, single cotyledons or triple cotyledons (left side, adapted from Willige et al. 2011). Cotyledons of the double mutant *djc31 djc62*(B. C. Willige et al., 2011) exhibit heart-shaped, triple and fused cotyledons (right side).

13.3% of the *Arabidopsis* seedlings lacking the auxin transporter PIN1 exhibited different altered cotyledon morphologies. Also in 1.8% of *ga1* seedlings, which are deficient in gibberellin (GA) biosynthesis, cotyledon defects could be observed (Figure 57). Crossing of the two mutants increased the occurrence of cotyledon defective seedlings to 25% in the *ga1*/*pin1* mutant, presumably caused by decreased PIN protein levels and auxin transport, which was already observed in GA pathway mutants (B. C. Willige et al., 2011). However, external supply of gibberellin could not significantly reduce the severe development and growth phenotype of *djc31 djc62*.

Also the *djc31 djc62* rosette leaves were affected by the double knockout. While *djc31* or *djc62* single mutants exhibited leaf shapes comparable to wild type, the leaves of *djc31 djc62* were shortened, thin and crumpled. A similar phenotype was already observed in overexpression mutants of the auxin transporter PIN5 (*PIN5 OX*) (Figure 58). *PIN5 OX* plants showed reduced activity of the synthetic auxin reporter DR5*rev::GFP* in root meristems. Furthermore, the level of free indole-3-acetic acid (IAA) was decreased in root tips and rosette leaves, whereas in the *pin5* knockout mutant both the auxin reporter activity in root meristems, as well as free IAA levels in root tips and rosette leaves were increased. Both findings indicate that the *PIN5 OX* phenotype might be caused by a disturbed auxin homeostasis (Mravec et al., 2009). Besides the strong leaf phenotype also other organs were affected by the knockout of *DJC31* and *DJC62*. *djc31 djc62* grew bushy with thinner stems, less side branches and extremely shortened roots, which barely formed lateral roots. Furthermore, the seed yield was tremendously decreased, which is most likely caused by the severe defects in flower development and morphology, since viable pollen was produced. Development of different organs in general largely depends on different plant hormones (di Donato & Geisler, 2019). Especially flower development is regulated by a complex interplay of different hormones like jasmonic acid for filament development and anther dehiscence, ethylene to promote carpel development, gibberellin as regulator of stamen and pollen development and auxin, which regulates size, number and location of flowers and their development (Smith & Zhao, 2016). Considering the strong

Figure 58: Comparison of the leaf phenotypes between PIN5 OX and djc31 djc62.

Adult plants of PIN5 OX exhibit wrinkled and narrow rosette leaves (Upper panel, adapted from Mravec et al. 2009). Rosette leaves of djc31 djc62 show a similar phenotype with narrow. wrinkled leaves (lower panel).

phenotype of the double mutant, which exhibits diverse defects at almost all organs, it is conceivable that DJC31 and DJC62 are involved in regulation of hormone biosynthesis, transport or signaling.

5.2. DJC31 and DJC62 are attached to the cytosolic side of the ER membrane

DJC31 and DJC62 were first described in an *in silico* study about carboxylate clamp type tetratricopeptide repeat proteins in *Arabidopsis*. Using different localization prediction tools, both proteins were predicted to be located in either the nucleus or the chloroplast (Prasad et al., 2010). Based on this study, Chiu et al included DJC31 and DJC62 in their study about chloroplast J-proteins and determined a plastidal localization of both proteins via chloroplast import experiments. However, the import efficiency was rather low and more than one mature form of the respective protein was observed on the gel after import, whereas the highest bands were close in size to the precursor proteins. To confirm this result, they repeated the import experiment, using truncated versions of the two proteins. Both fragments were imported, but again yielded more than one fragment after processing within the chloroplast. It was concluded, that DJC31 and DJC62 are both located in the chloroplast but possess only a very short transit peptide or a transit peptide which is not always removed (Chiu et al., 2013).

Since previous studies did not provide a clear evidence for a plastidal localization, localization studies on DJC31 and DJC62 were repeated in this study using a different approach. Using TargetP 1.1, a chloroplast transit peptide could be predicted, which was 48 amino acids in length for DJC31 and a very short transit peptide of only four amino acids in length for DJC62. To confirm this prediction experimentally, the first 80 amino acids of DJC31 and DJC62 were fused to GFP and were transiently expressed in tobacco. A localization to the chloroplast could not be observed for neither DJC31-TP-GFP, nor DJC62-TP-GFP, indicating that both proteins do not contain a chloroplast transit peptide. To determine the subcellular localization of DJC31 and DJC62, GFP localization studies were performed, using the N-terminal half of DJC31 or DJC62, C-terminally fused to GFP. The two GFP-fusion constructs were co-expressed in *Arabidopsis* protoplasts with fluorescent compartment markers for either the endoplasmic reticulum or the Golgi apparatus. Overlapping localization patterns could only be observed for DJC31Int-GFP or DJC62Int-GFP and the ER-marker, indicating both proteins to localize to the endoplasmic reticulum. Again an overlap between the GFP signals and the chlorophyll autofluorescence could not be detected, which supports the idea, that DJC31 and DJC62 are not located in the chloroplast. To prove this finding on a biochemical level, western blot analysis with isolated chloroplasts and microsomes was performed, using an antibody specific for either DJC31 or DJC62. Bands for DJC31 and DJC62 could only be detected in microsomes. Since microsomes do not only contain membranes derived from the ER, but also from the Golgi apparatus, plasma membrane and the outer mitochondrial membrane, a microsomal shift assay was performed (Fujiki et al., 1982).

This approach uses the feature of ribosomes to be attached to the ER membrane in the presence of Mg^{2+}. If microsomal membranes are isolated in presence of EDTA, ribosomes are removed, which causes a shift of ER derived membranes to lighter fractions in a sucrose gradient, thus providing a specific test for ER localized proteins (Schweiger et al., 2012). Both DJC31 and DJC62 showed a shift to lighter fractions in microsomal samples treated with EDTA as it could also be observed for the ER resident HSP70 chaperone BiP, which was used as a control. This finding was surprising, since neither DJC31, nor DJC62 carry typical signal sequences or motifs which mediate transport and retention to the ER. To analyze, whether DJC31 and DJC62 are located in the ER lumen or at the cytosolic side of the ER, split GFP was used. In this experiment a GFP signal could only be detected if the N-terminal half of either DJC31 or DJC62 fused to GFP11 was co-expressed with the cytosolic split GFP counterpart. This clearly showed, that DJC31 and DJC62 are located in the cytosol at the ER membrane. DJC31 and DJC62 could only be detected in western blot experiments, if isolated microsomes were used, which requires both proteins to be either enclosed by a membrane or to be attached to the ER. To gain more information about how DJC31 and DJC62 localize to the ER membrane, isolated microsomes were treated with different buffers and conditions. Carbonate treatment transforms vesicles into open membrane sheets, thus releasing the vesicles content and peripherally attached proteins like ribosomes (Fujiki et al., 1982). The band pattern on the western blot showed that carbonate treatment only partially removed DJC31 and DJC62 from the microsomal membranes. Also treatment with urea led only to release of a small portion into the soluble fraction. Only solubilization of the microsomes with SDS made DJC31 and DJC62 soluble, indicating that both proteins are tightly attached to the ER membrane. A previous *in silico* analysis, using the Kyte Doolittle hydrophobicity scale, indicated that presence of transmembrane domains in DJC31 and DJC62 is unlikely, since the threshold value was not reached, and the overall hydrophobicity was rather low. Besides transmembrane domains, proteins can also be anchored to membranes via lipid post-translational modifications. The subcellular GFP expression pattern of a construct, in which the flexible N-terminal part of DJC31 and DJC62 was replaced by GFP, did not match the expression pattern of the ER marker anymore. This indicates that attachment to the ER membrane is most likely mediated by the respective N-terminal part of the two proteins. Therefore, anchoring by glycosylphosphatidylinositol (GPI) anchors, farnesylation and geranylgeranylation can be excluded, since these modifications are added to the protein's C-terminus (Guan & Fierke, 2011; Zhou, 2019). Myristoyl groups are added to the N-terminus, however, DJC31 and DJC62 lack the respective myristoylation signal sequences (Guan & Fierke, 2011). S-acylation is so far not well studied and typical signal motifs for modification are still unknown. Although S-acylation usually occurs in combination with transmembrane domains or other lipid modifications, it cannot be excluded that DJC31 and DJC62 are attached to the ER membrane by S-acylation (Hurst & Hemsley,

2015). Another possibility of tethering to the ER membrane might be mediated by attachment to integral membrane proteins or protein complexes in the ER membrane.

5.3. DJC31 and DJC62 are co-chaperones of HSP70 and HSP90

DJC31 and DJC62 are composed of several TPR repeats in their C-terminal half, which form two TPR domains. Alignments with the two TPR domains of the human HSP70/HSP90 co-chaperone TPR2 showed that the TPR domains of DJC31 and DJC62 share the conserved K_5N_9-N_6-K_2R_6 motif, forming a carboxylate clamp, that recognizes the EEVD motif, which is present in cytosolic HSP70 and HSP90 chaperones (Brychzy et al., 2003; Prasad et al., 2010). Like TPR2, DJC31 and DJC62 carry a J-domain at the C-terminus, which is needed for activation of the HSP70 ATPase domain (Kampinga & Craig, 2010). This domain composition indicated that DJC31 and DJC62 might act as co-chaperones of cytosolic HSP70 and HSP90. Using BiFC, an interaction with HSP70.1 and HSP90.2 could be experimentally verified for both DJC31 and DJC62. However, no HSP70 or HSP90 protein could be identified as interaction partner in the yeast two-hybrid library screening. Since a fragmented cDNA-library was used, it might be that the respective fragments of HSP70 and HSP90, which are able to interact with DJC31, were not stable in yeast or not properly folded. Furthermore, yeast cytosolic HSP70 and HSP90 might compete with the respective library fragments for binding to the TPR or J-domains.

The protein folding pathway includes a handover of the client protein from HSP70 to HSP90, which is mediated via HOP. The human co-chaperone TPR2 was found to disrupt the HSP90-client interaction and by inducing ATP hydrolysis with its J-domain, the client is bound by HSP70. It was proposed that this mechanism constitutes the opportunity for certain polypeptides, which fail to fold properly after the first HSP70/HSP90 cycle, to re-enter the cycle again and thus reducing the risk of aggregation in the cytosol (Brychzy et al., 2003). Although DJC31 and DJC62 possess a long, disordered N-terminal part, which is not present in TPR2, they are the only cytosolic co-chaperones in *Arabidopsis thaliana* combining two carboxylate clamp type TPR domains with a J-domain (Prasad et al., 2010). Therefore, they might be functional homologs of the human co-chaperone TPR2 and might act in a similar way as mediators between HSP70 and HSP90 to prevent unstable proteins from aggregation and help them to re-enter the folding cycle.

Stable transformation of *djc31 djc62* with constructs carrying a mutation in the HPD motif could not rescue the double mutant phenotype. According to the literature, experiments using HPD-motif mutants often do not show an effect, since their function in binding/holding a client or in preventing aggregation is more prominent than the dependency as co-chaperone on HSP70 (Kampinga et al., 2019). This supports the idea that DJC31 and DJC62 are not predominantly involved in preventing aggregation but that their function is strongly dependent on HSP70 client binding. Therefore, the remaining mutant phenotype cannot be rescued, because DJC31 H1052Q and DJC62 H1006Q either

disturb the folding pathway by releasing the client from HSP90 but prevent HSP70 binding because of the missing ATPase activation. Additionally, there might be client proteins, for which activation or regulation is strictly dependent on the retrograde transfer from HSP90 back to HSP70.

5.4. DJC31 and DJC62 are involved in stress response and hormonal signaling

Chaperones in plants have been described to be involved in response to various stresses, such as cold and heat stress, drought, osmotic stress, light and pathogens (Jacob et al., 2017). Therefore, the response to different stresses was tested for the single mutants *djc31* and *djc62*, as well as for the double mutant *djc31 djc62*. Although DJC31 and DJC62 are located at the ER membrane, enhanced sensitivity to ER stress could not be observed. However, the double mutant seedlings exhibited enhanced sensitivity to salt stress, whereas single mutants and wild type were not affected. Besides osmotic stress, NaCl can also be harmful due to ionic toxicity. Therefore, growth on mannitol and glucose, as non-ionic osmotic stress agents, was also tested. Again, *djc31 djc62* seedlings were severely affected by the treatment. This indicated DJC31 and DJC62 to be of special importance during osmotic stress. Furthermore, *djc31 djc62* showed enhanced tolerance to drought, which was surprising, since the responses to osmotic stress and drought share different regulatory signaling pathways (Zhu, 2002). However, it must be noted that osmotic stress and drought were tested at different growth stages. Whereas water was withheld from two weeks old plants, osmotic stress was tested during germination and the early seedling stage. Whether older plants are also sensitive to osmotic stress should be analyzed in more detail to exclude effects, which are specific to defects in germination and early seedling growth. To analyze the drought response in more detail, transpiration rates of Col-0, *djc31*, *djc62* and *djc31 djc62* were determined. However, differences in water loss compared to wild type could not be observed for neither the single mutants, nor the double mutant, but it must be taken into account, that there are huge differences in overall size and the surface area between double mutant and wild type, which limits the comparability of the transpiration rates. Increased sensitivity to ABA was also observed for *djc31 djc62*, indicating a role in ABA signaling. Therefore, qPCR analysis was performed with *ABI5* and *RD29A*, two genes involved in ABA signaling and osmotic stress response (Clément et al., 2011; Park & Kim, 2014). Under non-stressed conditions expression levels of *ABI5* and *RD29A* were comparable between Col-0 and *djc31 djc62*. After treatment with 150 mM NaCl for six hours, *ABI5* was induced two-fold in Col-0 and four-fold in *djc31 djc62*. *RD29A* was also upregulated under salt stress, but the expression level in *djc31 djc62* was not significantly higher compared to wild type. However, this indicated that ABA signaling is enhanced in *djc31 djc62* under salt stress. Therefore the poor growth of *djc31 djc62* under osmotic stress can also be caused by the inhibitory effect of increased ABA levels and its associated pathways.

A similar behavior under osmotic and drought stress was observed for *ATJ1* mutants. AtJ1 is a J-protein, which was reported to be located in mitochondria. Seedlings of the two mutants *atj1* and *as793* were hypersensitive to glucose and salt but two weeks old plants on soil showed increased tolerance to drought, compared to wild type and the complementation line. Additionally, the water loss rate of detached leaves from *atj1* and *as793* was lower compared to wild type, which might contribute to the drought tolerance. Furthermore, both mutants are hypersensitive to abscisic acid (ABA). ABA levels were equal between wild type and mutant, but proline levels were increased in *as793,* which might enhance osmotolerance. Furthermore, expression of the proline biosynthetic gene *P5CS1* was increased under normal conditions, whereas under salt stress conditions expression levels were comparable between *as793* and wild type. Besides the aberrant behavior under stress conditions, *atj1* and *as793* exhibited slow growth and a delay in reaching the bolting stage, which might be caused by altered expression levels of genes involved in embryogenesis and flowering time. Besides that, deviations in expression levels of genes related to stress response could be observed (Park & Kim, 2014). Another research group reported that seedlings were sensitive to salt stress but four weeks old *atJ1* plants showed increased tolerance to osmotic stress when treated with 175 mM NaCl for two weeks, Furthermore, they detected higher glucose levels in a*tj1* plants, which might have influence on different developmental processes as a signal molecule. Furthermore, glucose signaling is linked to hormone biosynthesis and signaling, especially for ABA. Taken together, both studies propose that AtJ1 is a modulator of several genes involved in plant development and stress response (Park & Kim, 2014; Wang et al., 2014).

Considering the overlapping findings between *djc31 djc62* and *as793* or *atJ1* regarding seedling sensitivity to ABA, salt, glucose and mannitol and the enhanced drought tolerance, it is conceivable, that DJC31 and DJC62 might also be regulators of ABA signaling and developmental or stress related pathways and should be analyzed in more detail regarding concentration levels of compatible osmolytes, like proline. This is supported by RNAseq data of *djc31*, *djc62* and *djc31 djc62*, which show altered expression of factors involved in biotic and abiotic stress response, response to hormones and signal transduction. However, because of functional redundancy, deregulation of different genes might be compensated in *djc31* and *djc62*, since a mutant phenotype or altered response to stress was barely visible. Analysis of the RNAseq data using MapMan revealed, that especially different transcription factors were up or downregulated. Noticeably, calcium signaling was predominantly downregulated. In the DJC31 yeast two-hybrid screening, CaM4 and IQD11, two factors involved in calcium signaling, were identified as potential interaction partners. Unfortunately, this interaction could not be confirmed via BiFC. However, this was only tested under non-stress conditions and considering the relevance of DJC31 and DJC62 in stress response and the importance of calcium signaling for different stress pathways, this experiment should be repeated under stress conditions.

Another protein that was identified as a potential interaction partner in the screening was ENO2. Using BiFC an interaction with DJC31 and DJC62 could be confirmed. ENO2 is encoded by the *LOS2* gene, which also encodes the putative transcription factor AtMBP-1 that is translated from a second start codon and regulates the expression of ENO2. Both proteins were reported to be important for proper plant development and response to osmotic and drought stress (Z. J. Liu et al., 2020). The *los2/eno2* mutant shows several developmental defects, like dwarfism and disturbed flower development. Furthermore, *los2/eno2* mutants overaccumulate salicylic acid. The growth repressing effect of salicylic acid is not well understood so far, but it was reported, that salicylic acid has impact on gibberellin biosynthesis or signaling and mutants with increased salicylic acid levels show alterations in auxin levels and responsiveness (Eremina et al., 2015). The fact that ENO2 is involved in osmotic stress response makes it an interesting interaction partner to be analyzed in more detail. Furthermore, as a glycolytic enzyme it is involved in the production of phosphoenolpyruvate, which is a precursor for aromatic compounds and secondary metabolites (Eremina et al., 2015). Therefore, it is likely that the growth defects and the altered stress response of *djc31 djc62* might also be influenced by changes on the metabolic level.

5.5. DJC31 and DJC62 are regulated on the protein level by attachment to the ER membrane

Since the *djc31* and *djc62* single mutants did not show a strong phenotype, as observed for the *djc31 djc62* double mutant, it seemed likely, that the lack of one gene is compensated by the upregulation of the other gene. However, an up- or downregulation of either *DJC31* in *djc62* or *DJC62* in *djc31* could not be observed. Also western blot analysis did not show enhanced protein levels of the remaining protein in *djc31* or *djc62*. Under stress conditions *djc31 djc62* seedlings were severely affected, indicating DJC31 and DJC62 to be of special importance. Therefore, an enhanced expression of the two genes would be conceivable. However, significantly elevated or reduced expression levels under ER stress, heat or salt stress could neither be observed for *DJC31,* nor for *DJC62*. This can have several reasons. Either DJC31 and DJC62 are not directly involved in response to stress or DJC31 and DJC62 are available in amounts, which are sufficient also under stress conditions.

DJC31 and DJC62 were both found to be attached to the ER membrane. Since their predicted hydrophobicity is rather low, the presence of transmembrane domains or direct attachment to the membrane is rather unlikely. Therefore, DJC31 and DJC62 might be anchored by post-translational modification, which can be reversible in case of S-acylation, or by interaction with proteins in the ER membrane (Chamberlain & Shipston, 2015). Since both modes of attachment can be transient, it raises the question, whether DJC31 and DJC62 are always located at the ER or whether they change their localization under certain circumstances. Since previous experiments revealed DJC31 and DJC62 to be

of special importance for the response to stress, protoplasts co-expressing the N-terminus of either DJC31 or DJC62,fused to GFP, together with an ER marker, were treated with NaCl. After two hours, detachment of the DJC31 and DJC62 constructs from the ER membrane could be observed, with GFP spot formation in the cytosol. This indicated that DJC31 and DJC62 are released from the ER membrane into the cytosol under stress conditions.

Localization studies using constructs consisting of the C-terminal part of DJC31 or DJC62 fused N-terminally to GFP could show, that attachment to the ER membrane is mediated by the N-terminal half of the two proteins. Moreover, the full-length proteins N-terminally tagged with GFP were not able to properly attach to the ER membrane, as they were observed to be more distributed in the cytosol. These constructs were used to stably transform the *djc31 djc62* double mutant but failed to rescue the phenotype. This indicated that attachment to the membrane has a regulatory effect on DJC31 and DJC62 and restricts their function in a spatial and temporal manner, providing a mechanism for a fast response to developmental and stress related signals.

Taken together, it can be concluded that DJC31 and DJC62 are regulated on the protein level by attachment to the ER membrane, rather than on the transcriptional level.

6. Conclusion and Outlook

DJC31 and DJC62 are two class C J-proteins in *Arabidopsis thaliana*, which were determined to be attached to the cytosolic side of the ER membrane, mediated by their long, disordered N-terminal halves. At the C-terminus, both proteins carry several TPR repeats, which form two TPR domains, and a J-domain. This indicated, that both proteins act as co-chaperones of HSP70 and HSP90. Interaction with these two chaperones could experimentally be verified and additionally, a strong dependency on activation of the HSP70 ATPase domain and client binding could be determined. Knockout of both genes leads to impaired growth and development, which affects almost all organs. Moreover, DJC31 and DJC62 were found to be involved in the response to osmotic and drought stress. Instead of being up- or downregulated under salt stress, they were found to be released from the ER membrane into the cytosol. Together with the sensitivity to ABA, the altered expression of different factors involved in stress response and hormonal signaling, these findings indicated DJC31 and DJC62 to be regulators of different developmental and stress related pathways.

However, many open questions remain. How DJC31 and DJC62 are attached to the membrane is still not clear. It is conceivable that membrane binding is mediated by post-translational modification, e.g. S-acylation, which could be tested by measuring the incorporation of [^{3}H] palmitate. Furthermore, attachment could also be mediated by interaction with proteins of the ER membrane. Therefore, pull-down experiments, maybe with crosslinking to stabilize the interaction, could be performed to identify potential membrane proteins or complexes, which hold DJC31 and DJC62 at the membrane. That both proteins are released from the membrane under salt stress conditions raises the question, whether attachment to the ER represents a kind of inactive state or whether DJC31 and DJC62 are additionally of special importance for processes at and in the ER. However, interaction with HSP70 and HSP90 was also observed in the cytosol in absence of NaCl. This can either mean that a portion of DJC31 and DJC62 is soluble also under non-stress conditions or the release from the membrane might be caused by the experimental setup. On one side, microscopy can induce stress, on the other side, the two proteins were tagged with the BiFC fluorophores at their N-termini, which was shown to interfere with proper membrane attachment. To analyze this in more detail, cell fractionation by differential and gradient centrifugation with and without salt treatment could be performed to analyze localization changes without modifying the proteins. Furthermore, both the interaction between DJC31 and DJC62 with the chaperones and the stress induced release from the membrane were visible as GFP spots in the cytosol, whereas it has to be kept in mind that for the latter experiment only the N-terminus fused to GFP was used, which might lead to aggregation. For HOP proteins in Arabidopsis, spot formation in the cytosol was observed upon heat stress, which could be identified as localization to stress granules (Fernández-Bautista et al., 2018). Since stress granules are also formed under salt stress, it could be tested whether

DJC31 and DJC62 also localize to cytoplasmic stress granules by co-localization studies under stress conditions using a stress granule marker protein like (UBIQUITIN-SPECIFIC PROTEASE 1) UBP1 or isolation of stress granules and analysis of their composition (Fernández-Bautista et al., 2018; Kosmacz & Skirycz, 2020). DJC31 and DJC62 both possess a long, disordered N-terminus, which is presumably responsible for localization to the ER. Besides determining the protein's localization, it might be involved in selection and binding of client proteins, since some disordered proteins are known to mediate protein-protein interaction by undergoing a disorder-to-order transition upon recognition of a specific protein. This feature was observed especially in factors involved in signaling and regulation and can also be induced by special signals or post-translational modifications (Mészáros et al., 2018). Performing a yeast two-hybrid library screening, several potential client proteins could be determined for DJC31, which need to be verified using the full-length proteins, because a fragmented cDNA library was used. For ENO2 interaction with DJC31 and DJC62 could be confirmed by BiFC. Since also in this experiment DJC31 and DJC62 carried the fluorophore at the N-terminus, which might lead to impaired localization, it needs to be analyzed in more detail under which conditions this interaction takes place. Furthermore, it could be that DJC31 and DJC62 do not bind directly to ENO2, but a signal is detected by close proximity of the fluorophores, while ENO2 is actually bound by HSP70 or HSP90. In this case DJC31 and DJC62 could act as mediators between HSP70 and HSP90 as it is described for the human co-chaperone TPR2 (Brychzy et al., 2003). The phenotype of *djc31 djc62* exhibited different features that have been already observed in mutants altered in auxin homeostasis or transport. HSP90 and several of its co-chaperones have already been described in *Arabidopsis* to be involved in auxin dependent and regulatory processes (di Donato & Geisler, 2019). Therefore, auxin signaling and transport, especially the amount and localization of PIN proteins, should be analyzed in *djc31 djc62* in more detail.

7. References

Afgan, E., Baker, D., van den Beek, M., Blankenberg, D., Bouvier, D., Cech, M., Chilton, J., Clements, D., Coraor, N., Eberhard, C., Gruning, B., Guerler, A., Hillman-Jackson, J., Von Kuster, G., Rasche, E., Soranzo, N., Turaga, N., Taylor, J., Nekrutenko, A., & Goecks, J. (2016). The Galaxy platform for accessible, reproducible and collaborative biomedical analyses: 2016 update. *Nucleic Acids Res, 44*(W1), W3-W10. doi:10.1093/nar/gkw343

Ajit Tamadaddi, C., & Sahi, C. (2016). J domain independent functions of J proteins. *Cell Stress Chaperones, 21*(4), 563-570. doi:10.1007/s12192-016-0697-1

Ali, M. M., Roe, S. M., Vaughan, C. K., Meyer, P., Panaretou, B., Piper, P. W., Prodromou, C., & Pearl, L. H. (2006). Crystal structure of an Hsp90-nucleotide-p23/Sba1 closed chaperone complex. *Nature, 440*(7087), 1013-1017. doi:10.1038/nature04716

Almagro Armenteros, J. J., Salvatore, M., Emanuelsson, O., Winther, O., von Heijne, G., Elofsson, A., & Nielsen, H. (2019). Detecting sequence signals in targeting peptides using deep learning. *Life Sci Alliance, 2*(5). doi:10.26508/lsa.201900429

Altschul, S. F., Madden, T. L., Schaffer, A. A., Zhang, J., Zhang, Z., Miller, W., & Lipman, D. J. (1997). Gapped BLAST and PSI-BLAST: a new generation of protein database search programs. *Nucleic Acids Res, 25*(17), 3389-3402. doi:10.1093/nar/25.17.3389

Anfinsen, C. B. (1973). Principles that govern the folding of protein chains. *Science, 181*(4096), 223-230. doi:10.1126/science.181.4096.223

Balchin, D., Hayer-Hartl, M., & Hartl, F. U. (2016). In vivo aspects of protein folding and quality control. *Science, 353*(6294), aac4354. doi:10.1126/science.aac4354

Bertelsen, E. B., Chang, L., Gestwicki, J. E., & Zuiderweg, E. R. (2009). Solution conformation of wild-type E. coli Hsp70 (DnaK) chaperone complexed with ADP and substrate. *Proc Natl Acad Sci U S A, 106*(21), 8471-8476. doi:10.1073/pnas.0903503106

Boavida, L. C., & McCormick, S. (2007). Temperature as a determinant factor for increased and reproducible in vitro pollen germination in Arabidopsis thaliana. *Plant J, 52*(3), 570-582. doi:10.1111/j.1365-313X.2007.03248.x

Boyes, D. C., Zayed, A. M., Ascenzi, R., McCaskill, A. J., Hoffman, N. E., Davis, K. R., & Görlach, J. (2001). Growth stage-based phenotypic analysis of Arabidopsis: a model for high throughput functional genomics in plants. *Plant Cell, 13*(7), 1499-1510. doi:10.1105/tpc.010011

Bradford, M. M. (1976). A rapid and sensitive method for the quantitation of microgram quantities of protein utilizing the principle of protein-dye binding. *Anal Biochem, 72*, 248-254. doi:10.1006/abio.1976.9999

Brychzy, A., Rein, T., Winklhofer, K. F., Hartl, F. U., Young, J. C., & Obermann, W. M. (2003). Cofactor Tpr2 combines two TPR domains and a J domain to regulate the Hsp70/Hsp90 chaperone system. *EMBO J, 22*(14), 3613-3623. doi:10.1093/emboj/cdg362

Chamberlain, L. H., & Shipston, M. J. (2015). The physiology of protein S-acylation. *Physiol Rev, 95*(2), 341-376. doi:10.1152/physrev.00032.2014

Chen, Y., & Brandizzi, F. (2013). Analysis of unfolded protein response in Arabidopsis. *Methods Mol Biol, 1043*, 73-80. doi:10.1007/978-1-62703-532-3_8

Chiu, C. C., Chen, L. J., Su, P. H., & Li, H. M. (2013). Evolution of chloroplast J proteins. *PLoS One, 8*(7), e70384. doi:10.1371/journal.pone.0070384

Clément, M., Leonhardt, N., Droillard, M. J., Reiter, I., Montillet, J. L., Genty, B., Laurière, C., Nussaume, L., & Noël, L. D. (2011). The cytosolic/nuclear HSC70 and HSP90 molecular chaperones are important for stomatal closure and modulate abscisic acid-dependent physiological responses in Arabidopsis. *Plant Physiol, 156*(3), 1481-1492. doi:10.1104/pp.111.174425

Colebrook, E. H., Thomas, S. G., Phillips, A. L., & Hedden, P. (2014). The role of gibberellin signalling in plant responses to abiotic stress. *J Exp Biol, 217*(Pt 1), 67-75. doi:10.1242/jeb.089938

Craig, E. A., & Marszalek, J. (2017). How Do J-Proteins Get Hsp70 to Do So Many Different Things? *Trends Biochem Sci, 42*(5), 355-368. doi:10.1016/j.tibs.2017.02.007

D'Alessandro, S., Golin, S., Hardtke, C. S., Lo Schiavo, F., & Zottini, M. (2015). The co-chaperone p23 controls root development through the modulation of auxin distribution in the Arabidopsis root meristem. *J Exp Bot, 66*(16), 5113-5122. doi:10.1093/jxb/erv330

D'Andrea, L. D., & Regan, L. (2003). TPR proteins: the versatile helix. *Trends Biochem Sci, 28*(12), 655-662. doi:10.1016/j.tibs.2003.10.007

di Donato, M., & Geisler, M. (2019). HSP90 and co-chaperones: a multitaskers' view on plant hormone biology. *FEBS Lett, 593*(13), 1415-1430. doi:10.1002/1873-3468.13499

Dobin, A., Davis, C. A., Schlesinger, F., Drenkow, J., Zaleski, C., Jha, S., Batut, P., Chaisson, M., & Gingeras, T. R. (2013). STAR: ultrafast universal RNA-seq aligner. *Bioinformatics, 29*(1), 15-21. doi:10.1093/bioinformatics/bts635

Ellis, R. J., & Minton, A. P. (2006). Protein aggregation in crowded environments. *Biol Chem, 387*(5), 485-497. doi:10.1515/bc.2006.064

Emanuelsson, O., Nielsen, H., Brunak, S., & von Heijne, G. (2000). Predicting subcellular localization of proteins based on their N-terminal amino acid sequence. *J Mol Biol, 300*(4), 1005-1016. doi:10.1006/jmbi.2000.3903

Eremina, M., Rozhon, W., Yang, S., & Poppenberger, B. (2015). ENO2 activity is required for the development and reproductive success of plants, and is feedback-repressed by AtMBP-1. *Plant J, 81*(6), 895-906. doi:10.1111/tpj.12775

Fan, C. Y., Lee, S., Ren, H. Y., & Cyr, D. M. (2004). Exchangeable chaperone modules contribute to specification of type I and type II Hsp40 cellular function. *Mol Biol Cell, 15*(2), 761-773. doi:10.1091/mbc.e03-03-0146

Fernández-Bautista, N., Fernández-Calvino, L., Muñoz, A., Toribio, R., Mock, H. P., & Castellano, M. M. (2018). HOP family plays a major role in long-term acquired thermotolerance in Arabidopsis. *Plant Cell Environ, 41*(8), 1852-1869. doi:10.1111/pce.13326

Fields, S., & Song, O. (1989). A novel genetic system to detect protein-protein interactions. *Nature, 340*(6230), 245-246. doi:10.1038/340245a0

Finkelstein, R. R., & Lynch, T. J. (2000). The Arabidopsis abscisic acid response gene ABI5 encodes a basic leucine zipper transcription factor. *Plant Cell, 12*(4), 599-609. doi:10.1105/tpc.12.4.599

Fujiki, Y., Hubbard, A. L., Fowler, S., & Lazarow, P. B. (1982). Isolation of intracellular membranes by means of sodium carbonate treatment: application to endoplasmic reticulum. *J Cell Biol, 93*(1), 97-102. doi:10.1083/jcb.93.1.97

Gehl, C., Waadt, R., Kudla, J., Mendel, R. R., & Hänsch, R. (2009). New GATEWAY vectors for high throughput analyses of protein-protein interactions by bimolecular fluorescence complementation. *Mol Plant, 2*(5), 1051-1058. doi:10.1093/mp/ssp040

Genest, O., Wickner, S., & Doyle, S. M. (2019). Hsp90 and Hsp70 chaperones: Collaborators in protein remodeling. *J Biol Chem, 294*(6), 2109-2120. doi:10.1074/jbc.REV118.002806

Guan, X., & Fierke, C. A. (2011). Understanding Protein Palmitoylation: Biological Significance and Enzymology. *Sci China Chem, 54*(12), 1888-1897. doi:10.1007/s11426-011-4428-2

Hall, T. A. (1999). *BioEdit: a user-friendly biological sequence alignment editor and analysis program for Windows 95/98/NT.* Paper presented at the Nucleic acids symposium series.

Harb, A., Krishnan, A., Ambavaram, M. M. R., & Pereira, A. (2010). Molecular and Physiological Analysis of Drought Stress in Arabidopsis Reveals Early Responses Leading to Acclimation in Plant Growth. *Plant Physiol, 154*(3), 1254-1271. doi:10.1104/pp.110.161752

Hartl, F. U., Bracher, A., & Hayer-Hartl, M. (2011). Molecular chaperones in protein folding and proteostasis. *Nature, 475*(7356), 324-332. doi:10.1038/nature10317

Huang da, W., Sherman, B. T., & Lempicki, R. A. (2009). Systematic and integrative analysis of large gene lists using DAVID bioinformatics resources. *Nat Protoc, 4*(1), 44-57. doi:10.1038/nprot.2008.211

Huang, F., Zago, M. K., Abas, L., van Marion, A., Galván-Ampudia, C. S., & Offringa, R. (2010). Phosphorylation of conserved PIN motifs directs Arabidopsis PIN1 polarity and auxin transport. *Plant Cell, 22*(4), 1129-1142. doi:10.1105/tpc.109.072678

Hurst, C. H., & Hemsley, P. A. (2015). Current perspective on protein S-acylation in plants: more than just a fatty anchor? *J Exp Bot, 66*(6), 1599-1606. doi:10.1093/jxb/erv053

Jacob, P., Hirt, H., & Bendahmane, A. (2017). The heat-shock protein/chaperone network and multiple stress resistance. *Plant Biotechnol J, 15*(4), 405-414. doi:10.1111/pbi.12659

Johnson-Brousseau, S. A., & McCormick, S. (2004). A compendium of methods useful for characterizing Arabidopsis pollen mutants and gametophytically-expressed genes. *Plant J, 39*(5), 761-775. doi:10.1111/j.1365-313X.2004.02147.x

Kader, M. A., & Lindberg, S. (2010). Cytosolic calcium and pH signaling in plants under salinity stress. *Plant Signal Behav, 5*(3), 233-238. doi:10.4161/psb.5.3.10740

Kaiser, C. M., Goldman, D. H., Chodera, J. D., Tinoco, I., Jr., & Bustamante, C. (2011). The ribosome modulates nascent protein folding. *Science, 334*(6063), 1723-1727. doi:10.1126/science.1209740

Kampinga, H. H., Andreasson, C., Barducci, A., Cheetham, M. E., Cyr, D., Emanuelsson, C., Genevaux, P., Gestwicki, J. E., Goloubinoff, P., Huerta-Cepas, J., Kirstein, J., Liberek, K., Mayer, M. P., Nagata, K., Nillegoda, N. B., Pulido, P., Ramos, C., De Los Rios, P., Rospert, S., Rosenzweig, R., Sahi, C., Taipale, M., Tomiczek, B., Ushioda, R., Young, J. C., Zimmermann, R., Zylicz, A., Zylicz, M., Craig, E. A., & Marszalek, J. (2019). Function, evolution, and structure of J-domain proteins. *Cell Stress Chaperones, 24*(1), 7-15. doi:10.1007/s12192-018-0948-4

Kampinga, H. H., & Craig, E. A. (2010). The HSP70 chaperone machinery: J proteins as drivers of functional specificity. *Nat Rev Mol Cell Biol, 11*(8), 579-592. doi:10.1038/nrm2941

Kelley, L. A., Mezulis, S., Yates, C. M., Wass, M. N., & Sternberg, M. J. (2015). The Phyre2 web portal for protein modeling, prediction and analysis. *Nat Protoc, 10*(6), 845-858. doi:10.1038/nprot.2015.053

Kim, Y. E., Hipp, M. S., Bracher, A., Hayer-Hartl, M., & Hartl, F. U. (2013). Molecular chaperone functions in protein folding and proteostasis. *Annu Rev Biochem, 82*, 323-355. doi:10.1146/annurev-biochem-060208-092442

Kityk, R., Kopp, J., & Mayer, M. P. (2018). Molecular Mechanism of J-Domain-Triggered ATP Hydrolysis by Hsp70 Chaperones. *Mol Cell, 69*(2), 227-237.e224. doi:10.1016/j.molcel.2017.12.003

Kityk, R., Kopp, J., Sinning, I., & Mayer, M. P. (2012). Structure and dynamics of the ATP-bound open conformation of Hsp70 chaperones. *Mol Cell, 48*(6), 863-874. doi:10.1016/j.molcel.2012.09.023

Kosmacz, M., & Skirycz, A. (2020). The Isolation of Stress Granules From Plant Material. *Curr Protoc Plant Biol, 5*(3), e20118. doi:10.1002/cppb.20118

Krishna, P., & Gloor, G. (2001). The Hsp90 family of proteins in Arabidopsis thaliana. *Cell Stress Chaperones, 6*(3), 238-246. doi:10.1379/1466-1268(2001)006<0238:thfopi>2.0.co;2

Kunze, M., & Berger, J. (2015). The similarity between N-terminal targeting signals for protein import into different organelles and its evolutionary relevance. *Front Physiol, 6*, 259. doi:10.3389/fphys.2015.00259

Kyte, J., & Doolittle, R. F. (1982). A simple method for displaying the hydropathic character of a protein. *J Mol Biol, 157*(1), 105-132. doi:10.1016/0022-2836(82)90515-0

La Verde, V., Dominici, P., & Astegno, A. (2018). Towards Understanding Plant Calcium Signaling through Calmodulin-Like Proteins: A Biochemical and Structural Perspective. *Int J Mol Sci, 19*(5). doi:10.3390/ijms19051331

Laemmli, U. K. (1970). Cleavage of structural proteins during the assembly of the head of bacteriophage T4. *Nature, 227*(5259), 680-685. doi:10.1038/227680a0

Lamesch, P., Berardini, T. Z., Li, D., Swarbreck, D., Wilks, C., Sasidharan, R., Muller, R., Dreher, K., Alexander, D. L., Garcia-Hernandez, M., Karthikeyan, A. S., Lee, C. H., Nelson, W. D., Ploetz, L., Singh, S., Wensel, A., & Huala, E. (2012). The Arabidopsis Information Resource (TAIR): improved gene annotation and new tools. *Nucleic Acids Res, 40*, D1202-1210. doi:10.1093/nar/gkr1090

Lee, S. Y., Boon, N. J., Webb, A. A. R., & Tanaka, R. J. (2016). Synergistic Activation of RD29A Via Integration of Salinity Stress and Abscisic Acid in Arabidopsis thaliana. *Plant Cell Physiol, 57*(10), 2147-2160. doi:10.1093/pcp/pcw132

Leng, L., Liang, Q., Jiang, J., Zhang, C., Hao, Y., Wang, X., & Su, W. (2017). A subclass of HSP70s regulate development and abiotic stress responses in Arabidopsis thaliana. *J Plant Res, 130*(2), 349-363. doi:10.1007/s10265-016-0900-6

Lin, B. L., Wang, J. S., Liu, H. C., Chen, R. W., Meyer, Y., Barakat, A., & Delseny, M. (2001). Genomic analysis of the Hsp70 superfamily in Arabidopsis thaliana. *Cell Stress Chaperones, 6*(3), 201-208. doi:10.1379/1466-1268(2001)006<0201:gaoths>2.0.co;2

Liu, Y., & Li, J. (2014). Endoplasmic reticulum-mediated protein quality control in Arabidopsis. *Front Plant Sci, 5*(162). doi:10.3389/fpls.2014.00162

Liu, Z. J., Zhang, Y. H., Ma, X. F., Ye, P., Gao, F., Li, X. F., Zhou, Y. J., Shi, Z. H., Cheng, H. M., Zheng, C. X., Li, H. J., & Zhang, G. F. (2020). Biological functions of Arabidopsis thaliana MBP-1-like protein encoded by ENO2 in the response to drought and salt stresses. *Physiol Plant, 168*(3), 660-674. doi:10.1111/ppl.13013

Lu, S., Wang, J., Chitsaz, F., Derbyshire, M. K., Geer, R. C., Gonzales, N. R., Gwadz, M., Hurwitz, D. I., Marchler, G. H., Song, J. S., Thanki, N., Yamashita, R. A., Yang, M., Zhang, D., Zheng, C.,

Lanczycki, C. J., & Marchler-Bauer, A. (2020). CDD/SPARCLE: the conserved domain database in 2020. *Nucleic Acids Res, 48*(D1), D265-d268. doi:10.1093/nar/gkz991

Mészáros, B., Erdős, G., & Dosztányi, Z. (2018). IUPred2A: context-dependent prediction of protein disorder as a function of redox state and protein binding. *Nucleic Acids Res, 46*(W1), W329-W337. doi:10.1093/nar/gky384

Mravec, J., Skůpa, P., Bailly, A., Hoyerová, K., Krecek, P., Bielach, A., Petrásek, J., Zhang, J., Gaykova, V., Stierhof, Y. D., Dobrev, P. I., Schwarzerová, K., Rolcík, J., Seifertová, D., Luschnig, C., Benková, E., Zazímalová, E., Geisler, M., & Friml, J. (2009). Subcellular homeostasis of phytohormone auxin is mediated by the ER-localized PIN5 transporter. *Nature, 459*(7250), 1136-1140. doi:10.1038/nature08066

Nakabayashi, K., Okamoto, M., Koshiba, T., Kamiya, Y., & Nambara, E. (2005). Genome-wide profiling of stored mRNA in Arabidopsis thaliana seed germination: epigenetic and genetic regulation of transcription in seed. *Plant J, 41*(5), 697-709. doi:10.1111/j.1365-313X.2005.02337.x

Nelson, B. K., Cai, X., & Nebenführ, A. (2007). A multicolored set of in vivo organelle markers for co-localization studies in Arabidopsis and other plants. *Plant J, 51*(6), 1126-1136. doi:10.1111/j.1365-313X.2007.03212.x

Park, M. Y., & Kim, S. Y. (2014). The Arabidopsis J protein AtJ1 is essential for seedling growth, flowering time control and ABA response. *Plant Cell Physiol, 55*(12), 2152-2163. doi:10.1093/pcp/pcu145

Perales-Calvo, J., Muga, A., & Moro, F. (2010). Role of DnaJ G/F-rich domain in conformational recognition and binding of protein substrates. *J Biol Chem, 285*(44), 34231-34239. doi:10.1074/jbc.M110.144642

Pettersen, E. F., Goddard, T. D., Huang, C. C., Couch, G. S., Greenblatt, D. M., Meng, E. C., & Ferrin, T. E. (2004). UCSF Chimera--a visualization system for exploratory research and analysis. *J Comput Chem, 25*(13), 1605-1612. doi:10.1002/jcc.20084

Prasad, B. D., Goel, S., & Krishna, P. (2010). In silico identification of carboxylate clamp type tetratricopeptide repeat proteins in Arabidopsis and rice as putative co-chaperones of Hsp90/Hsp70. *PLoS One, 5*(9), e12761. doi:10.1371/journal.pone.0012761

Prasinos, C., Krampis, K., Samakovli, D., & Hatzopoulos, P. (2005). Tight regulation of expression of two Arabidopsis cytosolic Hsp90 genes during embryo development. *J Exp Bot, 56*(412), 633-644. doi:10.1093/jxb/eri035

Radli, M., & Rüdiger, S. G. D. (2018). Dancing with the Diva: Hsp90-Client Interactions. *J Mol Biol, 430*(18 Pt B), 3029-3040. doi:10.1016/j.jmb.2018.05.026

Rajan, V. B., & D'Silva, P. (2009). Arabidopsis thaliana J-class heat shock proteins: cellular stress sensors. *Funct Integr Genomics, 9*(4), 433-446. doi:10.1007/s10142-009-0132-0

Raudvere, U., Kolberg, L., Kuzmin, I., Arak, T., Adler, P., Peterson, H., & Vilo, J. (2019). g:Profiler: a web server for functional enrichment analysis and conversions of gene lists (2019 update). *Nucleic Acids Res, 47*(W1), W191-w198. doi:10.1093/nar/gkz369

Retzlaff, M., Stahl, M., Eberl, H. C., Lagleder, S., Beck, J., Kessler, H., & Buchner, J. (2009). Hsp90 is regulated by a switch point in the C-terminal domain. *EMBO rep, 10*(10), 1147-1153.

Robinson, D. G., & Aniento, F. (2020). A Model for ERD2 Function in Higher Plants. *Front Plant Sci, 11*, 343. doi:10.3389/fpls.2020.00343

Rosenzweig, R., Nillegoda, N. B., Mayer, M. P., & Bukau, B. (2019). The Hsp70 chaperone network. *Nat Rev Mol Cell Biol, 20*(11), 665-680. doi:10.1038/s41580-019-0133-3

Rüdiger, S., Germeroth, L., Schneider-Mergener, J., & Bukau, B. (1997). Substrate specificity of the DnaK chaperone determined by screening cellulose-bound peptide libraries. *EMBO J, 16*(7), 1501-1507. doi:10.1093/emboj/16.7.1501

Rüdiger, S., Schneider-Mergener, J., & Bukau, B. (2001). Its substrate specificity characterizes the DnaJ co-chaperone as a scanning factor for the DnaK chaperone. *EMBO J, 20*(5), 1042-1050. doi:10.1093/emboj/20.5.1042

Saint-Jore-Dupas, C., Nebenführ, A., Boulaflous, A., Follet-Gueye, M. L., Plasson, C., Hawes, C., Driouich, A., Faye, L., & Gomord, V. (2006). Plant N-glycan processing enzymes employ different targeting mechanisms for their spatial arrangement along the secretory pathway. *Plant Cell, 18*(11), 3182-3200. doi:10.1105/tpc.105.036400

Scheufler, C., Brinker, A., Bourenkov, G., Pegoraro, S., Moroder, L., Bartunik, H., Hartl, F. U., & Moarefi, I. (2000). Structure of TPR domain-peptide complexes: critical elements in the assembly of the Hsp70-Hsp90 multichaperone machine. *Cell, 101*(2), 199-210. doi:10.1016/s0092-8674(00)80830-2

Schmid, M., Davison, T. S., Henz, S. R., Pape, U. J., Demar, M., Vingron, M., Schölkopf, B., Weigel, D., & Lohmann, J. U. (2005). A gene expression map of Arabidopsis thaliana development. *Nat Genet, 37*(5), 501-506. doi:10.1038/ng1543

Schopf, F. H., Biebl, M. M., & Buchner, J. (2017). The HSP90 chaperone machinery. *Nat Rev Mol Cell Biol, 18*(6), 345-360. doi:10.1038/nrm.2017.20

Schott, A., Ravaud, S., Keller, S., Radzimanowski, J., Viotti, C., Hillmer, S., Sinning, I., & Strahl, S. (2010). Arabidopsis stromal-derived Factor2 (SDF2) is a crucial target of the unfolded protein response in the endoplasmic reticulum. *J Biol Chem, 285*(23), 18113-18121. doi:10.1074/jbc.M110.117176

Schwacke, R., Schneider, A., van der Graaff, E., Fischer, K., Catoni, E., Desimone, M., Frommer, W. B., Flugge, U. I., & Kunze, R. (2003). ARAMEMNON, a novel database for Arabidopsis integral membrane proteins. *Plant Physiol, 131*(1), 16-26. doi:10.1104/pp.011577

Schweiger, R., Müller, N. C., Schmitt, M. J., Soll, J., & Schwenkert, S. (2012). AtTPR7 is a chaperone-docking protein of the Sec translocon in Arabidopsis. *J Cell Sci, 125*(Pt 21), 5196-5207. doi:10.1242/jcs.111054

Shiau, A. K., Harris, S. F., Southworth, D. R., & Agard, D. A. (2006). Structural Analysis of E. coli hsp90 reveals dramatic nucleotide-dependent conformational rearrangements. *Cell, 127*(2), 329-340. doi:10.1016/j.cell.2006.09.027

Sima, S., & Richter, K. (2018). Regulation of the Hsp90 system. *Biochim Biophys Acta Mol Cell Res, 1865*(6), 889-897. doi:https://doi.org/10.1016/j.bbamcr.2018.03.008

Smith, A. R., & Zhao, D. (2016). Sterility Caused by Floral Organ Degeneration and Abiotic Stresses in Arabidopsis and Cereal Grains. *Front Plant Sci, 7*, 1503. doi:10.3389/fpls.2016.01503

Sung, D. Y., Vierling, E., & Guy, C. L. (2001). Comprehensive expression profile analysis of the Arabidopsis Hsp70 gene family. *Plant Physiol, 126*(2), 789-800. doi:10.1104/pp.126.2.789

Waese, J., Fan, J., Pasha, A., Yu, H., Fucile, G., Shi, R., Cumming, M., Kelley, L. A., Sternberg, M. J., Krishnakumar, V., Ferlanti, E., Miller, J., Town, C., Stuerzlinger, W., & Provart, N. J. (2017). ePlant: Visualizing and Exploring Multiple Levels of Data for Hypothesis Generation in Plant Biology. *Plant Cell, 29*(8), 1806-1821. doi:10.1105/tpc.17.00073

Wang, X., Jia, N., Zhao, C., Fang, Y., Lv, T., Zhou, W., Sun, Y., & Li, B. (2014). Knockout of AtDjB1, a J-domain protein from Arabidopsis thaliana, alters plant responses to osmotic stress and abscisic acid. *Physiol Plant, 152*(2), 286-300. doi:10.1111/ppl.12169

Willige, B. C., Isono, E., Richter, R., Zourelidou, M., & Schwechheimer, C. (2011). Gibberellin regulates PIN-FORMED abundance and is required for auxin transport-dependent growth and development in Arabidopsis thaliana. *Plant Cell, 23*(6), 2184-2195. doi:10.1105/tpc.111.086355

Willige, B. C., Isono, E., Richter, R., Zourelidou, M., & Schwechheimer, C. (2011). Gibberellin Regulates PIN-FORMED Abundance and Is Required for Auxin Transport–Dependent Growth and Development in Arabidopsis thaliana. *Plant Cell, 23*(6), 2184-2195. doi:10.1105/tpc.111.086355

Xie, W., Nielsen, M. E., Pedersen, C., & Thordal-Christensen, H. (2017). A Split-GFP Gateway Cloning System for Topology Analyses of Membrane Proteins in Plants. *PLoS One, 12*(1), e0170118. doi:10.1371/journal.pone.0170118

Xu, D., Marino, G., Klingl, A., Enderle, B., Monte, E., Kurth, J., Hiltbrunner, A., Leister, D., & Kleine, T. (2019). Extrachloroplastic PP7L Functions in Chloroplast Development and Abiotic Stress Tolerance. *Plant Physiol*. doi:10.1104/pp.19.00070

Yoo, S. D., Cho, Y. H., & Sheen, J. (2007). Arabidopsis mesophyll protoplasts: a versatile cell system for transient gene expression analysis. *Nat Protoc, 2*(7), 1565-1572. doi:10.1038/nprot.2007.199

Young, J. C. (2010). Mechanisms of the Hsp70 chaperone system. *Biochem Cell Biol, 88*(2), 291-300. doi:10.1139/o09-175

Zeytuni, N., & Zarivach, R. (2012). Structural and Functional Discussion of the Tetra-Trico-Peptide Repeat, a Protein Interaction Module. *Structure, 20*(3), 397-405. doi:https://doi.org/10.1016/j.str.2012.01.006

Zgajnar, N. R., De Leo, S. A., Lotufo, C. M., Erlejman, A. G., Piwien-Pilipuk, G., & Galigniana, M. D. (2019). Biological Actions of the Hsp90-binding Immunophilins FKBP51 and FKBP52. *Biomolecules, 9*(2). doi:10.3390/biom9020052

Zhou, K. (2019). Glycosylphosphatidylinositol-Anchored Proteins in Arabidopsis and One of Their Common Roles in Signaling Transduction. *Front Plant Sci, 10*, 1022. doi:10.3389/fpls.2019.01022

Zhu, J. K. (2002). Salt and drought stress signal transduction in plants. *Annu Rev Plant Biol, 53*, 247-273. doi:10.1146/annurev.arplant.53.091401.143329

Aus Datenschutzgründen entfernt.

Aus Datenschutzgründen entfernt.

Eidesstattliche Erklärung

Ich versichere hiermit an Eides statt, dass die vorgelegte Dissertation von mir selbstständig und ohne unerlaubte Hilfe angefertigt wurde. Ich habe weder versucht, anderweitig eine Dissertation einzureichen oder eine Doktorprüfung durchzuführen, noch habe ich diese Dissertation oder Teile derselben einer anderen Prüfungskommission vorgelegt.

München, den 02.02.2021 S. Dittmer

Sophie Isabell Dittmer